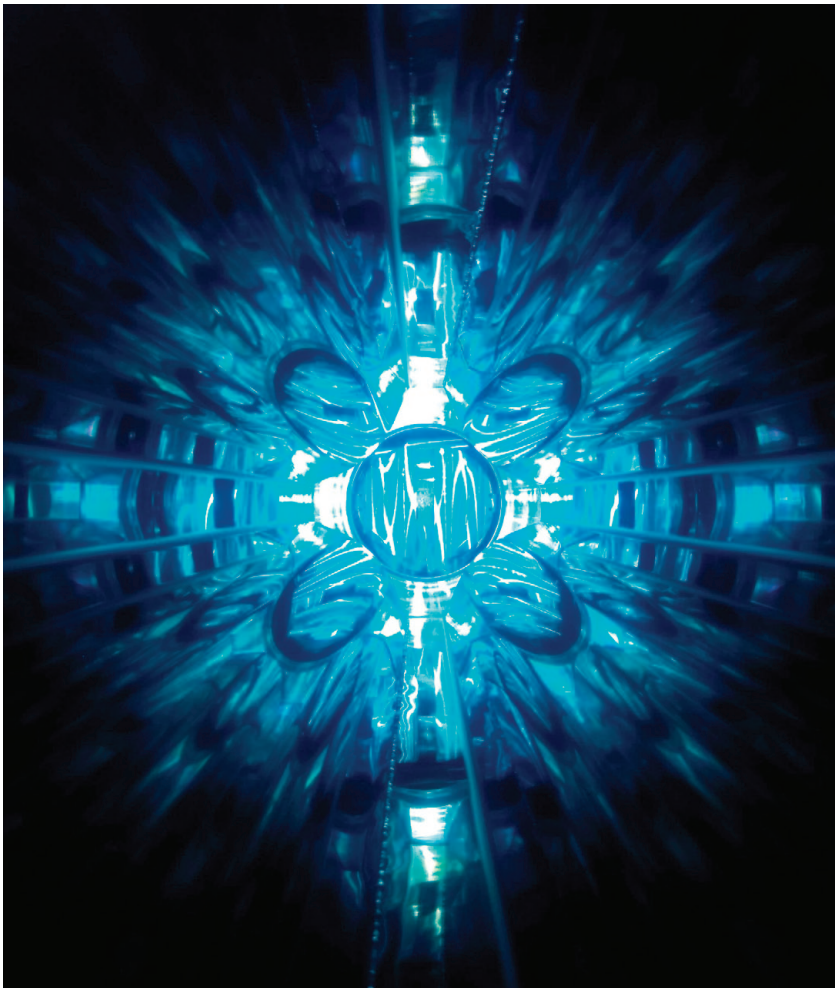

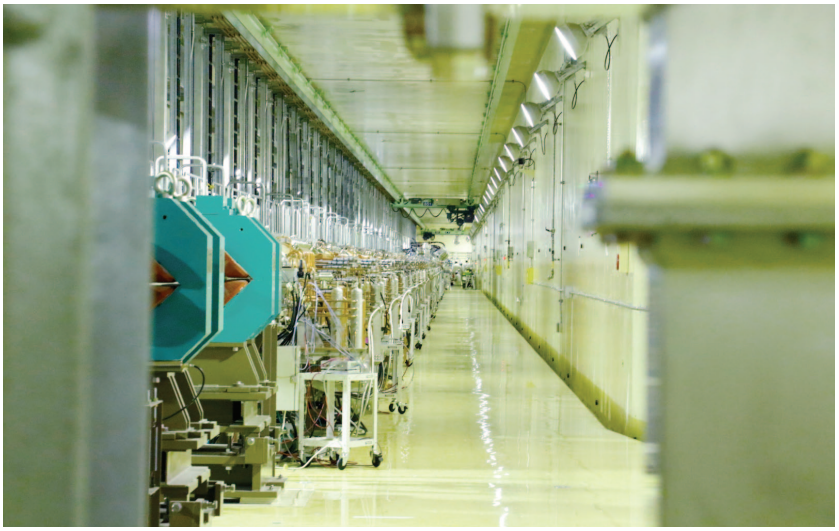

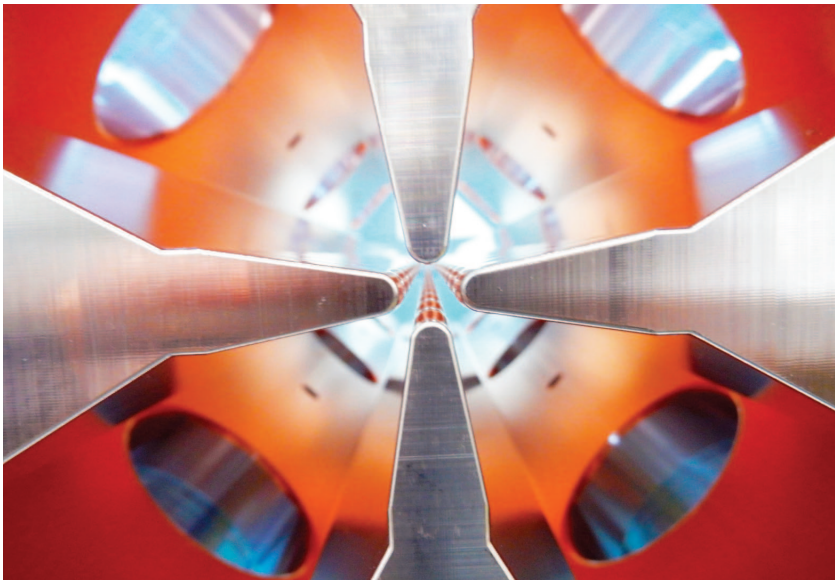

J-PARC

ANNUAL REPORT 2020

Vol.1: Highlight

Cover photographs

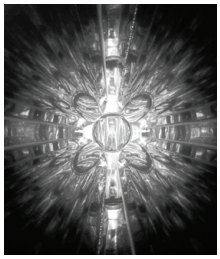

Photograph ① : Inside of a floral shaped beam duct
Image credit: Taihei ADACHI

Photograph ② : Beautiful view from the downstream
Image credit: Junko KITAGISHI

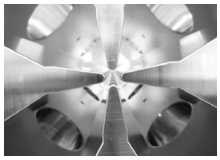

Photograph ③ : Radio-frequency quadruple linac, RFQ
Image credit: Masashi OTANI

J-PARC Annual Report 2020

Contents

Preface

In Japanese fiscal year (JFY) 2020, from April 2020 through March 2021, we made significant progress at J-PARC on many fronts and a few of our achievements are covered below.

Early in JFY2020, we faced an unexperienced and difficult situation as the first peak of COVID spread in Japan. Travel from abroad stopped, and domestic travel was also severely limited. In that situation, the MLF beam had to be suspended on April 20th to secure the safety of users and our staffs. After implementing preventive measures, we were able to restart the user beam on May 15th.

We achieved a 600-kW stable beam operation for the MLF. The total time provided for the user beam was about 3300 hrs (137 days) with the very high

availability of ~92 %. The Main Ring achieved a stable operation at 50 kW and 510 kW for hadron experiments and neutrino experiments, respectively. In JFY2020, 8 days of neutrino beams and 22 days of hadron beams were provided.

In the MLF, a new liquid mercury target with improved design for higher beam power was developed, installed, and successfully operated. Also, a test operation at ~1 MW (930 kW) beam power was successfully conducted for 36.5 hrs, which was also a major milestone toward realizing 1 MW stable user operation.

The neutrino group has established significant constraints on the CP phase. The hadron experimental facility is now equipped with a new target system, which can handle more beam power, and a new beamline, B-Line, to receive a primary proton beam.

In this volume, we report the progress made at J-PARC in JFY2020.

On behalf of the J-PARC staff members,
Director of J-PARC Center
Takashi KOBAYASHI

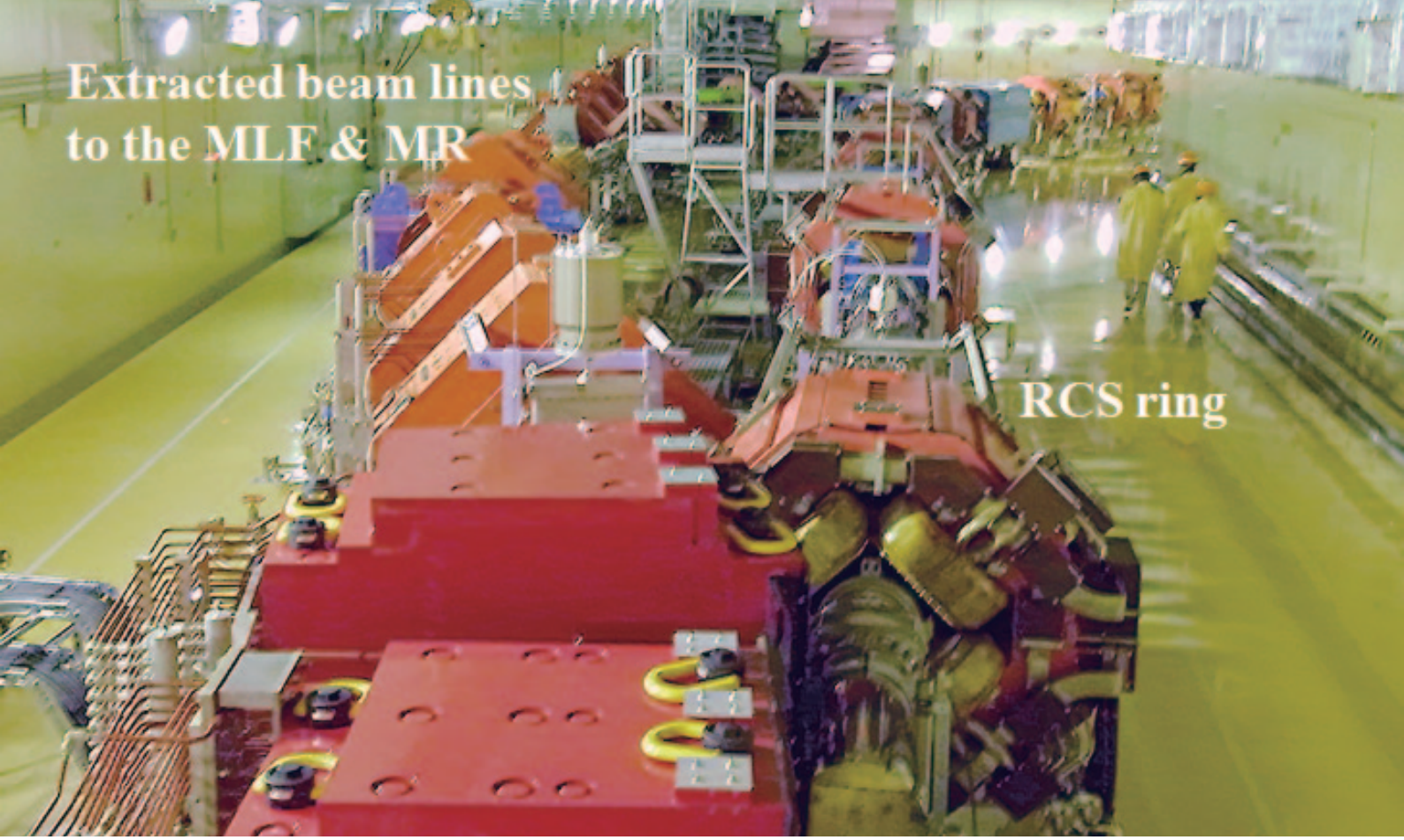

Accelerators

Overview of the Accelerator

The J-PARC accelerator complex consists of a 400 MeV linac, a 3 GeV Rapid Cycling Synchrotron (RCS) and a Main Ring Synchrotron (MR, 30 GeV). The proton beam from the RCS is delivered to the Materials and Life Science Experimental Facility (MLF) for neutron and muon experiments and is also injected into the MR. The MR has two beam extraction modes: fast extraction (FX) mode for the Neutrino experimental facility (NU) and slow extraction (SX) mode for the Hadron experimental facility (HD).

The operation in JFY2020 is illustrated in Fig. 1. The topics related to the beam operation are as follows:

(1) Operation for the MLF

The beam operation Run#84 was started in January and continued until April 20 when it was stopped due

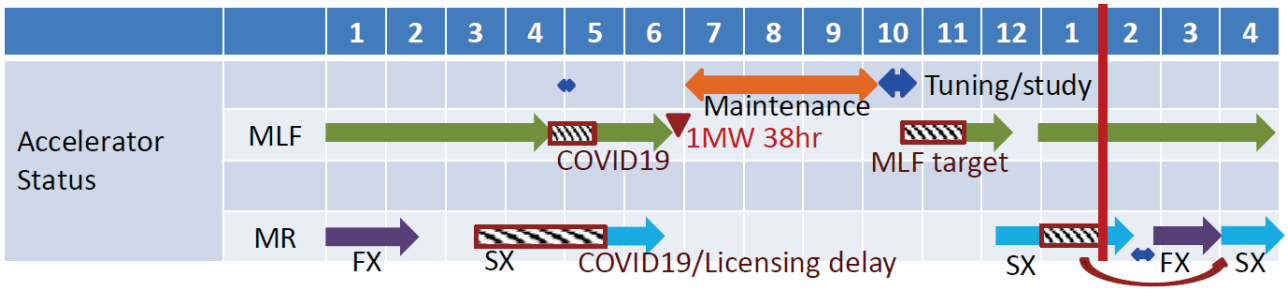

Fig. 1. Accelerator operation in JFY2020 (covers partially the end of JFY2019).

to the COVID-19 breakout. We also had a scheduled outage from May 1 to 10. The user operation was resumed from May 15 only for the MLF at a beam power of 500 kW, because the licensing for a new target and a new beam line in the HD was delayed by the authorities and the beam operation was postponed. The beam power to the MLF was increased to 600 kW from May 18. The user program was carried out as scheduled until June 27, also, an operation with the designed beam power of 1 MW was successfully executed from June 25 to 27. The user operation for the MLF ended on June 27 followed by a six-day accelerator study before the summer shutdown.

After the summer shutdown, the user program of the MLF restarted on December 1.

The neutron production target of the MLF was replaced during the summer shutdown. Due to the delay of the target-related work, the beam tuning and the user operation were postponed until the end of November, a two-week delay from the original schedule. The beam power for the user operation was 600 kW, the same as before the summer shutdown.

We had the usual shutdown period for about 2 weeks from the end of December until the beginning of January. The linac tuning started on January 7 followed by the RCS. The MLF user program started on January 12 and continued until the end of March as scheduled.

(2) Operation of the MR for the Neutrino Experiment (FX mode) and Hadron Experiment (SX mode)

The beam delivery to the Hadron experimental facility (HD) was started at a lower beam power on May 28. After fine tuning of the MR, we delivered beam at around 51 kW, a level similar to the previous operation. The HD user program was executed on June 25 and 26 at a beam power of around 51 kW, and a one-day beam study was carried out after the HD user program. The MR operation was completed on June 27 before the summer shutdown.

The beam studies at the MR after the summer maintenance started on December 10, and the beam delivery to the Hadron experimental facility (HD) resumed at beam power of 20 kW on December 14. After fine tuning of the MR, we delivered a beam at around 55 kW, the highest beam power for the HD user operation at the time.

However, due to the cooling water failure in the hadron facility, the HD user program was postponed until mid-February. The schedule was changed to install a new power supply and that work continued until February 7. The HD user operation was resumed on February 8. The beam power was gradually increased to 60 kW, which was the maximum beam power for the hadron user operation in J-PARC. The user program went on smoothly until February 28, but the ESS#1 (Electrostatic Septum #1) had a failure due to unexpected stoppage of few main quadrupole and sextupole magnets. The quadrupole magnets on three straight sections went down unexpectedly due to the accidental malfunction of the 22 kV circuit breaker causing a large deviation of the circulating beam towards the ESS#1. The deviation resulted in a large beam loss and breakage of some of the ESS#1 ribbons. The broken ribbons caused a short circuit failure of the ESS#1. Most of the lost beam spread throughout the Main Ring, and only a small fraction of the beam was extracted to the hadron target (no temperature rise was observed on the target). The broken ESS was removed from the beam line and a vacuum pipe was installed instead. Meanwhile, we started to prepare a spare ESS. The MR operation was changed for the neutrino user operation. We investigated the cause of malfunction of the circuit breaker. After identifying the cause and taking countermeasures, we restarted the hadron user operation. The neutrino user operation was restarted on March 8 at a beam power of 510 kW, and stopped on March 19 to prepare for the restart of the hadron user operation, which began on March 27.

The operation statistics for JFY2020 (from April 2020 to March 2021) are shown in Table 1 and Fig. 2. The total operation time, which included the shift leaders on duty time at the control room, the startup and the RF conditioning, was 4,632 hours. The net user operation hours and the beam availability rate for each experimental facility were as follows: 3,138 hours (95.3%) for the MLF; 134 hours (69.8%) for NU; and 344 hours (66%) for HD. These statistics show that the linac and the RCS operated with high availabilities. The cause of the lower availability for the NU operation was due to the trouble in the power supply of the injection magnet and also to a problem during the HD operation caused by the ESS ribbon failure in March 2021.

The downtime by components is shown in Fig. 3. There were several causes of the downtime. For the linac, HVDC and SDTL are still dominant. However, the cause of the stoppage incidents in SDTL was not the SDTL cavity, most of them are caused by the malfunction of LLRF. LLRF troubles were also counted as troubles in each cavity. The RCS outage was mainly due

to the RF and the cooling water. The RF outage was not due to the cavity, but to the failure of the capacitor and the end of life of the vacuum tube in the amplifier. Most of the RCS stops occurred during the 1-MW operation in late June. The MR had only one serious downtime event, which was the trouble of the ESS#1 in the "Slow ext." category. There was more than 100 hours downtime in the 3NBT caused by the trouble in the cooling water system, but it did not stop the user operation as the trouble occurred during the scheduled beam tuning period. These improved items, major downtime causes, achievements and history of the beam operation are described in the following chapters.

Table 1. Operation statistics in hours for JFY2020. Figures in the parentheses in trouble columns show the loss time contributions as percentage.

Facility	User Time (hours)	Trouble, Acc.only (hours)	Trouble, Faculty only (hours)	Net Time (hours)	Availability, Total (%)
MLF	3,291	143 (4.4%)	10 (0.3%)	3,138	95.3
Neutrino (FX)	192	45 (23.4%)	13 (6.8%)	134	69.8
Hadron (SX)	520	161 (31.0%)	15 (2.9%)	344	66.1

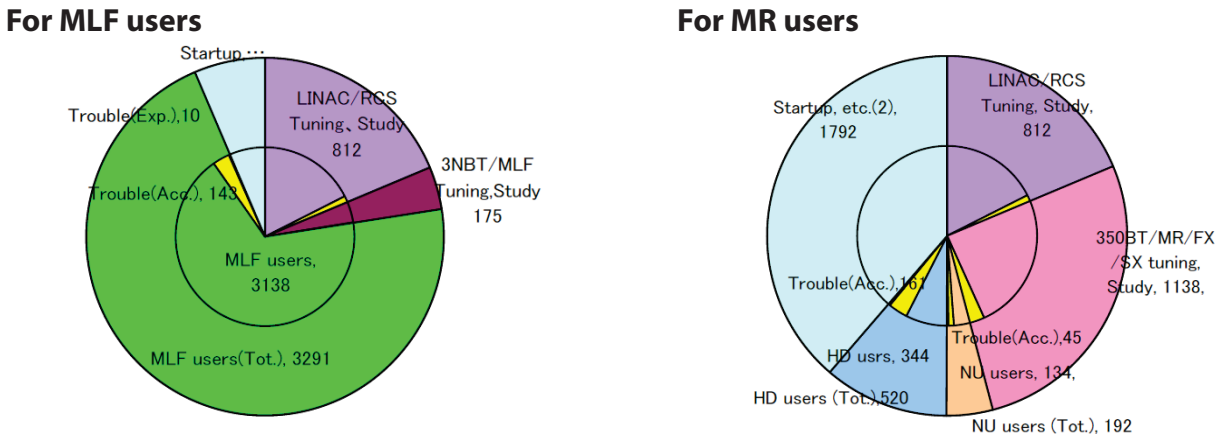

Fig. 2. Operation statistics for JFY2020. The total operation time was 4,632 hours.

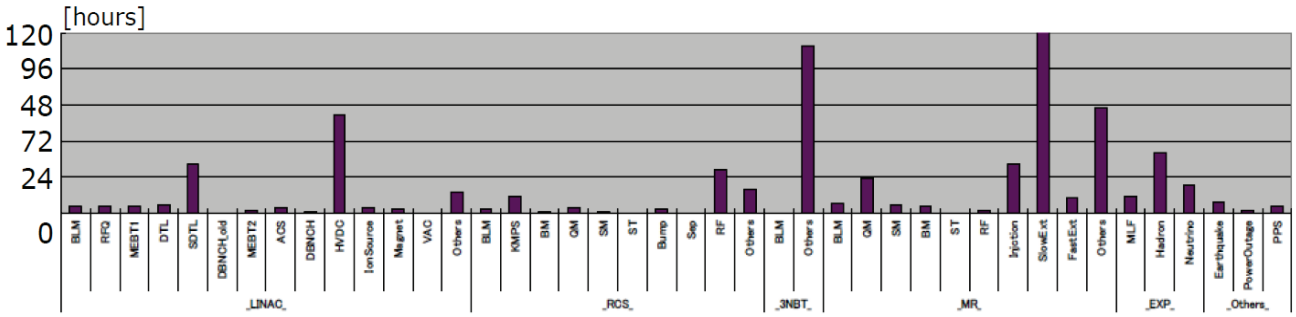

Fig. 3. Downtime by components in JFY2020.

Linac

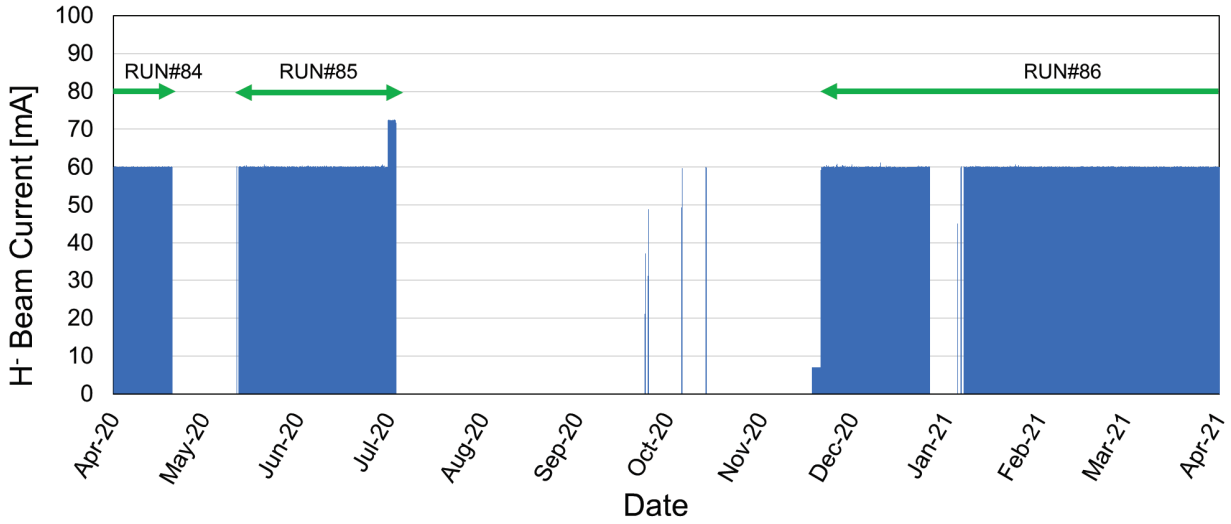

Fig. X-1. Operation history of the ion source in JFY2020.

Overview

The J-PARC linac has been operated with a nominal peak beam current of 50 mA. High availability of approximately more than 95% (to the MLF) was achieved during JFY2020 at the linac, the same as in JFY2019. Three 10-hour long beam stop events occurred due to the replacement of the klystron and the failure of the klystron peripheral devices. Beam studies have been conducted to resolve some issues, such as the beam loss mitigation, confirmation of feasibility for the further upgrade plan, and so on.

Accelerator components status

The operation history of the ion source in JFY2020 is shown in Fig. X-1. Presently, the ion source is being operated with a beam current of 60 mA for the user operation. At the end of RUN#85, the ion source extracted stable 72 mA beams for high-intensity beam studies at the linac. In RUN#84, a continuous operation of 2,445 hours with 60 mA was achieved, which was about 605 hours longer than the previous record. We skipped the replacement work of the ion source in this winter shutdown and took the challenge to achieve a continuous operation for more than 3,500 hours by the end of April 2021.

Figure X-2 shows the time variation of number of RFQ trips. The RFQ trip rate was approximately 10 times per day during the 25 Hz (MLF) beam operation in JFY2020, which is almost the same as before. To reduce the downtime of the linac due to the RFQ trip, we installed a new restart system for the RFQ. Previously, when the RFQ trip occurred, it took about 1 minute to resume the beam operation because the operator had to reset the MPS (machine protection system) manually. The new system can skip the MPS process and resume the beam operation automatically with the next macropulse (40 msec), therefore, the resume time can be significantly reduced from 1 minute to 40 msec. The new system saves about 10 minutes of no-beam time in a day, which can be expected to lead to a 1% improvement in the availability of the J-PARC accelerator.

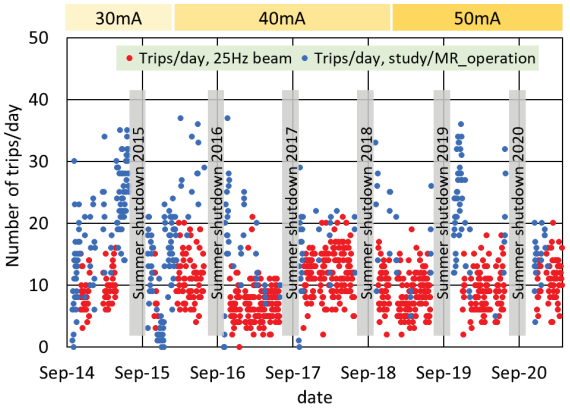

Fig. X-2. Time variation of the number of RFQ RF-trips.

After the Great East Japan Earthquake in 2011, we could not operate with the design rf power in some SDTL cavities due to the multipactor effect. By wiping the inner surface of the cavity with acetone, the multipactor region disappeared completely, except in the SDTL05A. Therefore, the input rf power of this

cavity and neighboring ones were slightly shifted to satisfy the beam quality while avoiding the multipactor region. Although this situation does not immediately affect the operation, we tried wiping with a different substance, diluted sulfuric acid, in the summer of 2020. As a result, the region did not disappear completely, but the rate of deterioration during the operation time was clearly slower than that with acetone. We will continue to observe the progress and verify the cleaning effect.

The operation of the ACS cavities was more stable than the other accelerator sections. The number of trips of all the ACS cavities was less than once per day.

RF system status

We have been handling two types of klystrons, a 324-MHz klystron and a 972-MHz one. The operation times of the klystrons as of March 2021 are shown in Fig. X-3. Eight out of twenty 324-MHz klystrons reached more than 75,000 hours of operation, which has been the entire period since the linac operation was started. Most of the 972-MHz klystrons reached more than 45,000 hours of operation.

In JFY2020, we suspended the beam operation once to replace a failed klystron (for SDTL09). The klystron failed due to a defective waveguide connection flange. The defect was caused by arching that occurred in a very small gap between the klystron and the waveguide connection flange. Although there was no problem with the performance of the klystron itself, we decided to replace it because the repair of the flange on site would have taken a lot of time.

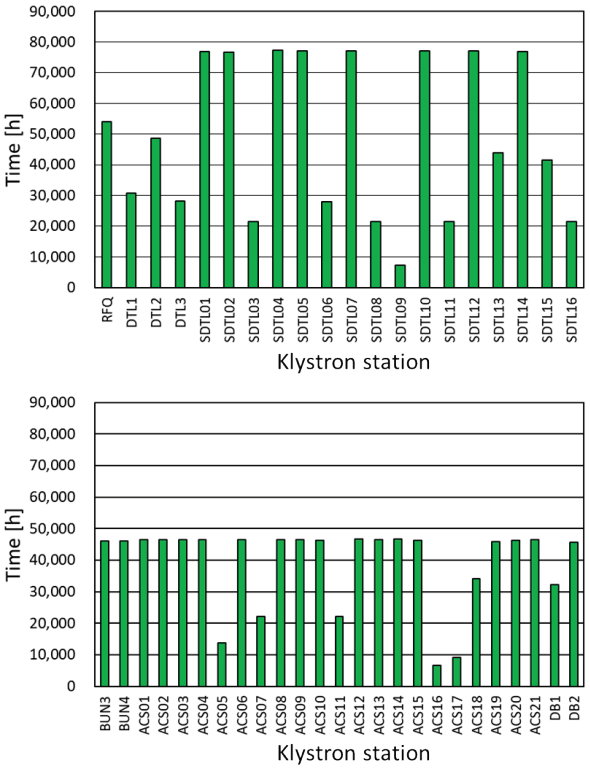

Fig. X-3. The operation time of the 324-MHz klystron (top) and 972-MHz klystron (bottom) as of March 2021.

Two failures in the klystron peripheral device stopped the beam operation for about 10 hours. The first failure was the malfunction of a power supply for a klystron main coil. The malfunction was caused by temperature rise inside the power supply housing after a cooling fan stopped. The second one was caused by a defect of a high voltage cable connecting the klystron and an anode modulator. It was restored by replacing the cable, but the beam was stopped for a long time because it took time to investigate the cause.

Beam monitor development

We are working to improve the beam quality of the linac by tuning the beam in a MEBT1 (medium energy beam transport1 located between the RFQ and the DTL). In the MEBT1, the beam energy is as low as 3 MeV, so the heat load on the beam irradiation portion of the beam monitor is very large, and as a result, the monitor has often failed. Therefore, we needed to develop new monitors with higher thermal load tolerance.

We developed a modified wire scanner monitor (WSM) based on the carbon nanotube (CNT) wire, which has high tensile strength and electric conductivity. After confirming that the CNT-WSM obtained almost the same result as the conventional WSM, all the WSMs at the MEBT1 were replaced with the CNT type in the summer of 2020.

We also developed a new bunch shape monitor (BSM) which can measure a longitudinal beam profile. The measurement of the profile at the MEBT1 was difficult with the conventional BSM using a tungsten wire as a secondary-electron production target due to the limitation of the thermal-fatigue damage. Therefore, a highly oriented pyrolytic graphite (HOPG), which has high thermal load tolerance, was adopted as the target. As a result of the off-line beam test, it was confirmed that the new BSM was able to withstand the 3-MeV beam sufficiently and worked fine to measure the bunch shape as did the conventional type. The new BSM was installed in the MEBT1 in the summer of 2020, and we utilize it as a beam tuning tool.

Beam study

The beam studies have been conducted at the interval of the user operation and before and after the long-term shutdown.

High residual radiation at DTL1 due to the beam loss was detected after the 50-mA operation commenced in 2018. Using a smooth local focusing correction scheme with the current of the DTQ (drift tube quadrupole) magnets set to maximum 60% higher than the design value, the beam loss was significantly decreased. After further detailed investigation, we confirmed that 30% correction could be sufficient to remove the beam loss.

At the ACS section, the dominant source of the beam loss was found to be the IBSt (intra-beam stripping) in the H- beam. Because the IBSt can be only mitigated by beam optics, some optics with a different temperature ratio between transverse and longitudinal planes (Tx/Tz) were examined (The optics of Tx/Tz=1.0 is the J-PARC linac baseline design based on the equipartitioning setting). Since it was confirmed that the beam loss at the case of Tx/Tz=0.7 was reduced by 40% compared to the Tx/Tz=1.0, the operation with Tx/Tz=0.7 was commenced from April 2019. Two years have passed since we commenced operation under the new condition, and the linac has been operated stably without any problems due to the new condition. In order to study the possibility of further reduction of the beam loss, we started beam test with Tx/Tz of 0.5 and 0.3.

We are considering a further upgrade plan to increase the RCS beam power to 1.5 MW. To realize the upgrade plan, the beam current and the beam pulse length must increase to approximately 60 mA and 600 μs respectively. We successfully extracted 60-mA and 600- s beam from the linac in July 2019. Although the beam current and the pulse length were satisfying the upgrade requirement, the linac output emittance was large. To improve the emittance, fine tuning of the beam parameter at the MEBT1 and re-matching in the three matching sections of the linac (SDTL, MEBT2, L3BT) were performed. As a result, a reduction of the beam loss of about 10% was achieved.

We also conducted the beam loss reduction study for the 60-mA operation. The result is shown in Fig. X-4. In this study, we applied a transverse-longitudinal matching, Tx/Tz = 0.7. The beam loss was mitigated at most of the BLM position, where a total reduction of 32% was achieved as compared to that with a Tx/Tz=1.0 optics. However, there are three "abnormal" points left as shown by the red circles. Further optimization of the Tx/Tz ratio is planned to improve the result in a near future study.

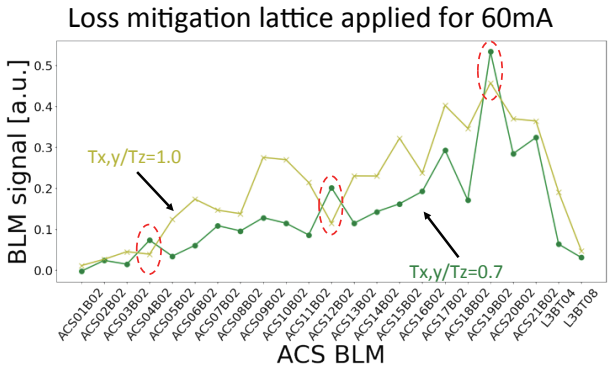

Fig. X-4. Distribution of the beam loss signal at the ACS section in case of Tx/Tz=1.0 and 0.7.

RCS

Operational status

At the beginning of JFY2020, RCS delivered a 500-kW proton beam for the neutron users in the MLF. Unfortunately, the whole operation at the J-PARC accelerator was suspended for about three weeks from mid-April due to the first pandemic of COVID-19 in Japan. The beam operation was resumed by increasing the beam power to 600 kW and continued at that level during JFY2020. Just before the summer shutdown period, we tried a two-day continuous operation at 1-MW beam power for the MLF. Meanwhile, the number of the protons for MR was 6.7e13 particles per pulse which corresponds to 515-kW output beam power of MR. Figure 1 shows the change in the RCS output beam power with respect to time.

This year, the operational status of the RCS was almost stable. One incident occurred at the cooling water pump of the 3NBT line. In mid-January 2021, a shaft wear sensor for a bearing motor in the pump sent a warning signal. We investigated the pump and found the sensor gave a wrong alert. We spent about one week to recover from this incident.

The availability of the RCS is summarized in the Table 1. The operation time for the MLF over the year was approximately 3291 h, excluding the commissioning time, and the downtime was approximately 38 h. The availability for the MLF, estimated by these values, was 98.9%. For the Neutrino and Hadron users, the availability of RCS was almost the same as in the MLF case, the value being around 99%.

Table 1. Summary of the RCS availability.

Facility	User time (h:m)	Trouble in RCS (h)	Availability of RCS (%)
MLF	3290:58	37:45	98.9
Neutrino	192:26	0:16	99.9
Hadron	511:56	9:37	98.2

Maintenance and improvements

- Radiation shielding installation around the injection chamber

At the recent operational condition, the major radio-activated point in the RCS is at the injection foil chamber. The residual dose value on the surface of the

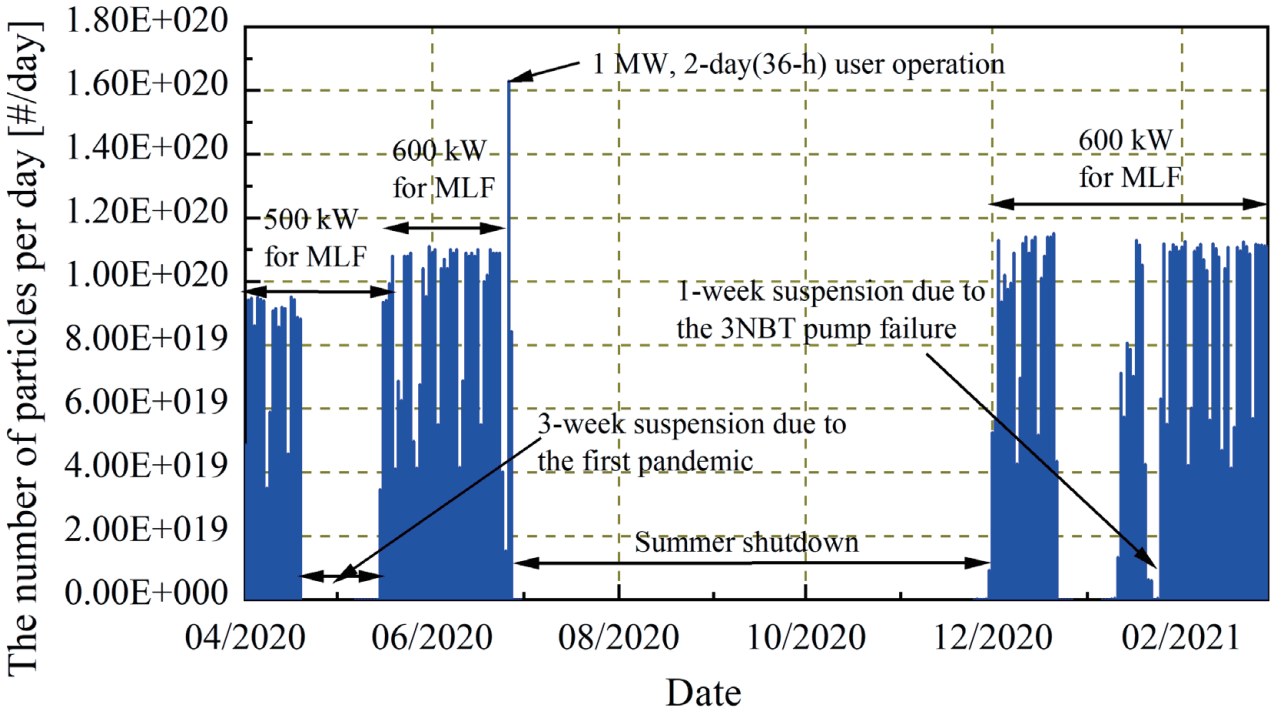

Fig. 1. xxxxxxxxxxxxxxxxxxxxxxxxxxxxxxxxxxxxxxxx

injection foil chamber was about 10 mSv/h at 4 h after the halt of the beam operation, and the worker dose around the injection point was quite high compared to that in other regions. Therefore, we considered countermeasures for the radiation around the injection region to reduce the worker dose at the high-intensity operation.

First, we considered changing the shape and location of the magnets near the injection point to install a permanent radiation shielding around the injection foil chamber. However, Monte Carlo simulation results indicated that a permanent radiation shielding would not reduce effectively the dose due to the residual activation because the radiation shielding itself would be activated.

Therefore, we changed our policy to prepare a temporary shielding under the present configuration. Two 10-ton cranes were present in the accelerator tunnel, and we moved and installed the temporary shielding using those cranes. However, since the original base of the foil chamber could not withstand the weight of the temporary shielding, we needed to replace it with a new one. We designed a new base and temporary shielding that can be easily attached using a crane. The replacement work on the new base was carried out in the summer shutdown period of 2020. Since a large amount of radiation exposure was expected during this operation, a detailed work plan was prepared. The work plan sheet included a work process, working conditions, job descriptions, positions of the workers, and dose rate for each position. We evaluated the worker doses using these data and controlled the personnel doses so that they would not be concentrated on one person. Thanks to these preparations, the work was completed with the doses of all workers below the expected value. Pictures of the injection point before and after the installation of the shielding are shown in Fig. 2.

Finally, we investigated the effect of this new temporary shielding just after the user operation. Figure 3 shows the measurement results of the dose rate near the foil chamber. The result showed that the residual dose rate was significantly reduced by the shielding.

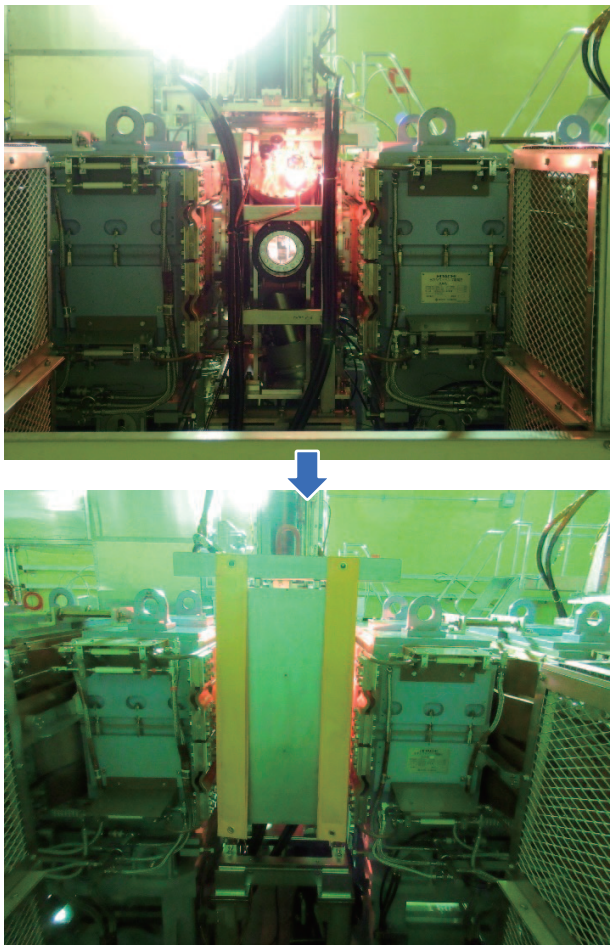

Fig. 2. Injection point of the RCS before (top) and after (bottom) installation of the temporary shielding.

1-MW demonstration

We attempted a two-day continuous user operation to the MLF with 1-MW beam power at the end of June 2020. During the 1-MW operation, two failures occurred at the capacitor and vacuum tube in the final stage amplifier of the RF cavity immediately after the 1-MW operation started. The recovery took approximately 12 h; thus, the 1-MW operation time was reduced to 36 h. We hypothesize that these failures were mainly caused by age-related deterioration, and the 1 MW beam power did not affect the deteriorations directly.

This 1-MW demonstration showed a serious issue that prevented a stable operation. We found that when the outside temperature increases, the supply

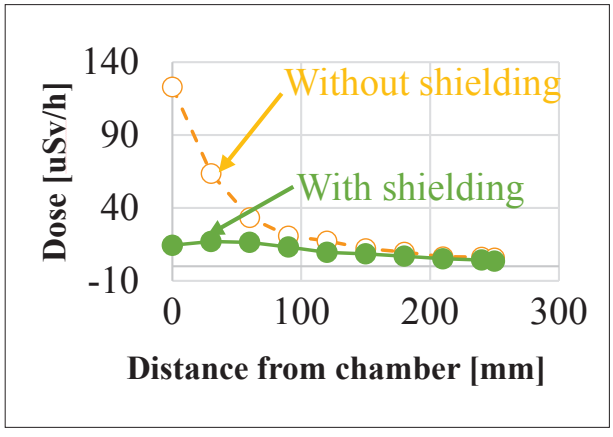

Fig. 3. Measured residual dose rate near the foil chamber.

temperature of the cooling water becomes uncontrollable and also increases. This induces the temperature interlock of the vacuum tube in the RF final stage amplifier. We need to improve the RF and/or the cooling water system to establish a stable 1-MW operation during summer.

After the1-MW user operation, we measured the residual dose values around the accelerator components and found that those were low enough to accept and the same as the results of the previous year. Considering the beam loss, it is still possible to deliver 1-MW beam power to users. Figure 4 shows the residual dose values in the RCS after the 600-kW and 1-MW operations. The dose values are almost proportional to the beam power.

Summary

RCS has almost achieved a continuous, stable user operation. In JFY2020, it delivers a 5.1e13 ppp (600 kW) beam to the MLF and 6.7e13 ppp (corresponding to a 515-kW beam of MR) beam to the MR. These values will be increased steadily with careful monitoring of the neutron target status and beam loss.

We attempted a 1-MW continuous operation at the end of June 2020. The 1-MW continuous operation revealed the problem of poor cooling water performance. To establish a stable 1-MW operation in all seasons, we have to consider improving the RF and the cooling water systems. We continue the study to establish a more stable condition.

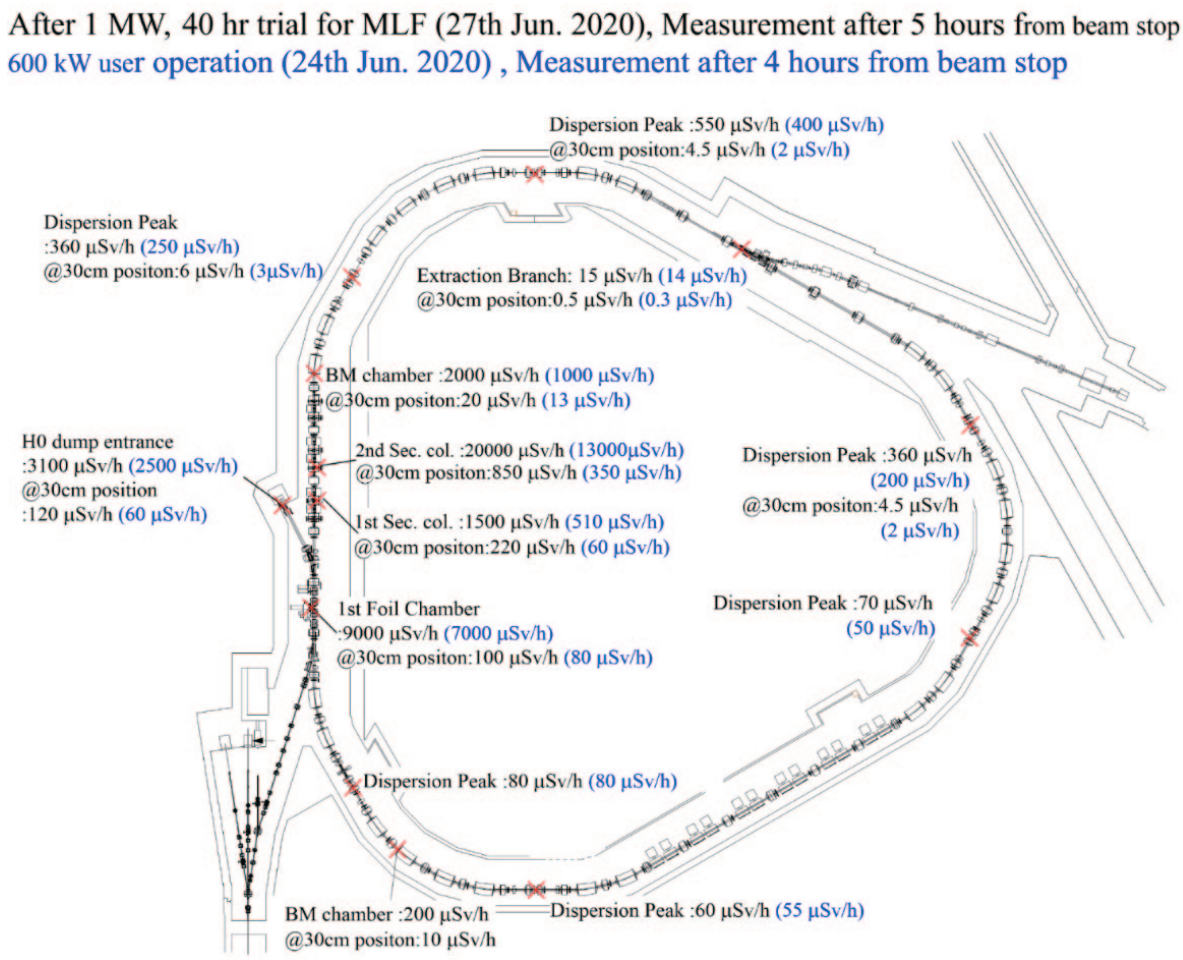

Fig. 4. Residual dose distribution in the RCS after 600-kW and 1-MW user operations.

MR

Overview

The Main Ring synchrotron (MR) is a high-power proton accelerator for experimental users of elementary-particle physics and nuclear physics. Proton beams of 3 GeV from RCS are injected in MR and accelerated to 30 GeV. The beams are delivered either to the hadron experimental hall with slow extraction (SX) mode or to the neutrino facility with fast extraction (FX) mode. For the SX operation the beam is extracted in about 2 s of debunched beam spill with the cycle of 5.2 s. The beam spill is delivered to the hadron experimental hall to produce various secondary particles for the experimental users. For the FX operation the beam is extracted in one turn with the cycle of 2.48 s. The beam is delivered to the neutrino facility for the T2K long baseline neutrino experiment.

Efforts have been made to increase the beam power for the SX mode. The main concern has been the beam instability, that has resulted in beam losses at the debunching process before the extraction. The beam power has been upgraded to 60 kW with suppression of the instability. For the FX mode, the beam power was 510 kW. Minimizing the beam losses and the localization are issues to be resolved.

Main magnet power supplies were constructed for the beam power upgrade. The test operation for the faster cycling was successful. Second harmonic RF cavities were installed during the summer shutdown. The FX septum magnet was tested for the faster cycling. Some of the upgrade works should be completed by the end of JFY2021 and the faster cycle operation of 1.32 s for FX is planned for JFY2022.

SX-mode operation

The beam power of the SX operation was 51 kW in JFY2019 because of the power limit of the hadron production target. Since the target was upgraded for the beam power of 95 kW, the MR operation was optimized for the higher beam power. The most serious issue was the transverse beam instability evoked by longitudinal microstructure during the debunching process that resulted in beam losses. It was mitigated with a RF phase offset at injection. The longitudinal beam emittance became large after dilution, and was effective for the instability suppression up to 51 kW. For a higher power beam, the instability was observed with only the phase offset injection and a further mitigation scheme was necessary. A new scheme of the RF voltage ramp down for debunch was discovered to be effective. The RF voltage was ramped down from the acceleration voltage of 256 kV to ~20 kV at the end of the acceleration, and after 80 ms it was ramped down to 0 kV for debunch. Longitudinal emittance became larger and the instability was significantly suppressed. The beam power of 60 kW was achieved for the user operation.

The beam availability for the hadron hall was 66.1% in JFY2020. Troubles occurred on the power supplies of the 3-50BT magnets, SX resonance sextupole magnets and SX septum magnets. They may have been caused by deterioration over time, because the components are 15 years old and some even older. The importance of maintenance to achieve better beam availability is recognized more and more. For instance, we found a damaged gate circuit board in the 3-50BT magnet power supply. Besides, the room temperature at the power supply is inappropriately high. The environment in the power supply buildings should be stabilized with an air-conditioner.

The circuit breaker was accidentally opened for the power supplies of the main quadrupole and sextupole magnets. The beam orbit then moved toward the SX electrostatic septum (ESS) unintentionally. This resulted in fatal damage to the ESS ribbons. We then had to reschedule the user operation to replace the ESS with a spare.

FX-mode operation

In March, just after the ESS ribbon failure, eleven days were assigned for the FX operation including the beam tuning. After the vacuum chamber baking with beam, the beam power of 510 kW was achieved for the

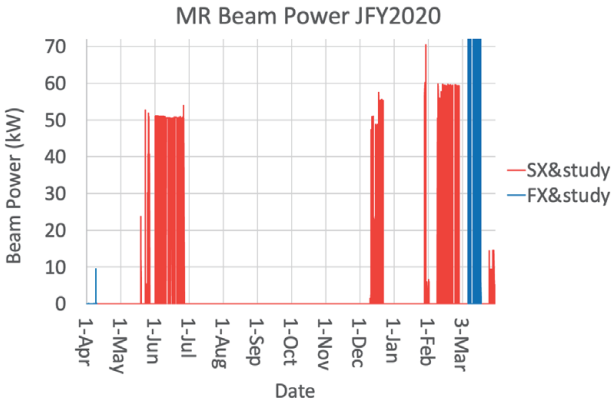

Fig. 1. MR beam power in JFY2020. The beam power of SX and study is shown in red and that of FX and study is shown in blue (out of scale).

FX operation, the same as the operation in JFY2019. The beam availability for the neutrino facility was 69.8% in JFY2020. A trouble occurred on the power supply of the injection septum 2 magnet. The photocoupler IC in the control board was found to be damaged. Because other parts of the power supply may not be reliable either, maintenance is again required for the stable operation.

Toward the 1.3-MW operation

The beam power of 500 kW was achieved with the cycle time of 2.48 s and accelerated protons of 2.6×10^{14} per pulse. The original beam power target is 750 kW with the cycle time of 1.32 s and 2.1×10^{14} protons per pulse (ppp). Even further beam power has been demanded from the neutrino user community for the discovery of CP violation and precise measurement of the mixing parameters in the lepton sector. A new target of 1.3 MW is planned with the cycle time of 1.16 s and 3.3×10^{14} ppp (Table 1).

Table 1. Beam Power Upgrade Concept.

	Beam Power	Cycle Time	Number of accelerated protons
Present	500 kW	2.48 s	2.6×10^{14} ppp
Original Design	750 kW	1.32 s	2.1×10^{14} ppp
New Plan	1.3 MW	1.16 s	3.3×10^{14} ppp

The new magnet power supplies have been constructed. All six power supplies for the bending magnets were completed by the end of JFY2020. The test operation of the 1.3 s cycle was successfully done. The production and installation of new magnet power supplies will be completed by JFY2021, and a test operation is planned for April and May of 2022.

Two second harmonic cavities were installed at insertion A during the summer shutdown (Fig. 3). The power amplifier will be installed in JFY2021. The present two second harmonic cavities will be converted to fundamental cavities. The total number of the fundamental cavities will then become nine, the accelerating voltage should be sufficient for the 1.32 s operation.

The injection and FX devices have been prepared for the faster cycling. For the injection kickers, design work is in progress for the cooling of the matching resistor box. Injection septum magnets and the power supplies were replaced and ready for the 1-Hz operation. For the FX kickers, a high voltage charger was upgraded and ready for the 1-Hz operation. New FX septum magnets are being tested. All these devices will be installed in JFY2021 and ready for the beam operation in JFY2022.

Two of additional collimators were constructed in JFY2020. They will be installed in JFY2021. Another collimator is planned to be constructed in JFY2021. The collimation system in the MR injection region must be upgraded for a capacity of 3.5 kW beam loss as compared to the present 2 kW.

Further upgrade is planned for the operation of 1.16 s. The number of RF cavities should be increased for the faster acceleration. The RF anode power supplies should be upgraded for the beam loading compensation of high-intensity beams. The upgrade is planned for JFY2025. Circuits of beam position monitors will be upgraded for high-intensity beams and more precise measurements by JFY2024. With the parameter tuning of the main magnet power supplies for the 1.16 s operation and the beam tuning for higher intensity, we plan to achieve the beam power of 1.3 MW in JFY2028.

Fig. 3. Second harmonic RF cavities installed at insertion A.

Materials and Life Science Experimental Facility

Overview

During the COVID-19 pandemic, a state of emergency was officially announced by the Government of Japan on April 14. J-PARC was forced to limit users visits for 47 days and imposed an unscheduled outage for 13 days in FY2020. The difficulties with the users visits affected seriously the user program of the MLF. Because domestic travel was limited and no user could visit the MLF from abroad for experiments, mail-in type experiments were performed with the dedicated support of the MLF staff. We tried to conduct as many experiments as possible in the 2020A period, however, many experiments were carried over to the 2020B period. Consequently, the available beam time to accept new proposals in the 2020B period decreased. 2020B and 2021A were called simultaneously.

Personnel exchange programs, such as AONSA Young Research Fellowship and SAKURA program with ESS, were postponed. Also, the annual meeting of industrial application at the MLF and the Neutron-Muon School were canceled. Meanwhile, Neutron Advisory Committee, Muon Advisory Committee, J-PARC International Advisory Committee, Quantum Beam Science Festa, which is an annual conference mainly for domestic users of MLF J-PARC and IMSS KEK, were held on-line.

The proton power ramp up on the neutron target and instrument upgrades were kept in progress under COVID-19. In fiscal year 2020, the beam operation started with beam power of 500 kW and the beam power was raised to 600 kW on May 18. At the end of the beam operation before the summer outage, high-power operation was maintained for 36.5 hours at 930 kW from June 25 to 27, much longer than the 10.5 hours achieved in 2019. The validity of the system design regarding a stable 1-MW operation was reconfirmed. A new detector module for a time-of-flight Laue

single-crystal diffractometer installed in BL18, SENJU, was developed based on scintillator and wavelength-shifting fiber technology. The thickness was reduced to 60% of the original detector. Constructions of the muon beam lines, H-line and S2 area, progressed. Automatic and remote experiment environments of neutron beam lines were implemented to realize efficient experiments under COVID-19.

The Efforts to make the user program successfully under COVID-19 conditions will be continued by discussions with users and sharing know-hows with international facilities.

Neutron Source Section

In fiscal year 2020, the neutron source section started the beam operation with beam power of 500 kW, but it was forced to stop it from April 20 to May 15 due to the coronavirus pandemic. After the beam operation was resumed, the beam power was raised to 600 kW on May 18 and the stable operation continued. This was the first achievement to operate over 500 kW for long term user program. At the end of the beam operation before the summer outage, high-power operation was maintained for 36.5 hours at 930 kW from June 25 to 27, much longer than the 10.5 hours achieved in 2019. This made it possible to obtain significant operation data, which normally would require long time to reach a stable value. Also, the validity of the system design with regard to the ultimate power goal was reconfirmed.

Another notable achievement was the successful operation of the new-type target vessel, target #11, in which the coupling-free structure between the inner mercury and the surrounding outer water shroud removes the structural cause of generating high thermal stress on the target. This was one of the major milestones to achieve stable and long term operation at 1 MW.

During the summer outage, replacement of the proton beam window was carried out after 3 years operation since the last replacement in 2017. Because the used proton beam window is a highly radioactive component irradiated within a relatively short period of time, in a situation similar to that of the used target vessel, it will be transported to RAM (Radio Activated Materials) building in near future.

There was also an important outcome in the pitting damage mitigation technology of the target vessel to achieve a stable 1-MW operation. Injection of micro-bubbles of helium gas into the mercury flow in the target vessel was used to reduce the intensity of the pressure waves which caused pitting damages. In addition to that, the narrow channel has been made by adding an inner wall at the forefront wall of the target vessel to mitigate the pitting damage by a steep velocity gradient of rapid mercury flow. Specimens were cut out from the forefront wall of target vessel #11 by hole-saw drilling machine. The bottom picture in Fig. 1 shows that the pitting damages on both the narrow channel side and the bulk side of the inner wall specimen are very small, even after the long run of the 600-kW operation. These results demonstrated the excellent effect of the present technology for pitting damage mitigation and are promising for further power ramp-up.

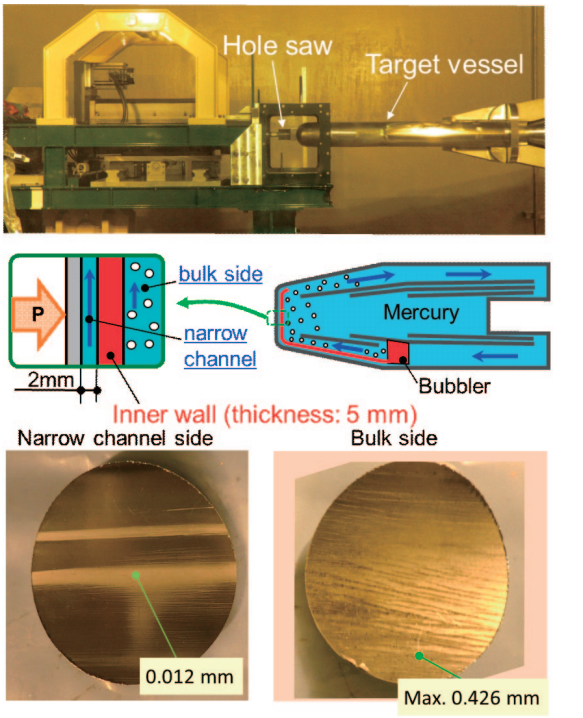

Fig. 1. Cutting machine (top) and structure of the target vessel (middle) and the surfaces of an inner wall specimen (bottom)

Target vessel #11 was replaced with a new target vessel but misalignment of the coolant pipe position led again to a target replacement with another spare target, which caused delay in the maintenance schedule. To prevent recurrence of this failure, the fabrication and inspection procedure for the target vessel was improved.

The beam operation for the user program started on December 1 after three weeks delay from the

original schedule. The neutron source continued its stable operation at 600 kW after the summer outage period and the average operational efficiency in fiscal year 2020 reached 91%.

Neutron Science Section

1. Renewal of Neutron Science Section

The Leader and Sub-Leaders of the Neutron Science Section were replaced in April 2020: Dr. Kenji Nakajima by Dr. Yukinobu Kawakita, Prof. Shinichi Itoh and Dr. Yukinobu Kawakita by Prof. Tetsuya Yokoo and Dr. Mitsutaka Nakamura, respectively.

2. Activities under the pandemic situation

In 2020, the COVID-19 pandemic situation became worse. A state of emergency was officially announced by the Government of Japan on April 14th, which caused the cancelation of the MLF beam operation from April 20th to May 14th. After the operation of the MLF resumed on May 15th, the accessibility was gradually extended from in-house use and mail-in experiments to all users access on June 19th. The experiments which could not be performed were carried over to 2020B term. To calm competition rate for new proposals, 2020B and 2021A were simultaneously called. Among 384 neutron general proposals, 200 were approved to be conducted by July 2021. The beamlines available for the Fast-Track Proposal (FTP) were timely added in the fall, so that 7 beamlines - BL08, BL11, BL16, BL17, BL18, BL21 and BL22, are available for FTP. The long-term proposal (LTP) was not called for the 2021 round, because all approved LTPs showed certain delay in the experimental plan and therefore a half-year elongation of the approved term was accepted. A new category, "one-year proposal", was introduced to BL11 PLANET aiming at promotion of research projects that include technology development in collaboration with the instrument group.

Under the pandemic, many user experiments were carried out by the instrument group, as shown in Fig. 1, instead of the users, because the latter were not able to come. For some of the beamlines popular among foreign researchers, this rate exceeded 50% of the conducted experiments. Developments of remote access and automation of the instruments have emerged as an urgent issue. The government also supported our activities by an additional budget (PRISM) of 55 million JY prompting collaboration among industry, government and academia.

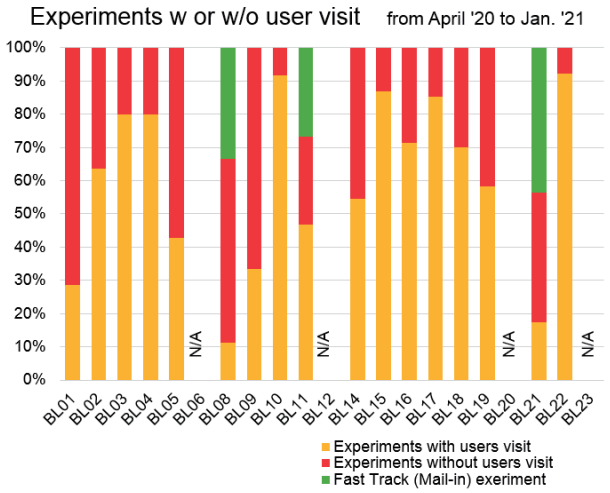

Fig. 1. Rate of the experiments with or without user visit among the conducted experiments.

3. Instrumentation kept up to date

The update of the new beamline instrument, POLANO (BL23) started as a part of the user program in 2019. POLANO is a polarization inelastic spectrometer, currently operating in an unpolarized-mode only for the user program. Unfortunately, all proposed experiments were canceled because of the COVID-19 issue. For the future polarization experiment, spin exchange optical pumping (SEOP) polarizer system, and several magnets for the guide field were almost ready to start commissioning. Vin Rose (BL06) is a neutron spin echo (NSE) spectrometer consisting of two different types of NSE instruments, namely, a modulated intensity by zero effort (MIEZE) type instrument and a neutron resonance spin echo (NRSE) type instrument. The user program was served by MIEZE with a 4-Kelvin GM cryostat and an electromagnet generating a field up to 0.6 Tesla.

4. Award

BL08 group (S. Torii, K. Oikawa, M. Hagihala, C. Kwanghee, T. Kamiyama) received the Technical Award by the 20th Annual Meeting of the Japanese Society for Neutron Science for the achievement of "Development of the World's Highest Resolution TOF Type Powder Neutron Diffractometer, SuperHRPD."

Neutron Device

The Neutron Instrumentation Section of the MLF Division has been engaged in the upgrade of the SENJU diffractometer. SENJU is a time-of-flight Laue single-crystal diffractometer installed in BL18 in the MLF. 37 detector modules have been in service since 2012 [1]. The recent upgrade includes additional new detector modules, which are placed in obliquely downward scattering direction to increase the total angle coverage. To fit in the tight space constraint, the thicknesses of the detector modules have been reduced to 60% of the original detector while maintaining the similar neutron-sensitive area and pixel size. The intensive development of the detector components led to the successful improvement of the count uniformities and efficiencies of the new detector.

Figure 1 shows a photograph of the prototype detector module. The detector is made on the basis of scintillator and wavelength-shifting fiber technology. Each detector module maintains a neutron-sensitive area of 256 × 256 mm with a pixel size of 4 × 4 mm. The ^{6}Li:ZnS scintillator screens purchased from SINTACOR with thicknesses of 0.25 and 0.45 mm are implemented for upstream and downstream of the WLS fibers, respectively. New discriminator electronics cards that have a 1.8-fold wider frequency bandwidth (~500 MHz) compared to the original ones [2] were developed and implemented to the detector as well. These new discriminator cards help the detector pick up weaker signals with 100 V less operational PMT voltage. Figure 2 shows the comparison of the count histograms when the detector is irradiated with neutrons uniformly over the detector face [3]. With the new cards the count uniformity improved to 4.3% from 6.0% of the original ones. As of the detection efficiency, the detector exceeded the original detector for neutron-wavelengths from 1 to 12 Å, which is 50-55% for the 2-Å neutron. The detector exhibited a ^{60}Co gamma-ray sensitivity of ~1 x 10^{-5} and background rate ~0.1 cps/hr, which are acceptable for use in the beam line. The specifications of the developed detector are shown in Table 1.

In summary, the new two-dimensional scintillation detector was developed for the new detector bank of SENJU. The produced four detector modules exhibited similar detector performances but had improved count uniformities and detection efficiencies compared to those in the original detector. These detectors have been implemented at obliquely downward scattering bank in the SENJU and have been in service since this year.

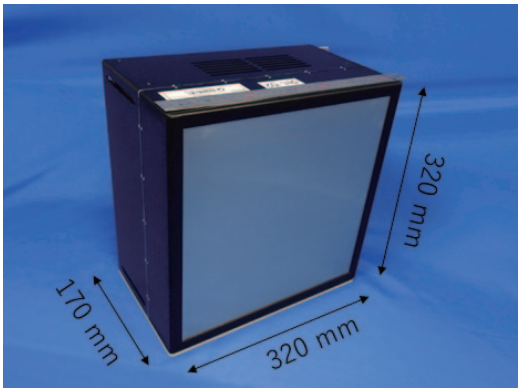

Fig. 1. A photograph of a prototype detector specifically designed for obliquely downward scattering bank of the SENJU.

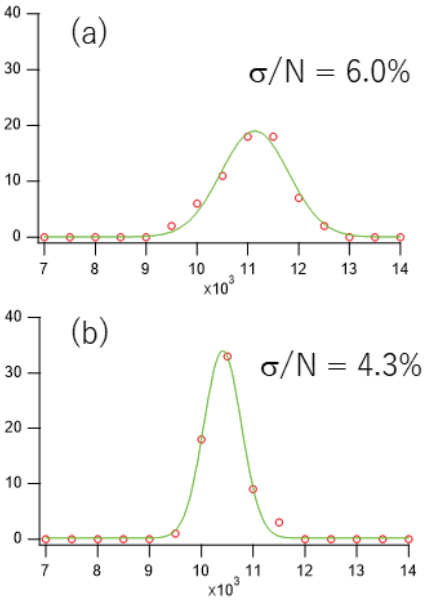

Fig. 2. Count histogram distribution for the x-projection data (a) with original discriminator cards, and (b) with new discriminator cards [3].

Table 1. Detector specifications

Pixel size	: 4 x 4 mm
Neutron-sensitive area	: 256 x 256 mm
Physical size	: 320 x 320 x 170[d] mm
Weight	: 16 kg
Detection efficiency	: 50-55% (@2 Å)
Gamma-ray sensitivity	: ~1 x 10^{-5} (^{60}Co)
Count uniformity	: 3-5%
Pulse pair resolution	: 5 μs

References

[1] T. Kawasaki, *et al*., Nucl. Instrum. & Meth. A 735 (2014) 444.

[2] T. Nakamura, *et al*., JPS Conf. Proc. 33 (2021) 011097.

[3] T. Nakamura, *et al*., 2020 IEEE NSS/MIC Conference Records, pp. 1-3, N20-215.

Muon Section

1. Development of real-time temperature monitoring system for the muon target

Real-time monitoring of the target temperature is extremely important to prevent severe accidents in the rotating target system. While thermocouples have been installed on the cooling jacket to measure the temperature rise due to thermal radiation from the rotating target, the slow response of thermocouples (typically in minutes) makes it difficult to detect a sudden temperature rise caused by some serious trouble, such as target rotation stoppage. For the real-time temperature detection, we have been developing a monitoring system based on the infrared (IR) camera.

Figure 1a shows the temperature distribution of the rotating target during the 1-MW operation observed by the IR camera. The high-temperature part (shown in yellow) can be observed flowing from the center of the target to the right (the direction of rotation). The measured temperature rise of the rotating target at the start of the beam operation is shown in Fig. 1b, where it takes about one hour using thermocouples to reach the actual temperature inferred from the IR camera.

The real-time sensitivity of the IR camera is also demonstrated by the temperature fluctuations associated with the fluctuations of the irradiated beam shown in Fig. 1b. The analysis regarding the relationship between the temperature change and thermal conductivity upon proton beam irradiation is in progress for the 1-MW operation.

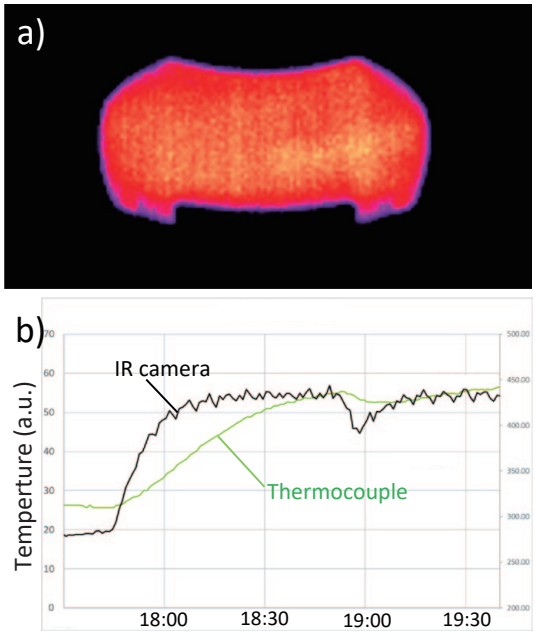

Fig. 1. a) An infrared (IR) camera image of the rotating target during 1-MW-beam operation. b) Temperature rise of the rotating target upon resump-tion of the beam operation. The temporary beam halt at around 18:50 is clearly identified by the target temperature monitored by the IR camera.

2. Construction of the H-Line

The H-line is a new beamline under construction since FY2012 in Experimental Hall #1 of the MLF building. Its layout drawing is shown in Fig. 2. It is a general-purpose beamline that can deliver both decay and surface muons and has branches to two experimental areas named H1 and H2. The designed surface muon flux reaches 10^8 muons/s with a proton beam power of 1 MW owing to a large acceptance (108 mSr) capture solenoid and other beamline magnets with large apertures.

In FY2020, the construction of the main (upstream) part of the H line and the first branch (to the H1 Area) progressed to secure the minimal components required to deliver muons to the H1 Area for beam commissioning. All vacuum devices were connected (see Fig. 2), electrical cabling and cooling water piping for two bending magnets (HB1 and HB2) were conducted, and a safety interlock system was implemented to be incorporated into the whole MLF system. Although the capture solenoid (HS1), transportation solenoids (HS2 and HS3), focusing quadrupole triplets, and a DC-separator are not ready, the surface muon flux is expected to be 6×10^5 muons/s without these components. In the next summer shutdown, we plan to conduct the remaining works such as electrical cabling and cooling water piping of all magnets and installation of a DC separator and beam slits to achieve the design intensity of 10^8 muons/s.

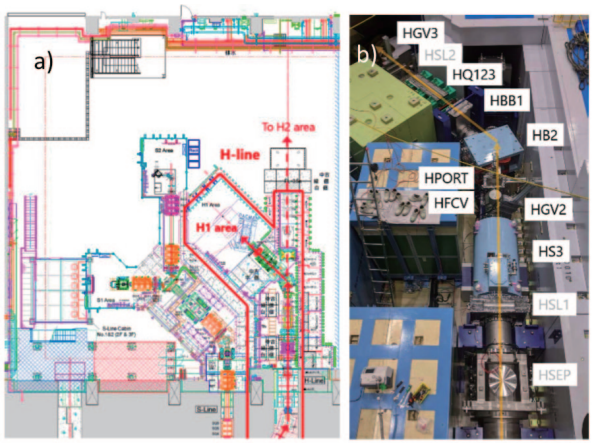

Fig. 2. a) A layout drawing of the H-line, and b) a snapshot showing vacuum devices for the beamline to the 1st branch, which were connected during the summer shutdown in FY2020.

Progress was also made in preparing the second branch of the H-line (to the H2 Area). Since the muon g-2/EDM experiment proposed for the H2 Area requires a 50-meter LINAC to accelerate muons to 212 MeV, the construction of an extension building is planned on the east side of the MLF where the parking lot is located. In FY2020, the detailed design of the extension building was completed, and geotechnical investigation and buried cultural property research were conducted on the construction site.

3. *Laser system for Ultra-slow muons*

Ultra-slow muons can be generated by resonant optical ionization of thermal muonium from hot-W foil target. Light pulses of 122.09 nm (Lyman-α) and 355 nm are required for the 1*s* to 2*p* state excitation and 2*p* to ionization, respectively. The high power pulsed coherent Lyman-α light source is one of the key elements for the efficient generation of ultra-slow muons.

In FY2020, more than 10 μJ Lyman-α pulses have been stably generated from 212.556 nm and 820 nm light pulses using the two-photon-resonant four-wave-mixing method attained by nonlinear wavelength conversions of a 100 mJ 1062.78 nm pulse delivered from Nd:YGAG (1 at.% Nd doped $Y_3Ga_2Al_3O_{15}$) ceramic laser amplifiers. Although we are targeting 1J-level 1062.78 nm pulses to achieve the required Lyman-α output power, the problem of Ga inhomogeneity in Nd:YGAG has prevented for years the realization of the large-aperture laser medium (>10 mm in diameter) for the amplifier required for this purpose.

To overcome this problem, we have been developing Nd:YSAG ceramic (Ga substituted with Sc), and a newly fabricated middle-size (ø9 mm, 112 mm long) Nd:YSAG ceramic was delivered for testing the amplification gain and wave-front distortion. While the amplification gain was satisfactory, distortion of the transmitted wavefront was exposed, which resulted in the reduction of the wavelength conversion efficiency in the subsequent stages due to the collapsed beam shape. In order to compensate for the distortion occurring inside the Nd:YSAG ceramic, we introduced an active 40-segment deformable mirror combined with the Shack-Hartmann wave-front sensor that was placed before and after the amplifier, respectively. The measured wavefront distortion is shown in Fig. 3, where the distortion is removed after the compensation. The method obtained by these studies will be applied to a practical laser system to implement the enhancement of Lyman-α optical intensity.

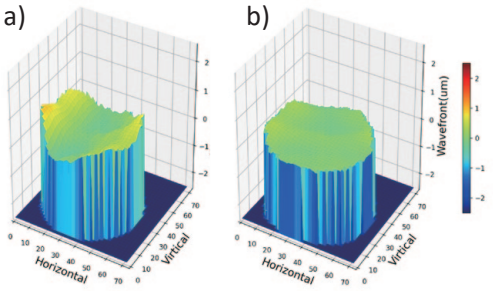

Fig. 3. The wavefront distortion in Nd:YSAG ceramic for final amplifier before (a) and after (b) after the compensation by a deformable mirror system.

4. Construction of the S2 Area

The S2 Area is under construction for the precise measurement of the muonium 1s-2s transition energy by the resonant laser ionization (S1-type proposal by Okayama U. group, supported by Kakenhi). To allow for the laser experiment and ensure safety, the entire area is shaded by walls and removable roofs. The muon beam interlock system is almost the same as that for the S1 Area. A laser hut has been installed next to the S2 Area for immediate access. The hut is made of a marine container, so that it can be easily moved by crane. The construction of the S2 Area has been nearly completed in the summer shutdown of FY2020. The rest of the work will be completed after the approval from the Nuclear Regulatory Commission to deliver the first beam in the early FY2021.

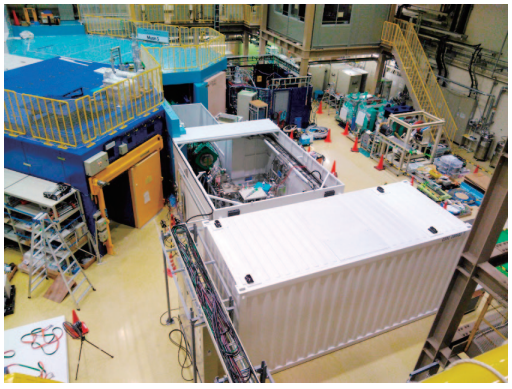

Fig. 4. A snapshot of the S2 Area (with roofs tempo-rally removed) and laser hut viewed from the down-stream of the S-line.

R. Kadono[1,2], K. Shimomura[1,2], A. Koda[1,2], P. Strasser[1,2], T. Yamazaki[1,2], S. Kanda[1,2], S. Takeshita[1,2], Y. Ikedo[1,2], Y. Kobayashi[1,2], J. Nakamura[1,2], T. Yuasa[1,2], N. Kawamura[1,2], Y. Oishi[1,2], Y. Nagatani[1,2], S. Mato-ba[1,2], S. Nishimura[1,2], S. K. Dey[1,2], W. Higemoto[2,3], and T. U. Ito[2,3]

[1]Institute of Materials Structure Science, KEK; [2]Muon Science Section, Materials and Life Science Division, J-PARC Center; [3]Advanced Science Research Center, JAEA

Technology Development Section

Neutron Bragg – edge transmission imaging

The time-of-flight neutron Bragg-edge transmission imaging, one of the advanced energy-resolved imaging techniques, can be used to directly visualize the two-dimensional distribution of crystallographic information and residual strain of bulk materials. We have developed this technique and applied it to various engineering materials at the MLF.

Applied to induction hardened gears at the MLF

Induction hardening, as an important heat treatment method, aiming for a hard martensitic microstructure in gear's teeth region, leads to significant improvement in the mechanical properties of the components. Residual stress and microstructure play an important role in forming the desired properties of gears. In the present study, we applied the Bragg-edge broadening analysis to gear products. Using this method, the residual strain and microstructural distribution of two types of induction-hardened gear products manufactured by Neturen Co., Ltd. were analyzed [1].

Figure 1 shows the Bragg-edge imaging experimental setup at BL22 RADEN [2]. Figure 2. shows a characteristic Bragg-edge transmission spectrum of the measured sample. The Bragg-edge position, d_{110}, and the Bragg-edge broadening, w_{110}, were obtained via single-edge fitting. Bragg-edge broadening was confirmed at a position in the gear's teeth region. This indicated the formation of a martensitic microstructure in the hardened zone due to induction heating.

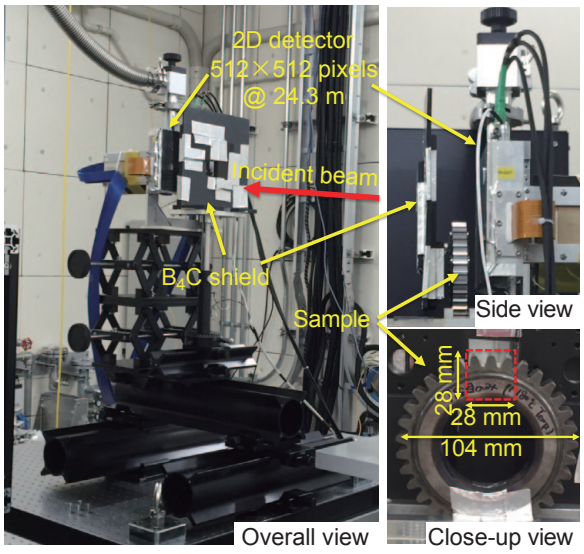

Fig. 1. Experimental setup at RADEN.

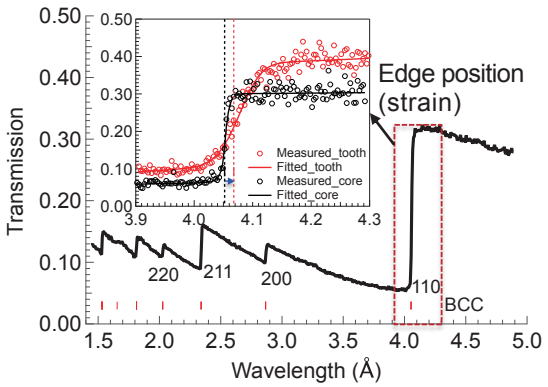

Fig. 2. An example of the Bragg-edge spectrum measured and BCC 110 edge fitting for edges from the core and the tooth region of a gear sample.

The obtained 2D maps for the elastic residual strain, ε_{110}, shown in Fig. 3, represent the first-ever maps made using the Bragg-edge imaging method. Compressive residual strains were generated in the martensite hardened zone of both gears, while the strain was almost zero in the core region. A steep compressive strain was introduced into the fine–grained martensite at the tooth surface of the finished product by the super rapid induction–heating process. The results were in accordance with those obtained using the XRD measurement.

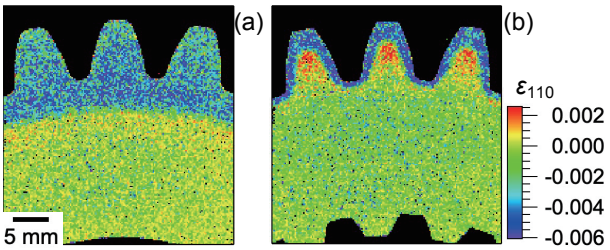

Fig. 3. 2D maps for residual strain of 110 lattice plane obtained via Bragg-edge imaging: (a) a precursor and (b) a finished product.

We have demonstrated that we can reveal microstructural features and residual strains in gears using the non-destructive Bragg-edge imaging. This technique would be applicable to other induction-hardened products or heat-treated machine parts.

References

[1] Y.H. Su *et al.*, Sci. Rep., **11** 4155 (2021).

[2] T.Shinohara *et al.*, Rev. Sci. Instrum. **91** 043302 (2020).

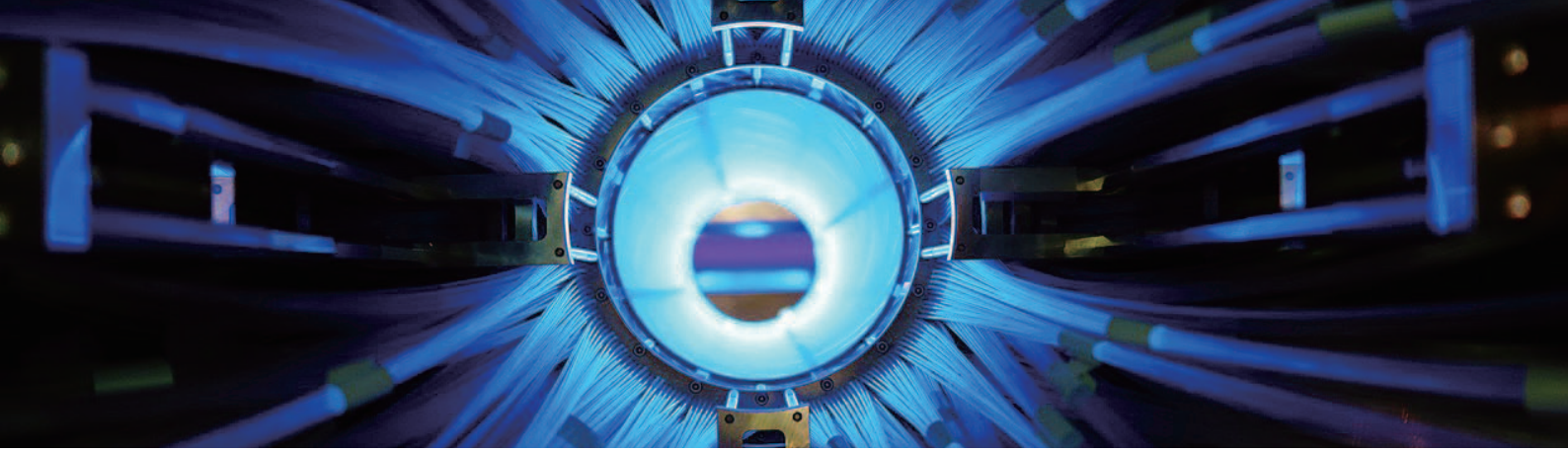

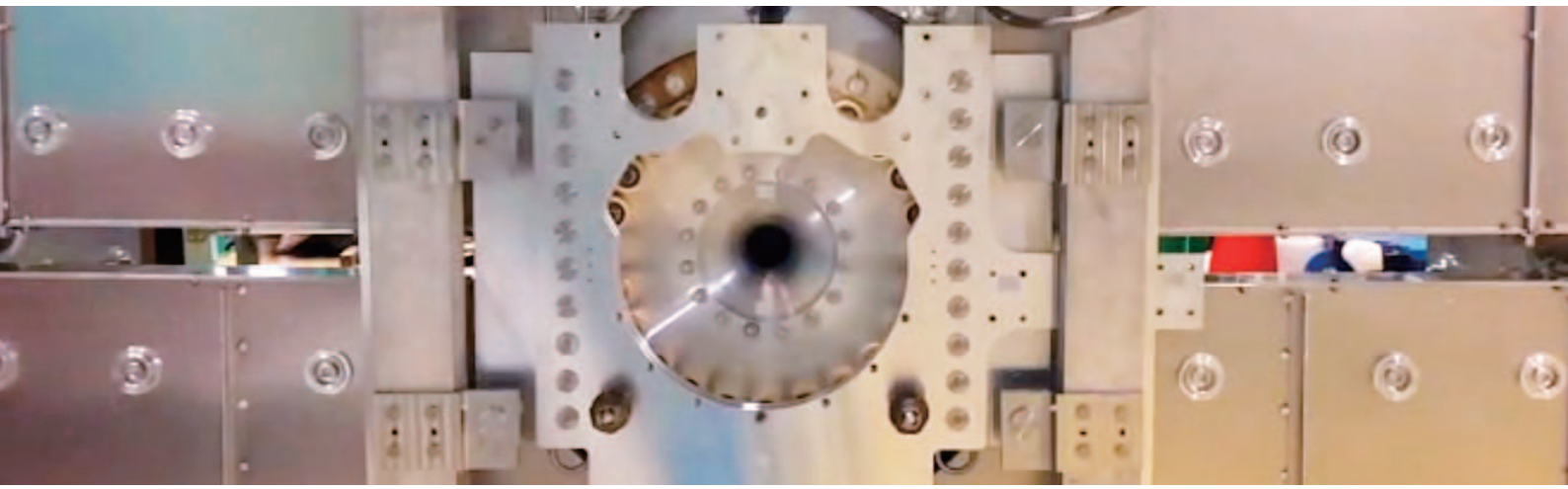

Particle and Nuclear Physics

Neutrino Experiment

After a one-year no-beam period, a T2K data acquisition was started in fiscal year 2020 in the neutrino mode on March 8, 2021. After vacuum chamber scrubbing and beam tuning, a stable operation of 510 kW beam power was successfully achieved. The accelerator operation continued until the end of April, with an interruption for hadron beam operation.

During this period, the T2K experiment was performed without the off-axis detector ND280 operation owing to COVID-19 travel restrictions. Three near detectors, Wagasci, BabyMIND, and on-axis INGRID, were operated by on-site experts and monitored remotely by collaborators overseas. The far-detector SuperKamiokande operated successfully for the first time with a beam after gadolinium was dissolved and demonstrated improved neutron detection capability. As of March 19th, since the beginning of the experiment, T2K accumulated 20.4×10^{20} POT in the neutrino mode, in addition to the 16.5×10^{20} POT accumulated in the anti-neutrino mode.

In April 2020, T2K published new analysis results regarding CP violation in Nature magazine. This imposed the world-first 3σ restriction on the CP phase, as shown in Fig. 1. This article was selected for the "10 remarkable discoveries from 2020."

A T2K extension, T2K-II, was proposed to further investigate the CP violation and perform a precise measurement of mixing parameters. It has been officially approved after recommendations from the J-PARC PAC. To improve the performance of on-site neutrino

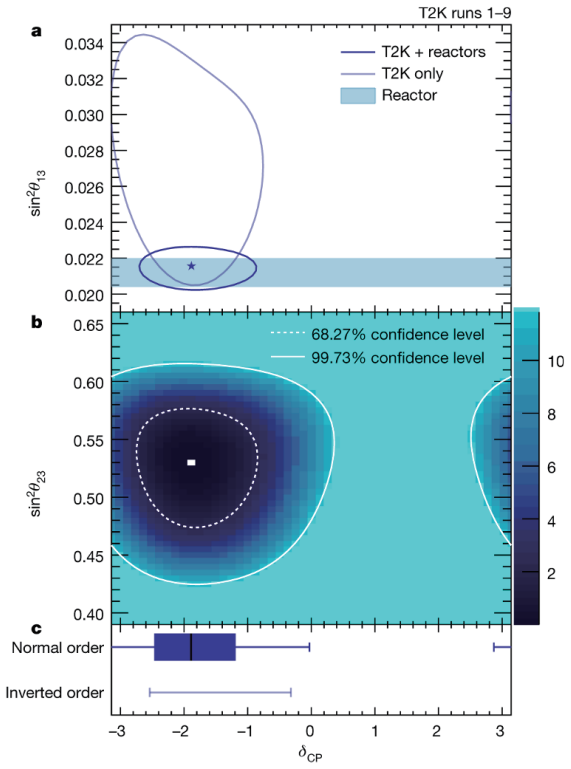

Fig. 1. Top: Two-dimensional confidence intervals at 68.3% confidence level for δ_{CP} vs. $\sin^2\theta_{13}$ in preferred normal mass ordering. Bottom: Two-dimensional confidence intervals at 68.3% and 99.7% confidence levels for δ_{CP} vs. $\sin^2\theta_{23}$ from T2K + reactors fit in normal mass ordering.

detector ND280 and to achieve a beam power beyond 1 MW, extensive efforts have been expended. The pre-assembling of two million scintillator cubes with supporting fibers was completed in one of the most important subdetectors of the ND upgrade program, i.e., the Super Fine Grain Detector (SuperFGD), as shown in the IPNS cover page. Also presented a schematic layout of cubes and wave-length-shifter fibers crossing in the x-,y-, and z-directions for a three-dimensional (3D) readout.

The E71 Ninja experiment is a precision study of neutrino–nucleus interactions with hybrid emulsion detectors. Their unique analysis procedure was provided in a press release on October 20th. The excellent spatial resolution of the emulsion combined with a novel timestamp mechanism enabled the reconstruction of neutrino interactions with unprecedented position precision. In March 2021, a pilot experiment with a heavy-water target was conducted.

The JSNS^2 experiment searches for sterile neutrinos with short baseline neutrino oscillations from $\overline{\nu}\mu$ to $\overline{\nu}e$ at the MLF. The experiment was commenced from January 2021, and data was acquired smoothly. Details regarding the JSNS^2 experiment are reported in the Research Highlights.

Hadron Experimental Facility

The Hadron Experimental Facility of J-PARC was developed for fixed-target particle and nuclear physics experiments. In FY2020, a primary proton beam can be used at a new beamline (B-line) in addition to the secondary hadron beams produced at the production target (A-line) based on a slowly extracted 30-GeV proton beam from the Main Ring accelerator. A small amount of the beam to the A-line was separated using a Lambertson magnet and delivered to the B-line experimental area.

Commissioning for the B-line was commenced and a new production target that can receive a 95 kW primary beam at the A-line was set on May 23rd. The first beam to the B-line was extracted on May 24th (Fig. 2). Beams were delivered to users until June 26th.

The second beam operation from December 14th was interrupted several times owing to several problems but was completed on April 7, 2021. During this time, 60 kW of beam power to the A-line was achieved. Several beam tunings of the B-line were performed, and the beam qualities such as beam stability and intensity fluctuation during extraction were improved.

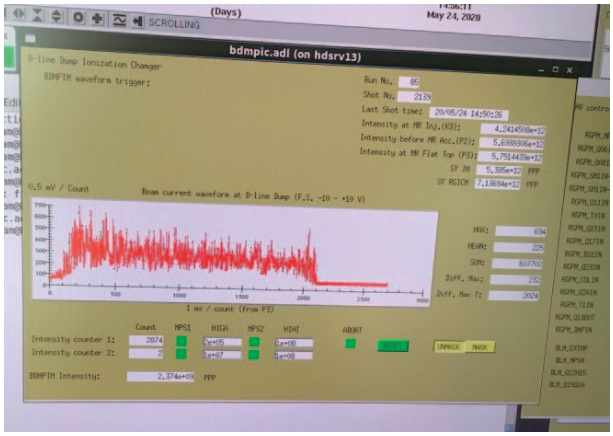

Fig. 2. The first shot to B-line measured with Ion Chamber (IC) at a beam-dump. Horizontal is time in millisecond while vertical is IC counts.

Strangeness/Hadron Physics Experiments

In the E40 experiment at the K1.8 beamline, which is a Σ hyperon-proton (*p*) scattering experiment, data acquisition of the Σ^+p scattering data was completed from May to June 2020. From the middle of December after the detector rearrangement at the K1.8 beamline, the E03 experiment was performed to observe Ξ-atomic X-rays for the first time and to obtain information regarding the Ξ-nucleus potential from the level shift and width.

At the K1.8BR beamline, pilot data were collected in June for the hyper-triton ($^3_\Lambda$H) lifetime measurement (E73), using a liquid ^{4}He target instead of ^{3}He to verify the methodology. The production and weak decay of $^4_\Lambda$H were identified.

Detector commissioning was performed and Run-0 data were acquired by the E16 experiment such that the primary proton beam at the B-line can be used. The aim of this experiment was to investigate the invariant-mass spectrum of di-electron pairs in the φ-meson region in proton– nucleus collisions.

Several results from the experiments were published in FY2020. The E15 experiment observed K^-pp-bound system and its binding energy and decay width were reported to be B_K = 42±3(stat.) $^{+3}_{-4}$(syst.) MeV and Γ_K = 100±7(stat.) $^{+19}_{-9}$(syst.) MeV, respectively. In the K^- + ^{11}B system, an event excess was observed in the deeply bound region of the missing-mass spectrum measured in E05. The corresponding binding energy was higher than that of the K^-pp system above. In the emulsion experiment, E07, several events of Ξ-hypernuclei (Ξ^-+^{14}N system) were observed.

Kaon Decay Experiment

The KOTO experiment was designed to investigate the decay of a long-lived neutral kaon into a neutral π meson (π^0) and a pair of neutrinos. It breaks the CP symmetry directly, and its branching fraction is theoretically well predicted in the SM as $(3.0 \pm 0.3) \times 10^{-11}$. The detection of this decay is challenging because only two photons from π^0 are observable, and the decay mode has not been observed. By examining this ultra-rare decay, a new source of CP symmetry breaking that can explain the matter-antimatter asymmetry in the universe may be revealed.

In FY2020, the results from data accumulated in 2016–2018 from the KOTO experiment were published. With a single event sensitivity of 7.2×10^{-10}, three events satisfied all the selection criteria, whereas the expected number of backgrounds was evaluated to be 1.22, which is statistically consistent with the observation. KOTO set the upper limit for the branching fraction of $K_L \to \pi^0\nu\nu$ in this dataset to 4.9×10^{-9} at the 90% confidence level. To reduce the newly found background due to the contamination of charged kaons in the neutral beam, a new detector, named the Upstream Charged Veto (UCV), was installed at the entrance of the KOTO detector in December. The activities performed are described comprehensively in Research Highlights of this report. Data acquisition using the UCV is being continued in the KOTO experiment to achieve better sensitivity.

Muon Experiments

COMET aims to identify muon-to-electron conversion with a sensitivity higher than 10^{-14}. Intensive research and development were conducted in 2020. A cylindrical drift chamber was successfully tested using cosmic-ray muons with a full setup of readout electronics and a remote control system. The construction of a straw tube tracker and the mass production of lutetium yttrium orthosilicate (LYSO) crystals for the electron calorimeter is currently in progress. The construction of a capture solenoid (CS), which is used to acquire and transport pions/muons produced by the COMET primary proton target, as well as the preparation of a cryogenic system, is in progress. The assembly of superconducting coils was completed in 2020. A cryostat to contain and cool coil assemblies down to the liquid helium temperature will be constructed in 2021, followed by coil installation

into the cryostat in 2022.

The E34 collaboration is preparing for precision measurements of the anomalous magnet moment (g-2) and electric dipole moment (EDM) of muons. The collaboration continued the development of the room-temperature muon source, linear accelerators, beam injection beamline, storage magnet, and positron detector. Preparation was performed for facility construction, such as grounding surveys, geotechnical surveys, and surveys of buried cultural properties at the construction site. Important achievements in the development of a muon source and a frontend ASIC for the silicon strip detector, which will be described in a later section (Fig. 3), have been published as technical papers.

Theory group

The mission of the theory group at the J-PARC branch is to investigate the theoretical aspects of particle and nuclear physics in collaboration with the experimental groups. The group consists of four IPNS staff members and five visiting researchers.

Owing to the COVID-19 pandemic, the activities of the theory group were mainly conducted online. Seminar series on J-PARC heavy-ion project, and two internal online workshops on "Physics of heavy-quark and exotic hadrons 2021" and "Beta decay, r-process, and related weak-interaction processes" were organized by the group members. More than ten research papers were published in 2020.

Technical Support Groups

The electronic system group constructs electronic systems through a framework known as "Open-It." Regarding the J-PARC experiments, the mass production of a 128 channel silicon strip readout application-specific integrated circuit was completed for the g-2/ EDM experiment (Fig. 3).

The predominant activities of the mechanical engineering group are collaborative investigations during various experiments, including T2K and COMET. The conceptual design for the COMET radiation shield has been completed.

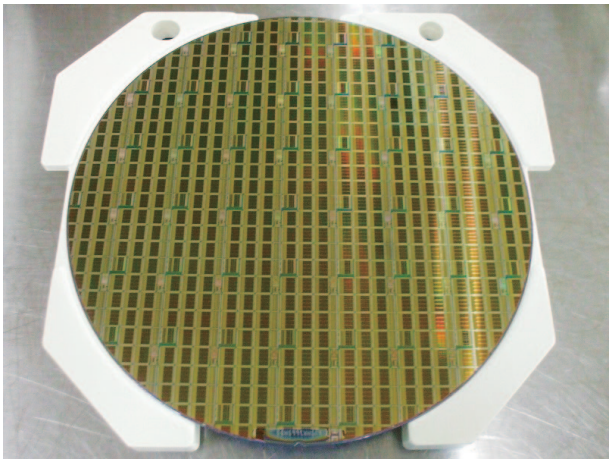

Fig. 3. Photograph of front-end ASICs for silicon-strip sensors in the g-2/ EDM experiment.

— Research Highlight —
The JSNS^2 experiment gets started!!

J-PARC Sterile Neutrino Search at J-PARC Spallation Neutron Source (JSNS^2) [1, 2] started data taking from January 2021. This article introduces the motivation, history and status of the JSNS^2.

JSNS^2 aims to search for sterile neutrinos, which are new particles that exist beyond the standard model of elementary particle physics. They had no weak interactions and felt only gravity. To explain the sterile neutrino, the simplest model is to introduce right-handed neutrinos in each generation. They were initially indicated by the Liquid Scintillator Neutrino Detector (LSND) experiment [3] in the 1990s, and several experiments have since been conducted to confirm or refute the existence of sterile neutrinos. Some claim positive results, while others show negative results. Please refer to the citation [4] for the experiments in the review. In this situation, the JSNS^2 experiment started data taking to confirm or refute their existence as a direct and ultimate test of the LSND.

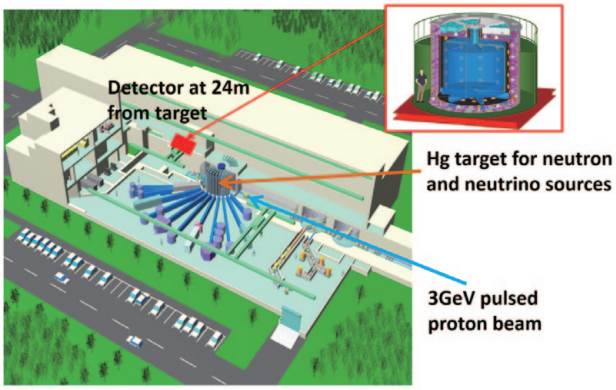

Fig. 1. Setup of the JSNS2 experiment.

Figure 1 shows the setup of the JSNS^2. We locate and move the detector every year twice, thus, seventeen tons fiducial volume of a (Gd-loaded liquid scintillator detector (50 tons in total) is placed on the third floor of the Materials and Life Science Experimental Facility (MLF) building.The mercury target of MLF produces a number of neutrons in the collisions of the three GeV short pulsed protons accelerated by the rapid-cycle synchrotron (RCS) of J-PARC to study the material and life sciences; however, many neutrinos are simultaneously produced. JSNS^2 uses the anti-muon-neutrinos produced by the decay-at-rest of the muons. Because the parent particles of neutrinos have zero momentum during production, neutrinos produced by the decay-at-rest have a well-known energy. The short pulsed three GeV proton beam can easily separate the background.

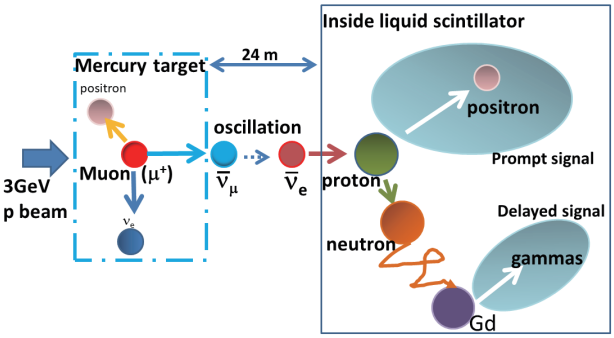

Fig. 2. The principle of the anti-neutrino production at the target and detection at the scintillator detector.

Figure 2 shows the experimental principle, particularly for neutrino production and detection. At the mercury target, the anti-muon-neutrinos are produced in collisions with three GeV protons through the muon decay-at-rest. After the production of anti-muon-neutrinos, neutrino oscillation between anti-muon-neutrinos and anti-electron-neutrinos occurred at 24 m through sterile neutrinos. The liquid scintillator detector is extremely effective in detecting anti-electron-neutrinos because they create inverse-beta-decay (IBD) signals ($\bar{\nu}_e + p \rightarrow e^+ + n$). The IBD signal produces two sequential signals from e^+ and neutron-Gd captured signals inside the liquid scintillator; therefore, the accidental background is significantly reduced by requiring the two signals for analysis.

JSNS^2 experiment was proposed in 2013 for the J-PARC. The final approval to start the experiment from the J-PARC was granted in November 2018. The construction of the detector began in 2017 and was completed in February 2020. Figure 3 shows the pictures of the detector. 10-inch photomultiplier tubes (PMTs), acrylic tank, and veto layer were used to observe the particles coming from outside the detector. The Gd-loaded liquid scintillator (Gd-LS) is filled inside the acrylic tank, while the Gd unloaded liquid scintillator (LS) is filled between the acrylic and stainless tanks. The IBD reaction is created in Gd-LS, as explained. The optical separator made of black boards that separates

the inner volume that detects IBDs and the veto region, which identifies the charged particles coming from outside, is as shown in Fig. 3. Approximately 20,000 L of Gd-LS was donated by the Daya-Bay experiment [5], and more than 80% of PMTs were donated by RENO and Double-Chooz experiments [6, 7]. Many electronics, such as flash ADC or front-end electronics (amplification circuit), were also donated by Double-Chooz. We express warm thanks to these experiments.

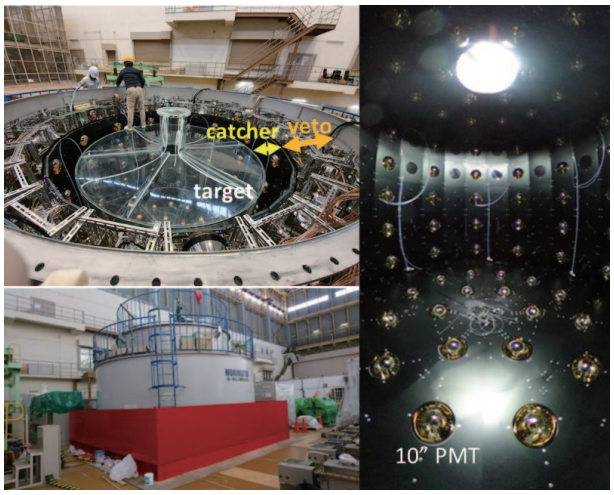

Fig. 3. (top-left): Overall detector structure inside the detector including acrylic tank. (right): 96 10-inch PMTs to see the scintillation light from the IBD. (bottom-left): the detector view from the outside.

The commissioning run was held in June 2020, and the first long physics run started from January 2021. During the first physics run, the beam power of the MLF was 600 kW until April 5, and approximately 700 kW after April 5. The beam power approaches the design value of 1.0 MW.

Figure 4 shows the activities around the beam timing. Several neutrons induced by the beam are observed in the beam timing; however, this background can be reduced using the timing of the production time of the anti-muon-neutrinos owing to the long lifetime of the muons decay-at-rest (2.2 μs). This indicates that effective search can be conducted for sterile neutrinos using timing information. With a beam power of one MW for three years, it will be concluded that most of the region can be indicated by LSND.

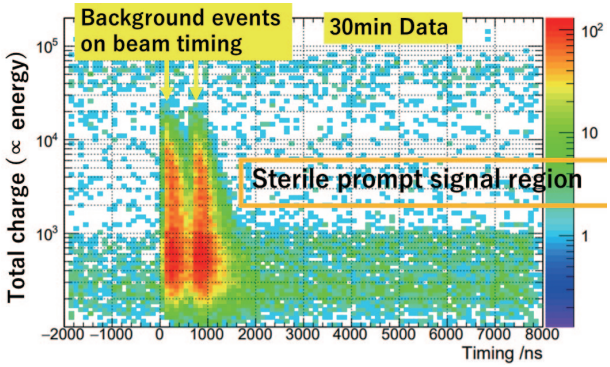

Fig. 4. Data around the proton beam timing. The activities (most of them are neutrons created by beam) are seen in the beam timing, while the IBD sterile neutrino search region (the orange rectangle) is dominated by cosmic ray induced background, which will be removed by the veto information and IBD selection criteria.

Recently, we proposed the second phase of the experiment, JSNS^2-II [8]. This experiment uses 35 tons of Gd-LS as a neutrino target with a baseline of 48 m; therefore, the low Δm^2 region of neutrino oscillation parameters, which is a stronger indication region by the global fit [4], and the weak points of the current JSNS^2 can be searched. We conclude the LSND anomaly in the near future.

References

[1] M. Harada *et al.*, arXiv:1310.1437 (2013).

[2] S. Ajimura *et al.*, arXiv:1705.08629 (2017).

[3] A. Aguilar *et al.*, Phys Rev D**64**, 112007 (2001).

[4] M. Dentler *et al.*, JHEP **08**, 010 (2018).

[5] M. Yeh *et al.*, Nucl. Inst. And Meth. A**584**, 238 (2008).

[6] J.K. Ahn *et al.*, Phys.Rev.Lett. **108**, 191802 (2012).

[7] Y. Abe *et al.*, Phys. Rev. Lett. **108**, 131801 (2012).

[8] S. Ajimura *et al.*, arXiv:2012.10807 [hep-ex].

— Research Highlight —
First determination of the binding energy of the Ξ hyperon in the Ξ hypernucleus

Elucidation of the nuclear force (strong interaction) that acts on nucleons (*N*s) and forms nuclei is one of major topics in fundamental physics. One trial is to extend the nucleons consisting of up (*u*) and down (*d*) quarks to the octet baryons, including Λ(*uds*), Σ^+(*uus*), Σ^0(*uds*), Σ^-(*dds*), Ξ^0(*uss*), and Ξ^-(*dss*) hyperons, by adding strange (*s*) quarks and to understand the interaction between octet baryons in a unified manner. Because of the difficulty of hyperon scattering experiments, the interaction of hyperons is obtained mainly from data on hypernuclei made of both hyperons and nucleons. In contrast to a relatively large amount of information on the strangeness of –1 (S = –1) Λ hypernuclei, data on the S = –2 system remain scarce. Double Λ hypernuclei have presented a good method for studying ΛΛ interaction, and the obtained binding energy of ${}^{\ 6}_{\Lambda\Lambda}$He has revealed that the ΛΛ interaction is weakly attractive [1]. Recently, the $\Xi^- p$ interaction was studied by ALICE experiment [2], in which attractive interaction was suggested based on a two-body correlation.

In line with Λ hypernuclei, the study of Ξ hypernuclei can provide meaningful information on Ξ*N* interactions. In the missing-mass spectra of the ^{12}C(K^-, K^+) reaction, no peak structure has been observed because of the insufficient energy resolution at KEK [3] and Brookhaven National Laboratory (BNL) [4]. However, the potential depth of 14 MeV has been deduced by assuming a Woods–Saxon type potential [4]. For the event named "KISO" identified in the emulsion experiment of KEK E373, its formation and decay were uniquely identified as $\Xi^- + {}^{14}\mathrm{N} \rightarrow {}^{10}_{\Lambda}\mathrm{Be} + {}^{5}_{\Lambda}\mathrm{He}$ [5]. Binding energy of Ξ^- (B_{Ξ^-}) of the formed state was obtained as 3.87 ± 0.21 MeV or 1.03 ± 0.18 MeV depending on whether ${}^{10}_{\Lambda}$Be was in the ground or excited state. In either case, the obtained B_{Ξ^-} of the $\Xi^- + {}^{14}$N system is deeper than that of the atomic 3*D* orbit of 0.17 MeV, and the observed system is a Ξ hypernucleus in which the Ξ hyperon is bound mainly by strong interaction. It turns out that the Ξ-nucleus potential and underlying Ξ*N* interaction are attractive. To determine B_{Ξ^-} uniquely and obtain the Ξ*N* interaction quantitatively, more events must be observed.

J-PARC E07 is an emulsion-counter hybrid experiment that aims to identify and observe approximately 10 times the number of events on S = –2 hypernuclei as those in KEK E373 using a high-intensity and high-purity K^- beam at the K1.8 beamline of the J-PARC Hadron Experimental Facility. In 2016 and 2017, 118 emulsion modules were exposed to Ξ^- hyperons produced by the (K^-, K^+) reaction on a diamond target located upstream of the emulsion module. Through the measured position and direction information of Ξ^- identified with the spectrometer system, the tracks of Ξ^- were automatically traced to the stopping point in the emulsion, and S = –2 hypernuclei were searched for using microscope systems.

Figure 1 depicts a remarkable event of the twin-Λ hypernuclear topology found in [6]. This event, named "IBUKI," was also uniquely identified as $\Xi^- + {}^{14}\mathrm{N} \rightarrow {}^{10}_{\Lambda}\mathrm{Be} + {}^{5}_{\Lambda}\mathrm{He}$, where a Ξ^- hyperon was captured by ^{14}N to form a bound system and decayed into ${}^{10}_{\Lambda}$Be and ${}^{5}_{\Lambda}$He through the $\Xi^- p \rightarrow \Lambda\Lambda$ conversion process. The B_{Ξ^-} was uniquely determined to be 1.27 ± 0.21 MeV because no possibility existed of the excited daughter Λ hypernuclei. The obtained 1.27 MeV is deeper than B_{Ξ^-} of the atomic *3D* orbit. In the case of Coulomb force only, the B_{Ξ^-} of the atomic *2P* orbit is calculated to be 0.39 MeV. The difference from the measured value is due to an additional force, namely, an attractive strong interaction between a Ξ^- and a

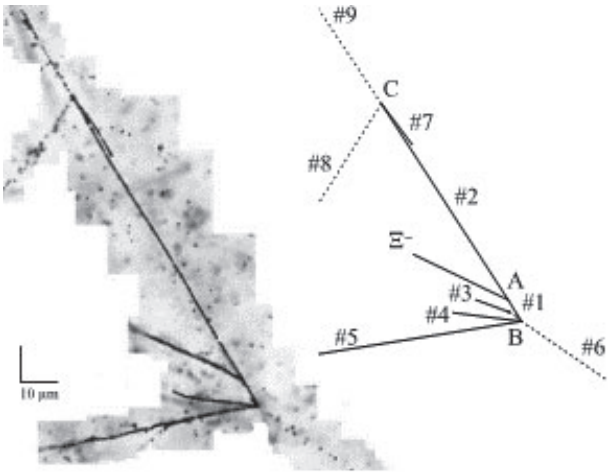

Fig. 1. Superimposed image and its schematic of the IBUKI event. A Ξ^- was captured by ^{14}N and decayed into a ${}^{10}_{\Lambda}$Be (#1) and a ${}^{5}_{\Lambda}$He (#2) at point A. The ${}^{10}_{\Lambda}$Be decayed into several nuclei (#3–6) and several neutrons (there were no recorded tracks because of no charge of neutron) at point B. The ${}^{5}_{\Lambda}$He decayed into a ^{4}He (#7), π^- (#8), and proton (#9) at point C.

nucleus. This is the first precise determination of B_{Ξ} of the Ξ hypernucleus, which provides us the strength of the Ξ-nucleus potential and the underlying Ξ*N* interaction. If the $\Xi^- p \to \Lambda\Lambda$ conversion is strong, the system decays before the Ξ^- reaches the nucleus and forms a Ξ hypernucleus. The present result indicates that the conversion is weak.

Most recently, a more deeply bound Ξ hypernuclear state was observed [7]. The event, named "IRRAWADDY," was identified as $\Xi^- + {}^{14}\mathrm{N} \to {}^{5}_{\Lambda}\mathrm{He} + {}^{5}_{\Lambda}\mathrm{He} + {}^{4}\mathrm{He} + n$ with $B_{\Xi^-} = 6.27 \pm 0.27$ MeV. Figure 2 shows the B_{Ξ^-} values of the $\Xi^- + {}^{14}\mathrm{N}$ system obtained from the emulsion events. For the "KINKA" event observed in KEK E373, the B_{Ξ^-} value was recently determined to be 8.00 ± 0.77 or 4.96 ± 0.77 MeV by reanalysis. With these events, the level structure of the $\Xi^- + {}^{14}\mathrm{N}$ system has become clear. A probable interpretation is that IBUKI and KISO (1.03 MeV) are states in which the Ξ^- is in nuclear *1p* orbit, whereas IRRAWADDY and KINKA are states in which the Ξ^- is in nuclear *1s* orbit.

Hyperons may stably exist in high-density matter such as the core of neutron stars, which are often described as giant nuclei. Which hyperons appear and at which density this happens depend in the interaction between the various baryons. The present results on Ξ*N* and $\Xi N \to \Lambda\Lambda$ interactions give us new insight into the origin of nuclei, namely, matter in the universe, as well as the structures of neutron stars.

Analysis of E07 emulsion is in progress. With the newly developed overall scanning method, which does not require counter information, 10 times the number of events as those under the present hybrid scanning method are expected to be detected. Then, S = –2 baryon interaction will become more apparent.

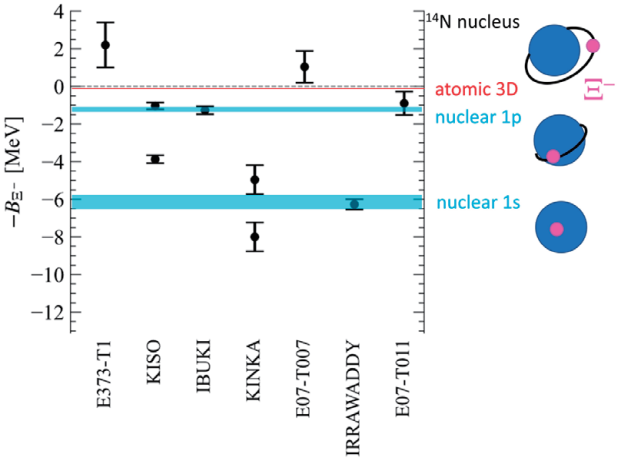

Fig. 2. Binding energies of Ξ^- in the $\Xi^- + {}^{14}\mathrm{N}$ system derived from the emulsion experiments at KEK E373 and J-PARC E07 [7]. For the atomic *3D* state, a Ξ^- is located far from the nuclear surface where the strong interaction does not work with the orbital angular momentum l = 2. However, a Ξ^- is located near the nuclear surface or inside the nucleus where strong interaction works with l = 1 or 0 for nuclear *1p* or *1s* states, respectively.

References

[1] H. Takahashi *et al.*, Phys. Rev. Lett. **87**, 212502 (2001); J.K. Ahn *et al.*, Phys. Rev. C **88**, 014003 (2013).

[2] S. Acharya *et al.*, Phys Rev. Lett. **123**, 112002 (2019); ALICE Collaboration, Nature **588**, 232 (2020).

[3] T. Fukuda *et al.*, Phys. Rev. C **58**, 1306 (1998).

[4] P. Khaustov *et al.*, Phys. Rev. C **61**, 054603 (2000).

[5] K. Nakazawa *et al.*, Prog. Theor. Exp. Phys. **2015**, 033D02 (2015); E. Hiyama and K. Nakazawa, Annu. Rev. Nucl. Part. Sci. **68**: 131 (2018).

[6] S.H. Hayakawa *et al.*, Phys. Rev. Lett. **128**, 062051 (2021)

[7] M. Yoshimoto *et al.*, Prog. Theor. Exp. Phys. 2021, 073D02 (2021)

— Research Highlight —
Updated results from KOTO

The $K_L \to \pi^0 \nu\bar{\nu}$ decay, in which a neutral kaon (K_L) decays into a neutral pion (π^0) and a neutrino-antineutrino pair ($\nu\bar{\nu}$), could potentially provide a clue to the new physics beyond the standard model (SM). In the SM, its branching ratio has been calculated to be as low as 3×10^{-11}, which implies that the effect of new physics on the decay could overwhelm that of the SM. Owing to the exceptionally small uncertainty in theoretical calculations, any observed deviation from the prediction is directly related to the existence of new physics.

The KOTO (standing for "K0 at Tokai") is a dedicated experiment to search for the $K_L \to \pi^0 \nu\bar{\nu}$ decay at the Hadron Experimental Facility of the Japan Proton Accelerator Research Complex. This international collaboration consists of 60 individuals from Japan, Korea, Russia, Taiwan, and the USA. The experiment began collecting data in 2013, and has continues to do so. The first dataset obtained in 2013 showed that the experimental method and all detector components worked properly [1]. With the second dataset obtained in 2015, the world's highest sensitivity was improved by one order of magnitude [2]. Analysis of the third dataset collected from 2016 to 2018 was completed in 2020; the published results are described in this article [3].

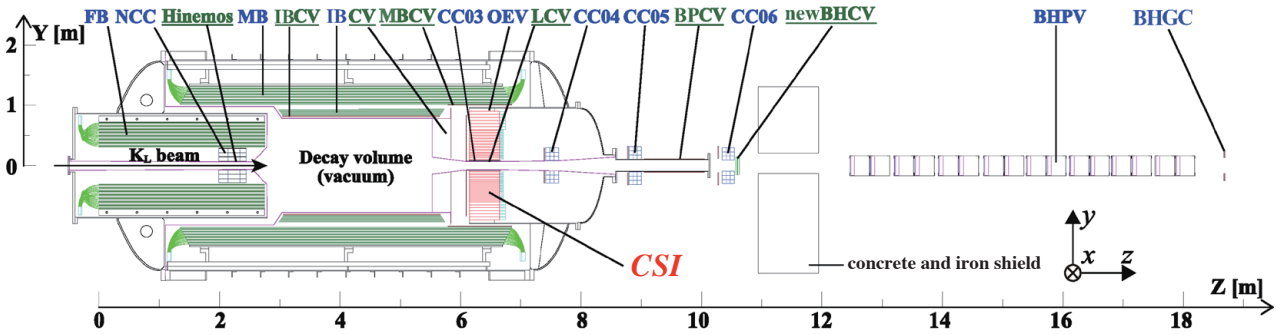

Fig. 1. Cross-sectional view of the KOTO detector.

Figure 1 shows a cross-sectional view of the detector. The energy and timing of two photons are measured in the electromagnetic calorimeter (labeled as CsI) made of 2716 undoped cesium iodide crystals. The decay position and momentum of the π^0 are reconstructed from them. Various types of veto counters surrounding the decay region hermetically confirm that there are no other particles accompanying the two photons.

It is an experimental challenge to operate the veto counters with high detection efficiency. For example, $K_L \to 2\pi^0$ decay has four photons in the final state, and is distinguished by two additional photons. Because its branching ratio is eight orders of magnitude greater than $K_L \to \pi^0 \nu\bar{\nu}$, the veto counters are required to detect a photon with 99.99% efficiency to avoid missing the two additional photons.

Another challenge is to reject π^0 production as a result of neutron interaction with matter because the K_L beam includes a large number of neutrons. To prevent the process from occurring, the decay volume should be maintained as a highly evacuated region. This is realized by placing most of the detectors, including the calorimeter, into a large vacuum chamber and placing veto counters far from the signal region.

New background sources appear along with improvement in experimental sensitivity, and they must be clearly understood. An important background source was found during the data analysis, in which a neutron entered the calorimeter and produced two photon-like activities. To remove the background, thin photon sensors, i.e., multi-pixel photon counters, were installed in front of the calorimeter in 2018 after accumulating the third dataset. With this improvement, KOTO continuously accumulated data, which are being analyzed to achieve higher experimental sensitivity.

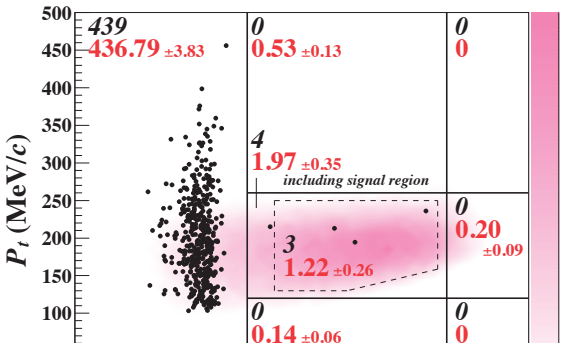

Fig. 2. Reconstructed π^0 transverse momentum (P_t) versus π^0 decay vertex position (Z_{vtx}) plot indicating the signal region for the $K_L \to \pi^0 \nu\bar{\nu}$ decay.

Figure 2 shows the distribution of remaining events for the third dataset after applying all selection criteria in the plane of the reconstructed π^0 decay position (Z_{vtx}) and its transverse momentum (P_t). The region inside the polygon indicated by dashed lines is the signal region searching for the $K_L \to \pi^0 \nu\bar{\nu}$ decay. The block dots represent the observed events. The colored contour indicates the expected density distribution of the signal events obtained by Monte Carlo simulation. For the three events in the signal region, the single-event sensitivity of the analyzed data was calculated as 7.2×10^{-10}. In the process of investigating their nature to declare them as genuine signal events, the study of the decay of the charged kaon ($K^{\pm}$) along with the K_L was proposed. A $K^{\pm}$ can be generated during the collision of K_L with dense materials at the inner surface of the beam line, which enter the decay volume. Even with a small number of $K^{\pm}$, it could become a serious background source through $K^{\pm} \to \pi^0 e^{\pm} \nu$ decay. This is mainly because the kinematics of the π^0 is similar to that of $K_L \to \pi^0 \nu\bar{\nu}$ decay. However, it was not possible to evaluate the number of the background correctly due to the uncertainty in the number of $K^{\pm}$ because a reliable Monte Carlo calculation related to the process does not exist.

In 2020, a special experiment was performed to measure the $K^{\pm}$ flux. As a result, 847 $K^{\pm} \to \pi^{\pm} \pi^0$ decays were successfully reconstructed. This means that the ratio of the $K^{\pm}$ and K_L flux is $(7.2 \pm 0.1) \times 10^{-5}$. That is, the number of $K^{\pm} \to \pi^0 e^{\pm} \nu$ backgrounds is expected to be 0.9. Summing up all contributions of K_L decays and neutron interactions to this $K^{\pm}$ result, the expected number of background events is 1.22 ± 0.26. This value is statistically consistent with the number of observed events. With the assumption of Poisson statistics, the upper limit of the branching ratio of the $K_L \to \pi^0 \nu\bar{\nu}$ decay was set as 4.9×10^{-9}.

To suppress the newly observed background events, a charged particle detector, made of scintillating fibers of 0.5 mm × 0.5 mm in cross-section, was fabricated and installed in front of the detector. Data collection was scheduled for two months starting in May 2021. This will provide a similar amount of data as the third dataset. This dataset will improve the understanding of the $K^{\pm}$ background and its rejection by a newly installed detector.

References

[1] J. K. Ahn *et al.*, (KOTO collaboration), Prog. Theor. Exp. Phys. 2017, no. 2, 021C01 (2017).

[2] J. K. Ahn *et al.*, (KOTO collaboration), Phys. Rev. Lett. 122, 021802 (2019).

[3] J. K. Ahn *et al.*, (KOTO collaboration), Phys. Rev. Lett. 126, 121801 (2021).

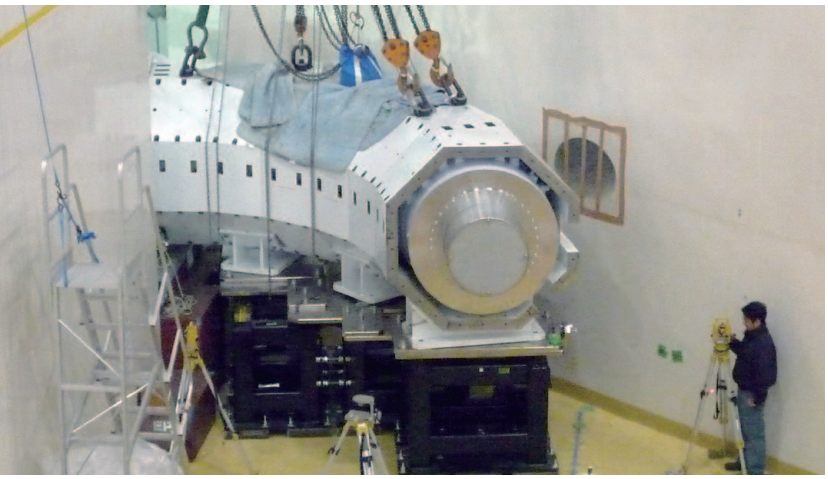

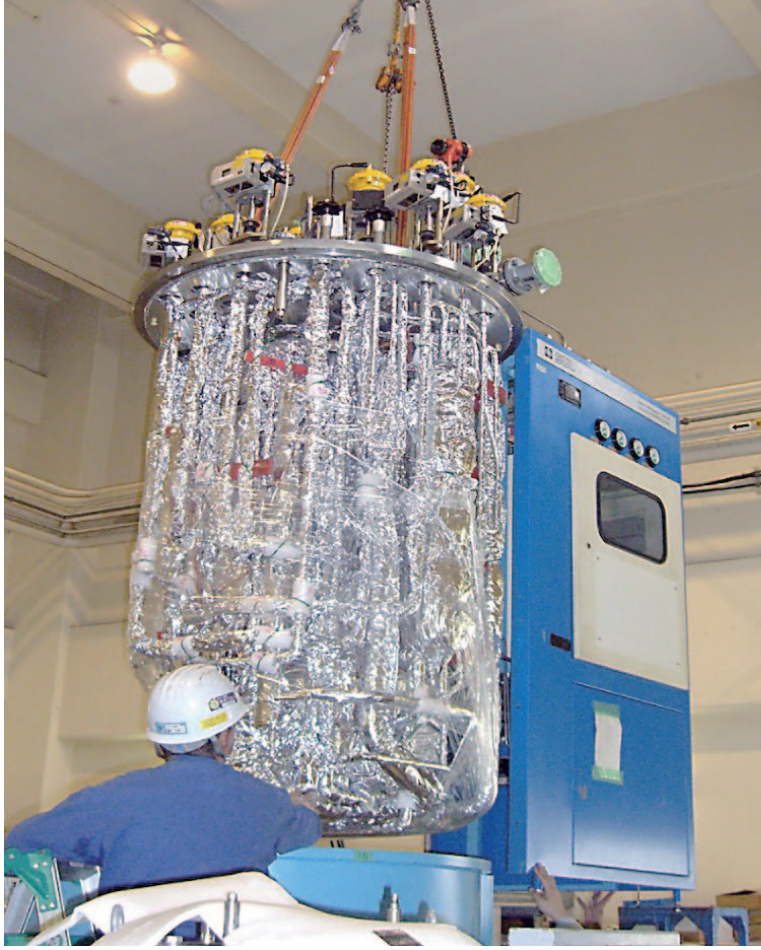

Cryogenics Section

Overview

The Cryogenics Section supports scientific activities in applied superconductivity and cryogenic engineering, carried out at J-PARC. It also supplies cryogen of liquid helium and liquid nitrogen. The support work includes maintainance and operation of the superconducting magnet systems for the T2K neutrino beamline and the muon beamlines at the Materials and Life Science Experimental Facility (MLF) and construction of the magnet systems at the Hadron Experimental Facility (HEF). It also actively conducts R&D works for future projects at J-PARC.

Cryogen Supply and Technical Support

The Cryogenics Section provides liquid helium cryogen for physics experiments at J-PARC. The used helium is recycled by the helium gas recovery facility at the Cryogenics Section. Figure 1 summarizes the liquid helium supply in FY2020.

Liquid nitrogen was also supplied to the users for their convenience. Its amount in FY2020 is summarized in Fig. 2. Liquid nitrogen has been regularly provided to the Radiation Safety Section for operation of a gas chromatograph. It was also supplied to the users in the MLF, the HEF and the Cryogenics Section.

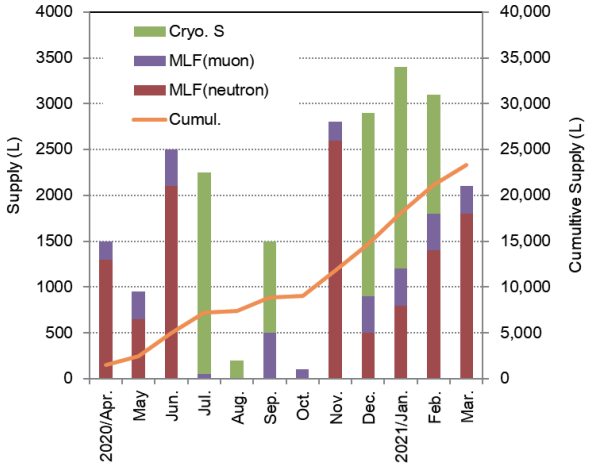

Fig. 1. Liquid helium supply at J-PARC from April 2020 to March 2021.

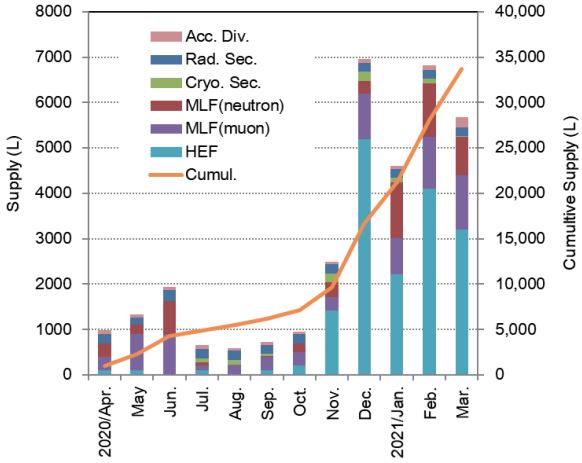

Fig. 2. Liquid nitrogen supply at J-PARC from April 2020 to March 2021.

Superconducting Magnet System for T2K

The superconducting magnet system for the T2K experiment operated during the periods shown in Table 1. The system worked well without disturbing the beam time. The operation time in FY2020 was only 49 days and regular maintenance works were carried out in the summer. Figure 3 summarizes the incidents in the refrigeration system from FY2009 on. The system was suspended only in its early period due to problems in the hardware and control parameters. Although a few problems with hardware parts occurred in the recent years, the troubles had been resolved without interrupting the operation. The system was very stable in FY2020 as well.

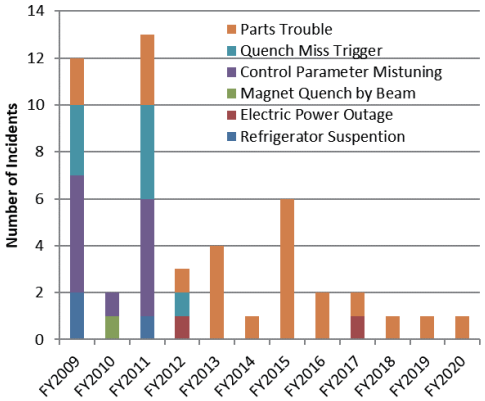

Fig. 3. Summary of incidents in the Refrigerator System for T2K.

Table 1. Operation history of the T2K superconducting magnet system.

	2020 Apr.	May	June	Jul.	Aug.	Sep.	Oct.	Nov.	Dec.	2021 Jan.	Feb.	Mar.
Operation											⟷ 2/3-3/23	
Maintenance						⟷						

Superconducting Magnet Systems at the MLF

The Cryogenic Section contributes to the operation and maintenance of the superconducting magnet systems at the Muon Science Facility (MUSE) in the MLF. The superconducting solenoid in the Decay Muon Line (D-line) was operated from January to June 1, 2019, although the operation was temporally stopped from April 20 to May 11 due to the coronavirus. Annual maintenance, such as exchange of the oil separation filter, safety valve maintenance and so on, was performed from July to the end of November. During the maintenance work, a small leak was found on a flexible horse of the He high pressure line, therefore, four horses, including three horses without a leak, were replaced just in case (Fig. 4). The cryogenic operation was restarted on November 24. It was stopped on December 24 for the New Year holidays, and it resumed on January 6.

Fig. 4. Exchange work of the He flexible horses.

Superconducting Magnet Systems at the HEF

The COMET experiment is under construction in the Hadron South Experimental Hall (HDS) of the Hadron Experimental Facility (HEF). The Cryogenics Section was involved in the construction of the cryogenic system and superconducting magnets. Production of the superconducting solenoid magnet for the muon source is in progress. Superconducting coils for the Pion Capture Solenoid (PCS) were inserted in the support shell structure and impregnated with the radiation resistant resin. The coil structure is shown in Fig. 6.

The magnets are designed to be cooled by a two-phase flow of liquid helium, which is supplied by a helium refrigeration system built in HDS. The current lead box (CLB) for the PCS was fabricated and installed in the HDS in FY2020 (Fig. 1). Five High Temperature Superconductor (HTS) current leads for 3 kA, 500 A and 250 A are installed. They are cooled not only by cryocoolers but also by the shield helium gas with

Fig. 5. Insert of the current lead box for the Pion Capture Solenoid.

Fig. 6. The coldmass of the Pion Capture Solenoid (CSMS coils).

temperature of 40K supplied from the helium refrigerator. Performance test of the CLB will be done in FY2021.

The transfer line was connected to the small cryostat for protection diodes, which is separated from the cryostat of the MTS magnet. Since the cooling port of MTS has an aluminum cooling pipe, an aluminum pipe should connect the diode and the magnet. Connecting the aluminum pipe, which ensures leak-free conditions in cryogenic temperature with thermal shocks and thermal cycles, requires a great deal of skill. We performed the aluminum pipe welding with high reliability and high yield. After this welding, we also confirmed that all welding points were leak free (less than 10^{-10} Pa·m^3/sec) after a thermal shock with liquid nitrogen temperature.

R&D for the Future Projects at J-PARC

The g-2/EDM project aims for the precise measurement of the anomalous magnetic moment and the electric dipole moment of muons. This experiment was proposed at the MUSE H-Line. A superconducting solenoid with a high field homogeneity, better than 1 ppm locally, plays a very important role as a muon storage ring. The numerical study of cold box on vibration conduction was carried out. Mechanical vibration causes errors in the magnetic field. The cold box has four GM cryocoolers to re-condensate evaporated helium gas, and they generate vibration. The cryocoolers were supported by the stage separated from the vacuum vessel of the cold box and connected to the cold box with soft bellows in order to avoid direct conduction of the vibration. The frequency response analysis was carried out with FEM software to evaluate the vibration conduction performance. The simulation study shows that the resonant vibration modes were higher than 20 Hz, that is sufficiently higher than the main vibration frequency of the cryocooler, 1 Hz. The coil vibration, that is error field, caused by the conducted vibration from the cold box will be evaluated in the next fiscal year.

A muonium hyperfine structure measurement, called MuSEUM experiment, has been proposed for the same beam line as the g-2/EDM project. In the experiment, the energy state transition in muonium will be observed under a static magnetic field with local homogeneity of 1 ppm. A new NMR readout board were designed and manufactured (Fig. 7). It must be installed close to the measurement dynamic region in order to optimize the LC resonant circuit. Surface mount devices were carefully selected, and the board size was minimized in order to decrease the magnetic field distortion caused by the magnetization of the board.

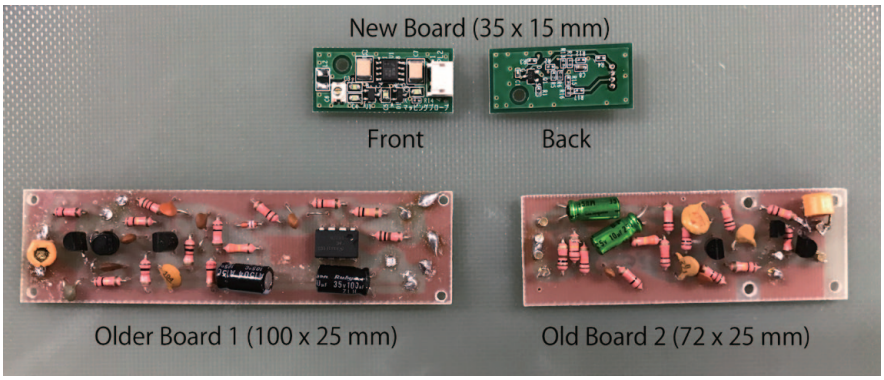

Fig. 7. Newly developed read out board. Two older boards are also shown at the bottom.

Information System

Overview

The Information System Section plans, designs, manages and operates the network infrastructure of J-PARC and also provides support to ensure its information security. In terms of computing, until now, J-PARC has owed its major computer resource for analyzing and storing data from neutrinos, nuclear physics and MLF experiments to the KEK central computer system. The section connects the J-PARC network to the KEK central computing system directory and helps the users to utilize the system effectively.

Status of Networking

Since 2002, the J-PARC network infrastructure, called JLAN, has been operated independently from KEK LAN and JAEA LAN in terms of logical structure and operational policy. In 2020, the total number of hosts on JLAN exceeded 5,600, which was a 106% increase compared to the last year. The growth curve of edge switches, wireless LAN access points and hosts (servers and PCs) connected to JLAN are shown in Fig. 1.

In April 2016, the National Institute of Informatics (NII) upgraded SINET (Japan Science Information Network https://www.sinet.ad.jp) from version 4 to 5. SINET is not only a gateway from JLAN to the internet but also an important connection between Tokai and the KEK Tsukuba site in J-PARC.

Figures 2 and 3 show the network utilization of the internet from/to JLAN. Since the bandwidth capacity for the internet through the SINET is 10 Gbps, it is clear that there is enough space for additional activity. Figures 4 and 5 show the statistics of data transfer between the Tokai site and the Tsukuba site. The network bandwidth capacity between the two sites is 10 Gbps. This shows that the usage level has been approaching a half of it, especially during the period when the Hadron facility was running. In addition to the current bandwidth, the upgrade offers a future option of 20 Gbps for both of internet and Tokai-Tsukuba connections, if the J-PARC network can be adapted.

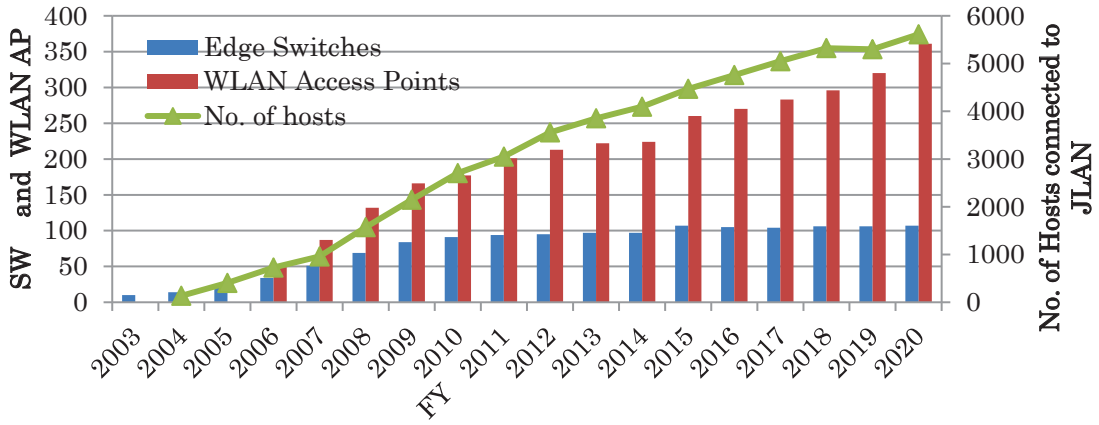

Fig. 1. Number of hosts, edge SW and wireless AP on JLAN.

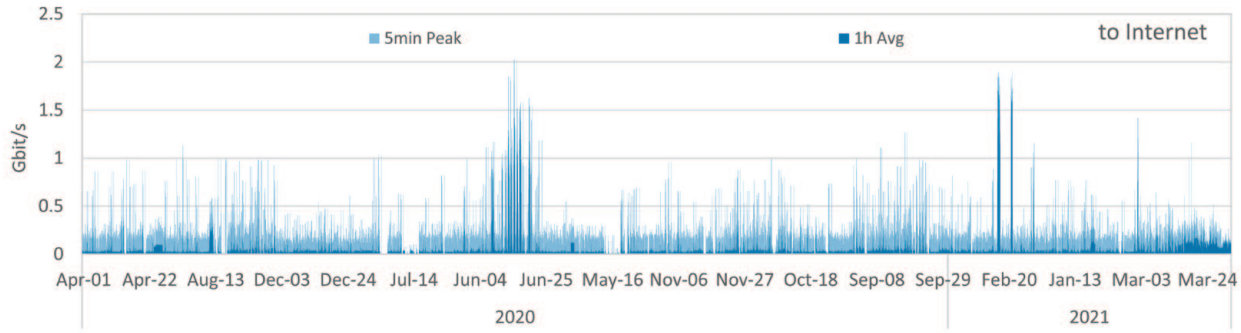

Fig. 2. Network traffic from JLAN to the internet.
(1 hour average and 5 minutes peak value)

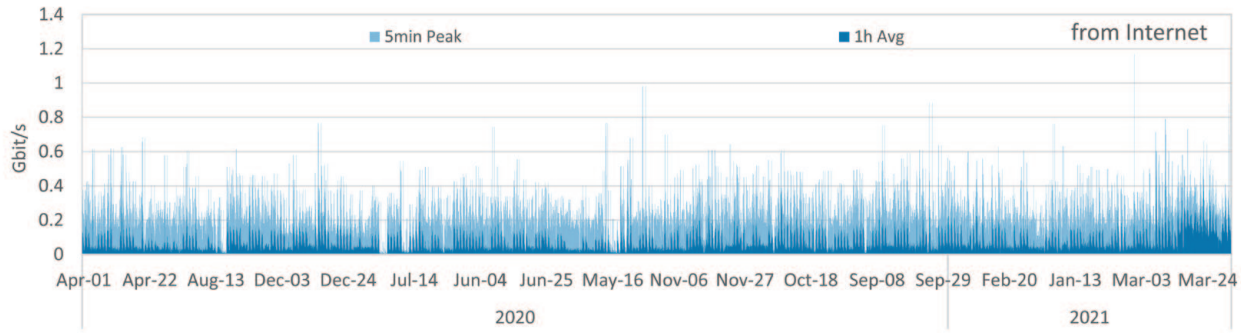

Fig. 3. Network traffic from the internet to JLAN.

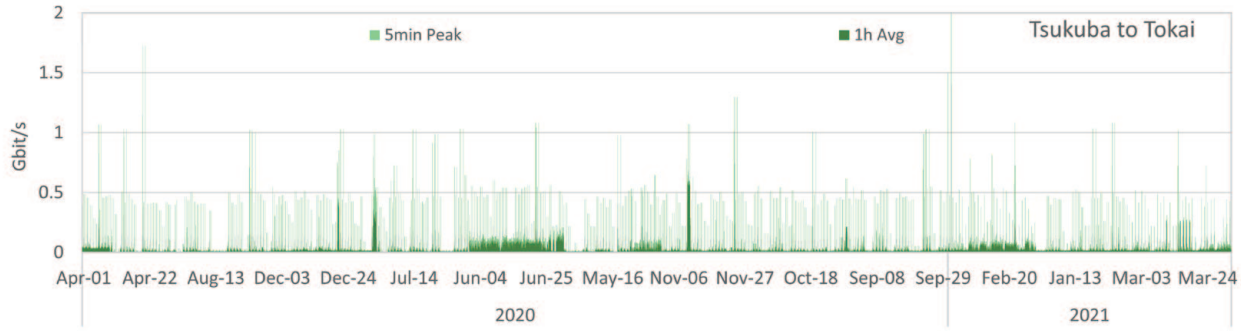

Fig. 4. Network traffic from the Tsukuba site to the Tokai site.

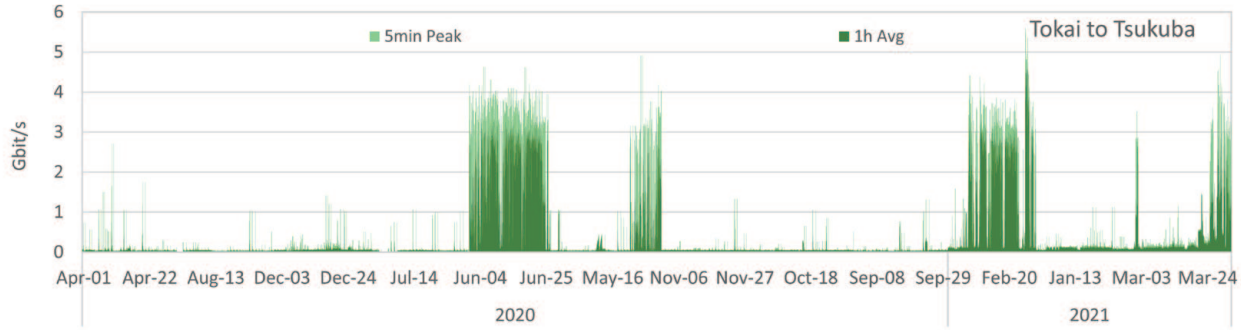

Fig. 5. Network traffic from the Tokai site to the Tsukuba site.

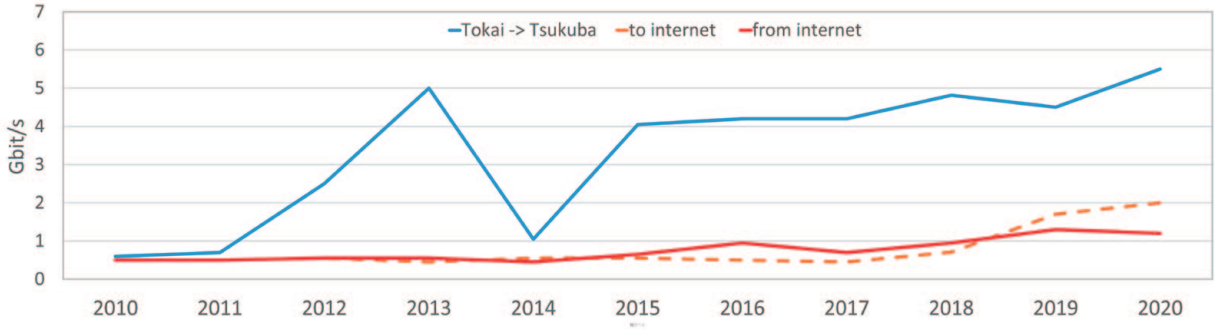

Fig. 6. Peak network traffic for the recent years.

Internet Connection Services for Visitors and Public Users of J-PARC

Since 2009, J-PARC has offered a Guest network (GWLAN) service, which is a wireless internet connection service for short-term visitors, available in almost all J-PARC buildings. In the end of 2014, additional network service called User LAN has started. To use the GWLAN, users are required to receive a password at the J-PARC Users Office beforehand, while in the User LAN, they are authenticated by the same ID and password for the User Support System, which is also used for dormitory reservation and so on. From March 2016, a new service called "eduroam" has been started. The eduroam (https://www.eduroam.org/) is a secure roaming access service developed for the international research and education community and mutually used among a huge number of research institutes, universities, and other institutions around the world. The eduroam service will be a convenient third option of internet connection service for J-PARC visitors. Figure 7 shows this fiscal year's usage statistics of GWLAN, User LAN and the newly introduced eduroam service.

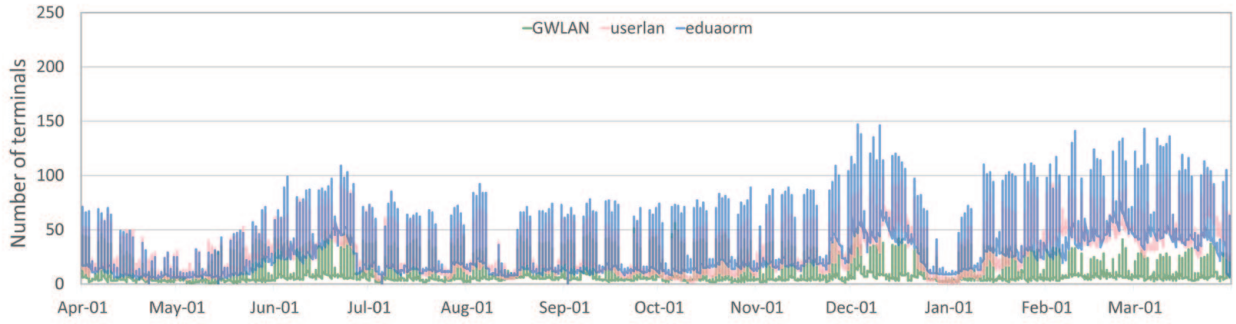

Fig. 7. Usage trends of GWLAN, User LAN and eduroam.

Status of Computing

Since J-PARC does not have computing resources for physics analysis, starting from 2009, the KEK central computing system (KEKCC) at the KEK Tsukuba campus has been mainly used for that purpose. KEKCC is shared by most of the research groups of KEK, including J-PARC. At the Neutrino (T2K), Hadron and Neutron (MLF) experiments, the data taken in J-PARC are temporarily saved at their facilities and then promptly transferred, stored, and analyzed at the system in Tsukuba. The storage of the system is also utilized as a permanent data archive for their data. The third upgrade of the system was completed in 2020, and the computing resources are shown in Table 1. Figures 8-10 show the utilization statistics of the computing resources in FY2020. The main users who used the CPU and storage constantly were from the Hadron and Neutrino experiment groups. The MLF group also started to store data to tapes on the system.

Table 1. Computing resources in the KEKCC.

CPU (Intel Xeon Gold 6230)	15000 cores
RAID Disk (GPFS)	25.5 Peta Bytes
Tape Library (HSM)	100 Peta Bytes

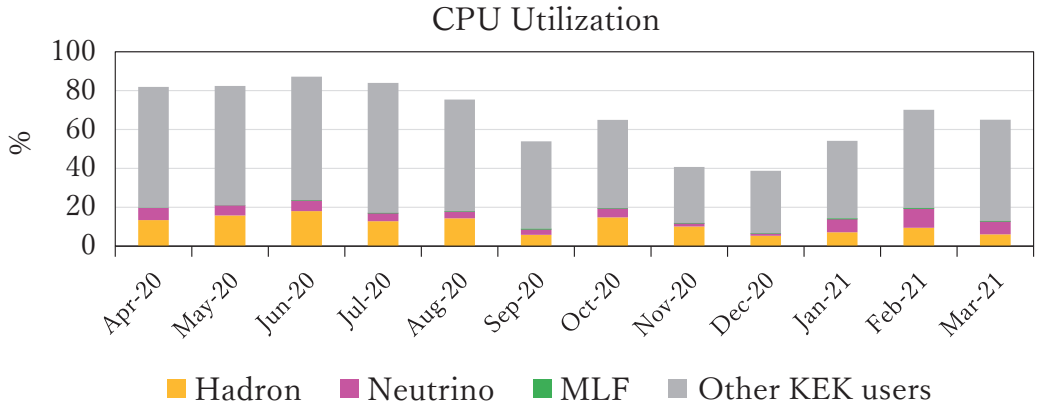

Fig. 8. CPU usage statistics of KEKCC in FY2020.

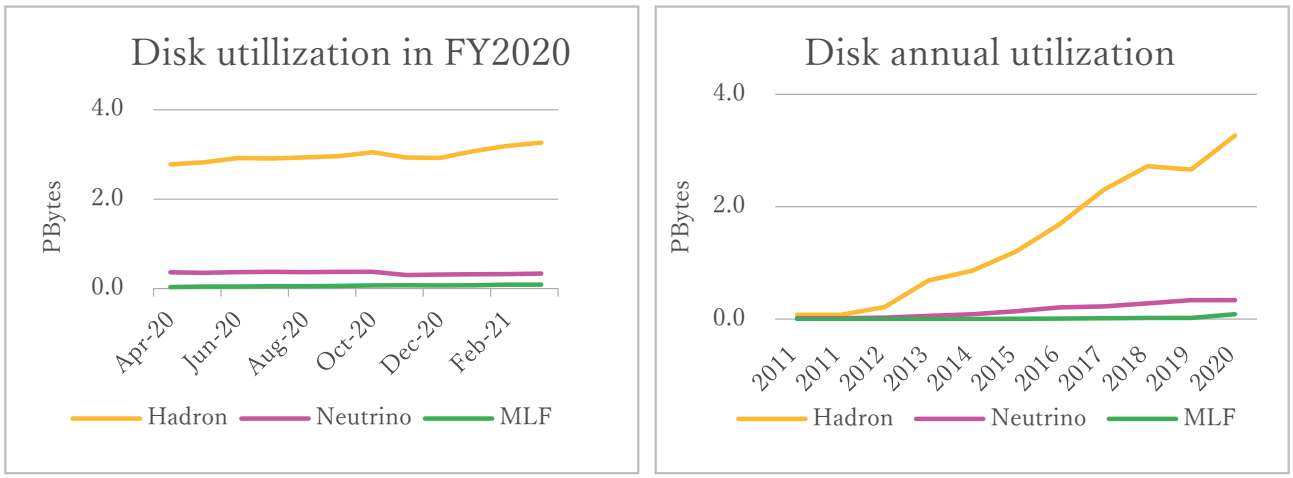

Fig. 9. Disk usage statistics (left: trend of FY2020; right: annual trend).

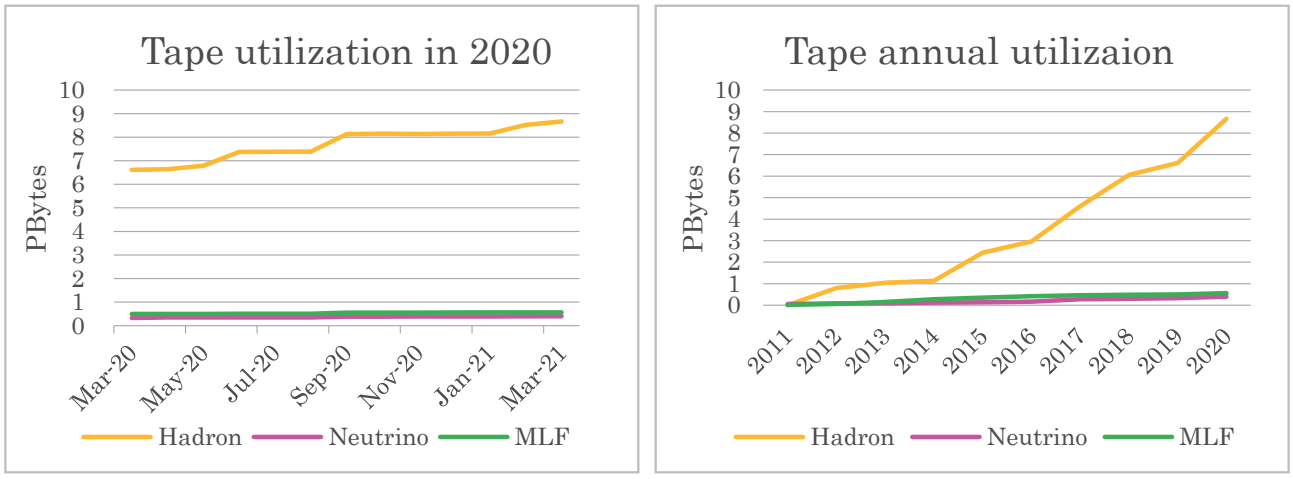

Fig. 10. Tape library usage statistics (left: trend for FY2020, right: annual trend).

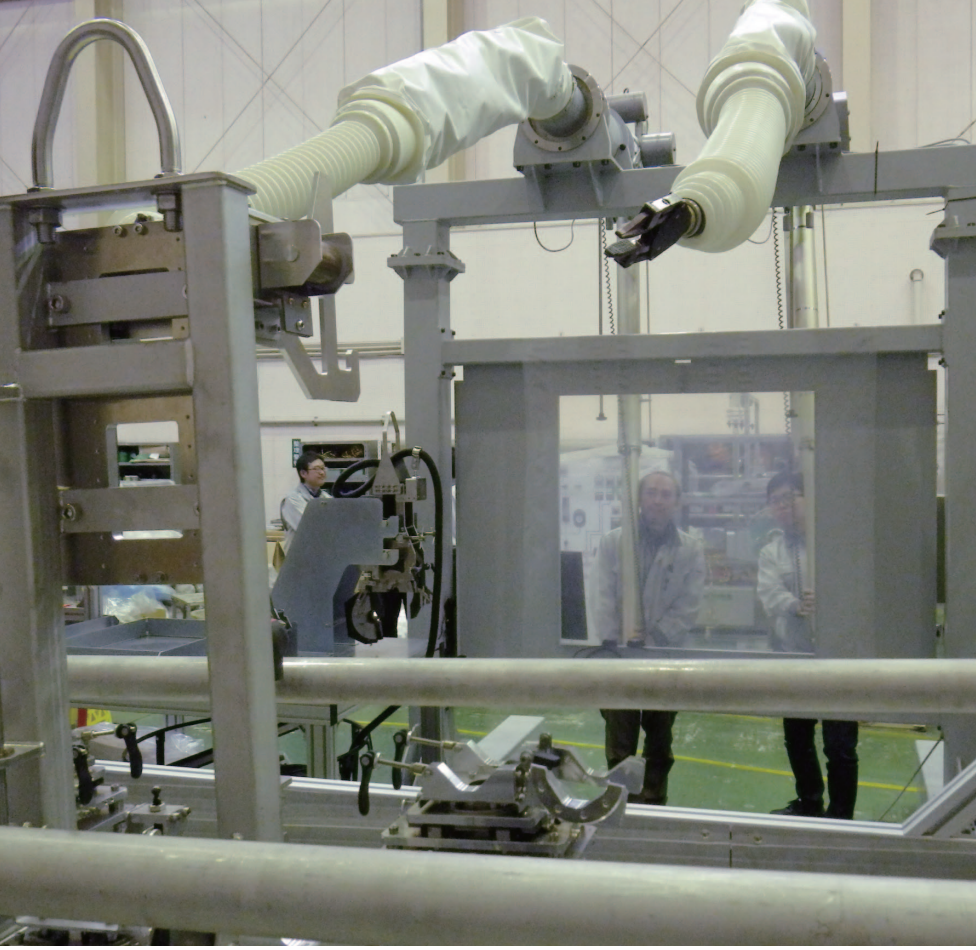

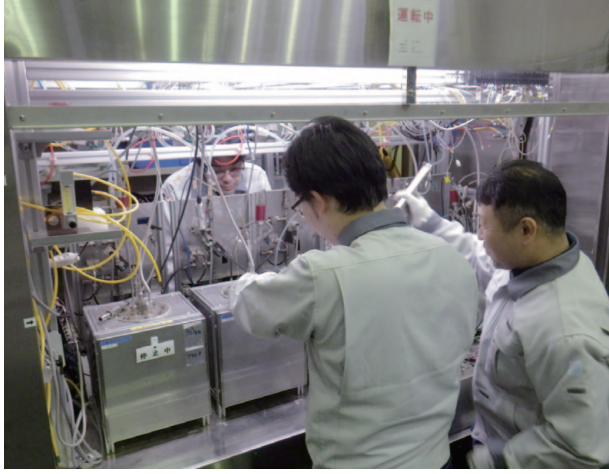

Transmutation Studies

Overview

We are developing nuclear transmutation technology with accelerator-driven systems (ADS) using the J-PARC's research resources and expertise in high-power accelerator and target technologies. The ADS is an effective nuclear system for volume reduction and mitigation of harmfulness of high-level radioactive waste produced in nuclear reactors. We believe that the ADS is one of the most beneficial applications of high-power accelerators for contributing to human society.

The baseline design of the J-PARC Transmutation Experimental Facility (TEF) was completed in FY2017 (JAEA-Technology 2017-003 and 2017-033). To make the facility more attractive and effective by introducing leading edge knowledge to its purpose and specifications, we are changing the concept of the TEF to a new one. The main purpose of the new facility is to acquire irradiation damage data of ADS's beam window materials by impinging a proton beam to a lead-bismuth eutectic target in which the sample materials are located. In addition, it is under consideration to irradiate the beam window and target materials used in high-power accelerator facilities, such as J-PARC, by the proton beam directly to acquire irradiation data of the materials to ensure a safe and efficient operation of those facilities. We also plan to equip the new facility with a hot laboratory for efficient post-irradiation examination (PIE). Accordingly, it is expected that the new facility can contribute not only to the development of ADS but it will also help to upgrade the J-PARC's existing facilities.

As for the R&D activities on the lead-bismuth eutectic (LBE) target technology, we successfully established automatic control of the oxygen concentration in LBE,

and this enabled us to launch in November 2020 a series of materials corrosion test campaigns using the OLLOCHI LBE loop.

Our recent R&D activities on nuclear data for nuclear transmutation received the following awards:

- H. Iwamoto, S. Meigo, "Unified description of the fission probability for highly excited nuclei", Academic Award of Nuclear Data Subcommittee, Atomic Energy Society of Japan (AESJ)
- K. Nakano, "Isotope production in proton- and deuteron-induced spallation reactions on ^{93}Zr and ^{93}Nb", Incentive Award of Nuclear Data Sub-committee, AESJ
- H. Matsuda, S. Meigo, Y. Iwamoto, et al., "Measurement of displacement cross-sections of copper and iron for proton with kinetic energies in the range 0.4 – 3 GeV", J. Nucl. Sci. Tech. 57, 1141 (2020), Treatise Award of AESJ (Fig. 1)
- S. Meigo, et al., "Experimental study on displacement cross section of structural materials for nuclear transmutation systems", Exploit R&D Award of JAEA's President Award

In addition, we issued two press releases:

- "How much are metals damaged by high-intensity proton beam irradiation?", July 2020
- "Development of proton beam controlling technology for nuclear transmutation research", December 2020

Fig. 1. Members of the Treatise Award of AESJ, Drs. Y. Iwamoto, H. Matsuda, S. Meigo from the left.

On January 22, 26 and February 2, 2021, the seventh TEF Technical Advisory Committee (T-TAC) was held on-line. This year, the T-TAC was specifically asked for an advice on the progress in the ongoing R&D activities from the viewpoint of ADS activities in the world. The main conclusions of the T-TAC were as follows: *"T-TAC congratulates for the recent start of the OLLOCHI installation."* and *"T-TAC considers the R&D works carried out by J-PARC as valuable contributions to the international ADS community."*

Research and development

The management of the lead-bismuth eutectic, which are highly corrosive under high temperature, is one of the key issues of the ADS. To overcome the issue, a new method of applying oxygen potential control technique to form an oxide layer on the steel surface has been tested. Various research activities, operation of spallation target mockup loop, preparation of the corrosion database, and development of the LBE measurement sensors are underway.

OLLOCHI

Oxygen concentration (OC) control tests in OLLOCHI (Oxygen-controlled LBE LOop Corrosion tests in High-temperature) started in January 2020 and we managed to maintain the OC automatically within a certain range by mixing inlet gases. We started the first campaign of the long-term corrosion test in November 2020 and finished in February 2021. The total operation period was about 2,000 hours. The test conditions were as follows; the maximum temperature and the temperature difference were 450˚C and 100˚C, respectively. The flow rate was about 1 m/s at the samples' position. OC was kept at 1×10^{-6} wt%. Tested samples were taken out from the specimen holders shown in Fig. 2 and are being observed.

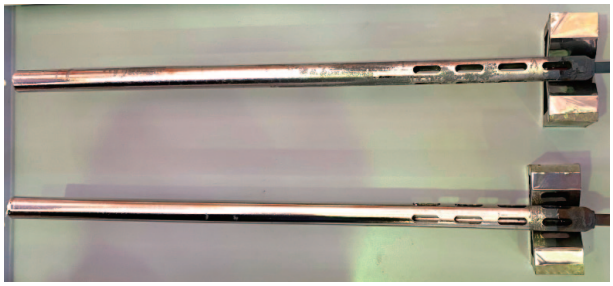

Fig. 2. Outline of specimen holders after the corrosion test operation.

IMMORTAL

IMMORTAL is a mock-up test loop of a future LBE spallation target in TEF-T. Several modifications were progressed to enhance the operability and the thermal stability of the loop. In addition, the number of measurement points were increased by the modifications. In the future, a transient heat-transfer experiment of LBE under non-isothermal condition will be performed after the evaluation test of the modified components.

LAPIN

LAPIN (**L**BE **A**pparatus for **P**urification of **I**mpurities by **N**atural convection) is a small LBE loop to understand the natural convection behavior of LBE and evaluate mixed impurities behavior. The LBE inventory is limited to less than 8 liters, and it can be easily exchanged to apply various impurities in LBE. The temperature difference of LBE along the triangle flow channel is generated by a heater unit and an air-cooled heat exchanger. As a representative impurity, Ni will be applied because its large solubility can cause various harmful effects on the loop operation. In near future, the behavior of LBE flow velocity and the oxygen concentration will be evaluated.

Fig. 3. Exterior of LAPIN

NALTO

To develop electromagnet flow velocity probe (EM probe) for LBE, a rotating test apparatus named NALTO (**N**imble velocity measurement **A**pparatus in **L**BE with controlled **T**emperature and **O**xygen potential) was newly designed and installed. Figure 4 shows the exterior of NALTO. It consists mainly of a chamber containing a rotating annular vessel, gas atmosphere control system and vessel rotating system. Because the rigid body rotation of the LBE can be assumed, molten LBE in the vessel rotates together with the vessel. Then, we obtain the circumferential velocity of the LBE from the rotation speed of the vessel.

Fig. 4. Exterior of NALTO

Prototype EM probe was applied to the high temperature LBE. As a result, we obtained successfully a clear linearity between the velocity and the output voltage from the probe up to about 500˚C, which was higher than Currie temperature of the permanent magnet and suitable for the LBE spallation target operation. To obtain the local flow direction, multi-velocity components will be measured with 4-electrodes type EM probe in FY2021.

Research and development

Measurement of nuclide production cross sections

For predicting the radioactivity of the components of ADS and their nuclear inventory calculation, nuclide production cross sections play a vital role. We have newly measured nuclide production cross sections in high energy proton-induced reactions on heavy nuclei, such as ^{165}Ho, ^{nat}Lu, ^{nat}Re, and ^{209}Bi, by using the activation method as a part of a systematic measurement of the cross-sections.

The irradiation experiment was performed at 3NBT. The stacked metal foils were irradiated by 0.4, 1.3, 2.2, and 3.0 GeV protons. After the irradiation, gamma-ray measurement was performed for three months. The production cross sections were derived from the decay curve of the detected gamma-rays.

We identified the production of 44 nuclides for the

^{209}Bi target, including nuclides whose cross-sections have never been measured, and successfully obtained 114 production cross-sections in all incident energy regions. Figure 5 shows the ^{206}Po production cross-section from the proton-induced reaction on Bi as a function of incident proton energy. Our data support Titarenko's data. The calculation using INCL4.6 and GEM models shows excellent agreement with the measured data.

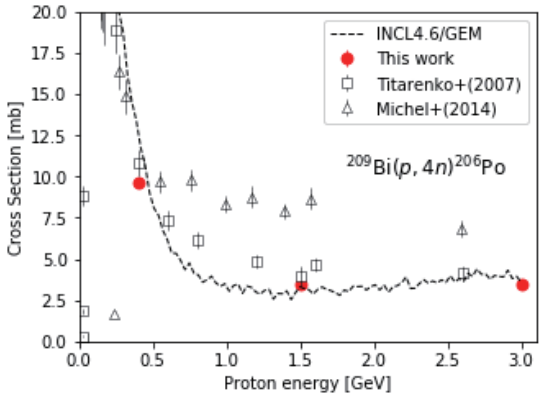

Fig. 5. ^{206}Po production cross section from the proton-induced reaction on ^{209}Bi.

Nuclear data measurement for ADS

An experimental program on nuclear data for research and development of ADS was launched in 2019, entrusted by MEXT. In the framework of this program, neutron energy spectrum measurements have been conducted using the Fixed-Field Alternating Gradient (FFAG) proton accelerator at Kyoto University (Fig. 6). As the first experiment, we measured the double-differential thick target neutron yields (TTNY) and double-differential cross-sections (DDX) for an iron target, which is the major constituent material of ADS, using 107-MeV proton beams accelerated from the FFAG accelerator. The preliminary results show that we have successfully obtained the angle-dependent neutron energy spectra. As a next step, we will continue to measure the TTNY and DDX, focusing on lead and bismuth targets, which are essential materials for the ADS.

Fig. 6. FFAG accelerator.

Proton accelerator for ADS

The Accelerator-driven subcritical system (ADS) requires strict control of the number of beam trips to avoid thermal stress in the beam windows. To this end, the proton accelerator for ADS pursues a robust beam optics design, Fault-tolerance capabilities, and repairability to become a reliability-oriented accelerator.

This work investigated the Fault-tolerance compensation schemes (FTCS) to reduce the system downtime and consequently to allow the accelerator to reach the reliability requirements for a JAEA-ADS machine.

Fault-tolerance is accomplished by using the none Faulty-element to counteract the unwanted effect of the Faulty-element. Figure 7 top shows the readjustment of the accelerating gradient (Eacc) to compensate for a failure in the last five-cell Elliptical cavity resonator 1 (EllipR1). The energy recovery is shown in the bottom plot in Fig. 7.

The results showed that the FTCS for SRF cavities and magnets produced acceptable beam performance, except for the Half-wave Resonator (HWR) region, the first SRF section of the linac. Thus, these studies showed the capability of FTCS for fast recovery in the rest of the proton accelerator to satisfy the reliability requirements for the ADS project.

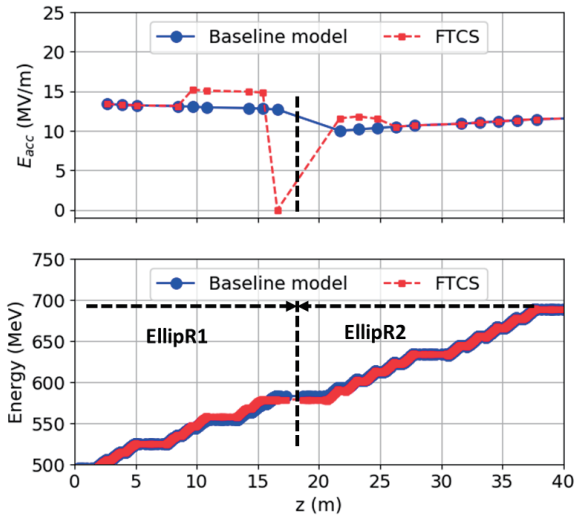

Fig. 7. TCS for the failure in the last EllipR1's cavity. The black dotted vertical line indicates the transition between the EllipR1 and EllipR2 regions.

MA Irradiation Experiments

To develop an accelerator-driven system (ADS), it is necessary to verify the nuclear data of minor actinides (MAs) in a fast neutron core, such as the transmutation physics experimental facility (TEF-P) designed in J-PARC. As planned in TEF-P, one of the verifications is to use fission chambers containing MA as fissionable material and a well-known material such as ^{235}U as reference in the critical or sub-critical core, where the neutron spectrum in ADS core can be simulated. To achieve high-accuracy verification, precise fabrication of the chamber (e.g. accountancy and purity of MA, uniformity of MA layer, and hermeticity) is important, but the fabrication itself requires R&D because the preparation of pure raw MA and its treatment are possible in very limited facilities. We have recently fabricated several chambers (Fig. 8) containing ^{237}Np, ^{241}Am, ^{243}Am, or ^{244}Cm in NUCEF in JAEA and measured the ratios of the ^{237}Np/^{235}U and ^{243}Am/^{235}U fission rates at the Kyoto University Critical Assembly (KUCA).

Figure 9 shows the pulse height distributions of ^{237}Np and ^{235}U fission reactions as an example. The fission rate ratios of ^{237}Np/^{235}U and ^{243}Am/^{235}U obtained by each pulse height were 0.048 ± 0.003 and 0.042 ± 0.004, respectively. According to the tentative calculations, the result of ^{237}Np/^{235}U was in good agreement with the measurement, but the result of ^{243}Am/^{235}U underestimated the measurement. These experimental data were obtained with high accuracy and would be usable for verification of evaluated nuclear data by conducting detailed analyses [1].

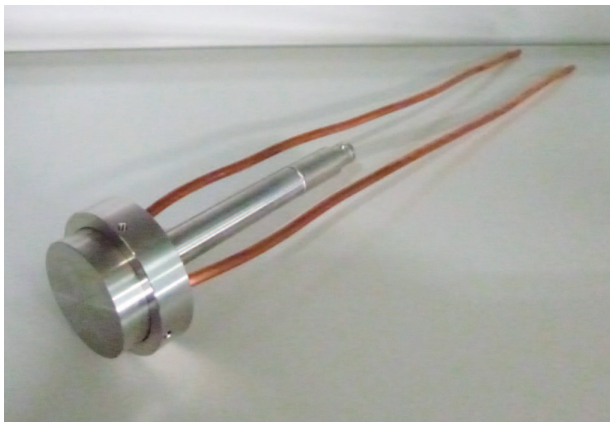

Fig. 8. Photograph of the JAEA single fission chamber.

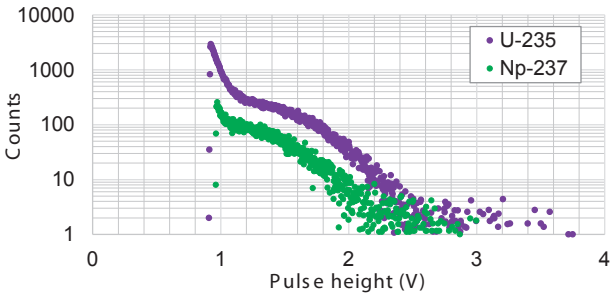

Fig. 9. Fission signals of the ^{237}Np and ^{235}U fission chambers [1]

Reference

[1] A. Oizumi *et al.*, KURNS Progress Report 2020, (2021).

International and Domestic Cooperation

In spite of the severe restrictions due to the COVID-19, we proceeded steadily with the international cooperation.

We are collaborating closely with the Belgian Nuclear Research Centre (SCK CEN) for the ADS development under the collaboration arrangement between SCK CEN and JAEA. SCK CEN is promoting the MYRRHA (Multi-purpose hYbrid Research Reactor for High-tech Application) project, which is the world's first large scale ADS project at power levels scalable to industrial systems. There are three important topics of cooperation, i.e., neutronics, LBE technology and ADS's accelerator development. As for the neutronics, experimental data obtained at J-PARC, such as proton-induced nuclide production cross section and neutron spectral flux intensity from the MLF's mercury target, were shared with SCK CEN for validating the neutronics calculation codes. In the case of the LBE technology, the performance of the oxygen sensors produced by SCK CEN was compared with that of JAEA's oxygen sensors. It was found that the sensors produced by the two institutes indicated a consistent and valid output. As for the ADS's accelerator development, one young scientist of the J-PARC's Linac team, Dr. Jun Tamura, visited Louvain-la-Neuve in Belgium from January to December 2020. He joined the MYRRHA accelerator team and contributed to producing a prototype of the MYRRHA linac of up to 100 MeV (Fig. 10).

In addition, "Arrangement in the field of nuclear research as pertaining to accelerator driven systems and their safety" between Karlsruhe Institute of Technology (KIT) in Germany and JAEA was agreed upon on June 18, 2020. An on-line meeting between KIT and JAEA was held on October 8, 2020 where the two parties agreed on the Specific Topic of Cooperation in the field of the LBE technology.

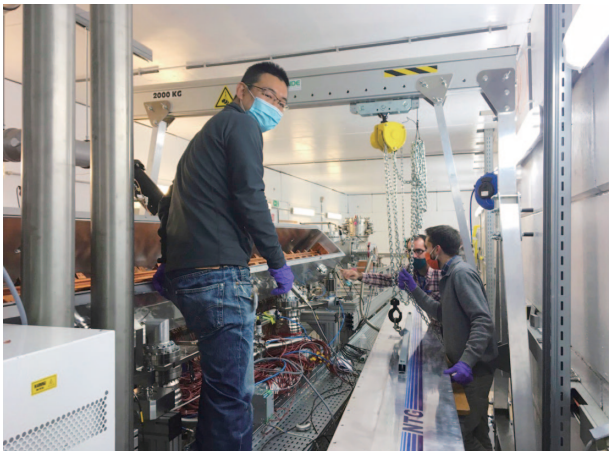

Fig. 10. Dr. Jun Tamura working with the MYRRHA accelerator team at Louvain-la-Neuve, Belgium.

On March 30 and 31, 2021, two on-line workshops related to the J-PARC's irradiation facility were held. In the first workshop, possibilities of the J-PARC's irradiation facility were discussed. The most important message was that "the J-PARC's facility will be very effective not only for materials irradiation research but also for education of young scientists under the current situation when the number of research reactors is decreasing." The second workshop was focused on the soft error of semiconductor devices, which would be one of the important themes to be studied by using the intense high-energy neutron beam from the LBE target. It was concluded that the J-PARC's facility would provide a very suitable soft error test environment because its flux intensity is the highest in the world.

Safety

Safety

1. Major events on safety culture and safety activities in the J-PARC

Through our experiences of the various accidents and incidents, the J-PARC has reaffirmed that "The safety of the facility is achieved by the efforts of every person involved", and we actively implement safety culture development activities to upgrade the safety awareness and skills of each person. Our efforts to enforce the safety culture in the J-PARC include sharing safety information, enhancement of safety awareness, education and training, etc. For these purposes, new approaches are being introduced sequentially. In addition, these activities are being reviewed internally and by external experts to ensure continuous improvement.

In fiscal year 2020, responding to the global outbreak of the novel coronavirus (COVID-19), the annual safety policy was determined as "Creating work safety style that incorporates new lifestyles." On the basis of this policy, we tried to effectively and flexibly integrate the anti-COVID-19 measures with the normal safety measures. In order to prevent the increase of potential risks such as heatstroke, fires, falls, etc. when focused too excessively on infectious disease countermeasures, we continued steadily the safety activities that we have been conducting so far, such as sharing good practices and commendation, experience-based safety trainings, e-learning on safety issues, certification training for radiation measurement technique, sharing of safety information using video materials, etc. In addition, we newly introduced the "KY"[1] training to promote proactive and creative efforts in the workplaces and to improve the skills on safety matters.

Table 1 lists the major events on safety culture and safety activities in the J-PARC. The J-PARC Center had held "the J-PARC Safety Day" around May 23, the date when the radioactive material leak incident occurred in 2013. However, due to concerns related to COVID-19, Safety Day 2020 was postponed and held on September 9 online. Following the introductory talk by the J-PARC director, some good practices related to safety and health were awarded. The main talk entitled "Introduction to occupational behavior analysis" was given by Dr. Rieko Hojo (National Institute of Occupational Safety and Health, Japan). Further, a newly produced video on the radioactive material leak incident in 2013 was presented.

An emergency drill was conducted on October 21 at the Hadron Experimental Facility (HD) by supposing that the beam operation was started when two workers were left in the experimental area of HD. The drill included transportation and decontamination of the exposed workers, estimation of exposure doses, setup of the command post and communication with the accident site, report to the headquarters via TV conference, and a simulated press release.

The J-PARC safety audit in fiscal year 2020 was conducted by two auditors on December 7. They reviewed the following points: 1) Organization of safety management, 2) Management of work safety, 3) Emergency preparedness, and 4) Safety education and promotion and continuation of the safety culture. An on-site inspection of the works at the MLF facility was also conducted. The auditors gave us valuable recommendations on safety measures with considerations for the development of the J-PARC over the next 10 years.

2. Radiological license update and facility inspection

Applications to update the radiological license were submitted to the Nuclear Regulation Authority on October 5. Table 2 lists the main changes in the applications. The permit for the applications was issued on June 9, 2021.

The facility inspection for the construction of a new High-p beamline at the Hadron Experimental Facility and the associated change with the shielding structure, which was applied for on December 6, 2019, and approved on April 28, 2020, was conducted on June 22, 2020, as part of the regular inspection, and passed on June 24, 2020.

3. Meeting of the committee on the radiation safety matters

The J-PARC Radiation Safety Committee is organized as an advisory committee to both JAEA and KEK to discuss the policy on radiation safety in the J-PARC. Meanwhile, the Radiation Safety Review Committee has been established to discuss specific subjects of radiation safety in the J-PARC.

In FY2020, the J-PARC Radiation Safety Committee met twice, and the Radiation Safety Review Committee met three times. Table 3 lists the major issues for the committees.

1 "KY" is a Japanese word meaning a briefing in which workers discuss and confirm the potential risks in their work shortly before it starts. "KY" is an abbreviation of "Kiken Yochi" meaning "Hazard Prediction."

4. Radiation exposure of radiation workers

The number of persons subject to annual measurement of external exposure in FY2020 was 2,705 due to a decrease in the number of users engaged in radiation work due to the impact of the spread of the new coronavirus infection.

Table 4 lists the distribution of annual exposed doses for each category of workers. There was no exposure exceeding the dose limit specified in the local radiation protection rule for the J-PARC and the administrative dose limits (7 mSv/year) specified in the detailed rule of local radiation protection rule for the J-PARC. The total annual effective dose was 27.1 person·mSv, and the maximum effective dose was 0.9 mSv.

Table 1. List of major events on safety in FY2020.

Day	Events
June 30, 2020	Liaison committee on safety and health for contractors
September 9, 2020	Safety Day (Meeting to exchange safety information between each section, Workshop for fostering safety culture)
October-December	Refresher course on radiation safety for in-house staff (e-learning)
October 21,2020	Emergency drill assuming while the workers were in the Hadron experimental area, the beam was withdrawn, causing massive exposure
December 7, 2020	FY2020 J-PARC Safety Audit
January 7, 2021	KY training (Using an illustration sheet depicting the work situation, the participants discuss, think about it, come to an understanding r about possible hazards and countermeasures, and finally confirm the action goal by pointing and calling.)

Table 2. Major application items of the radiological license.

Facility	Items of an application
MLF	• Installation of the Fast Muon Experimental Facility • Expansion of the Slow Muon Experimental Facility
NU	• Addition of the drainage system (storage tank)
All	• A change of the site boundary of the J-PARC

Table 3. Radiation Safety Committee (RSC) and Radiation Safety Review Committee (RSRC) in FY2020

No.	Date	Major Issues
The Radiation Safety Committee		
35th	August 6, 2020	• The policy for radiological license update in FY2020
36th	March 22, 2021	• The proposal to increase the beam intensity from the original plan • The plan for radiological license update in FY2020
The Radiation Safety Review Committee		
27th	July 29, 2020	• Update of the radiological license for the Neutrino facilities • Installation of an X-ray generator • Revision of the local radiation protection rule of the J-PARC
28th	October 16, 2020	• Revision of the detailed rule of local radiation protection rule for J-PARC. • The policy for revision of the operational rules
29th	March 12, 2021	• Update of the radiological license for the Neutrino facilities • Installation of an X-ray generator

Table 4. Annual exposed doses in FY2020

	# of workers	Dose range x (mSv)				Collective dose (person · mSv)	Maximum dose (mSv)
		ND	0.1≤ x ≤1.0	1.0< x ≤5.0	5.0< x		
In-house staff	680	648	32	0	0	9.0	0.7
Users	717	717	0	0	0	0.0	0.0
Contractors	1,315	1,250	65	0	0	18.0	0.9
Total	2,705	2,608	97	0	0	27.1	0.9

User Service

Users Office (UO)

Outline

The J-PARC Users Office (UO) was established in 2007. It opened an office on the first floor of the IBARAKI Quantum Beam Research Center in Tokai-mura, in December 2008. The UO maintains the Tokai Dormitory for the J-PARC users. The UO provides on-site and WEB support with one-stop service for the utilization of the J-PARC. As of March 31, 2020, the UO had 12 staffs and 6 WEB Support SE staffs in the Users Affairs Section. The J-PARC Users, after the approval of their experiment, follow the administrative procedures outlined on the Users Office (UO) WEB Portal Site, related to their registration as a J-PARC User, radiation worker registration, safety education, accommodation, visa invitation letter and other requirements. Then, the UO staffs provide them with support by e-mail. After their arrival at the J-PARC, the UO provides on-site assistance to the J-PARC Users, like receiving the J-PARC ID, glass badge, and safety education. Since 2015, the UO had been doing its part to improve the J-PARC on-line experiment system and make it more user-friendly.

After completion of the experiments, the UO may return the experiment samples at User's cost after cooling the radioactive materials.

Map to the J-PARC Users Office

Activities of the UO

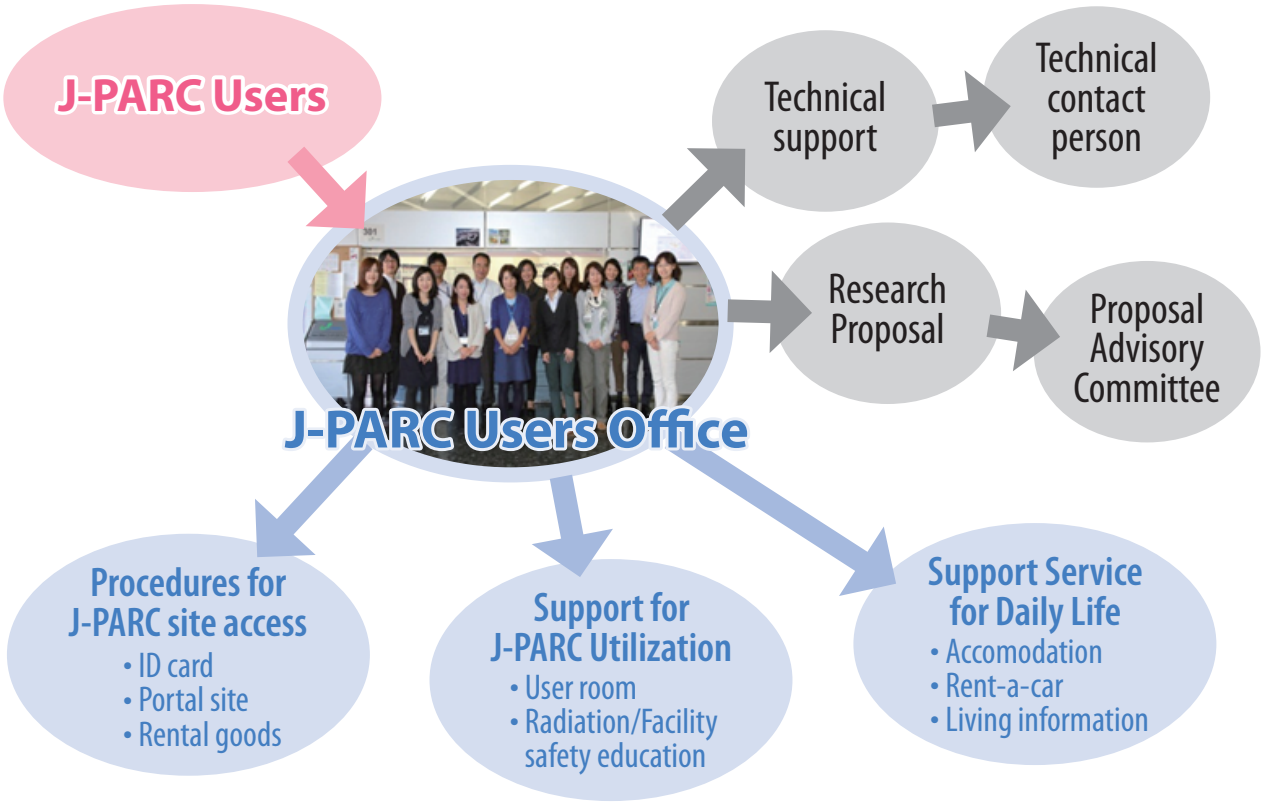

One stop service for J-PARC users

on the web

Step 1 User registration

New user: Getting user ID

Registered user: Annual registration, specifying of the visit

Approval of UO

Step 2-1 Obligatory application

Application form to visit J-PARC
Visit proposal (foreign nationality)
Reservation of safety training
On-line education video

Step 2-2 Optional application

J-PARC Card for facility access
Network registration
Radiation worker registration
Reservation of Dormitory
Invitation letter for Visa

on-site support

Step 3

Procedures upon arrival at the first day

Recieve J-Parc User ID card

Vehicle Permission pass

Safety education and dosimeter

Rental goods
Bicyle
PHS
Cafeteria card
Locker key
Office key

Step 4 J-PARC Experiment and meeting

Step 5 Leaving procedures

Retern all cards, keys, rental goods UO (office hours) or return box!

Users Office at IQBRC
Office hours(9:00-17:00, Mon.-Fri.)

Rental bicycle

Return box at IQBRC

User Statistics

Users in 2020 (Japanese/Foreigners, person-days)

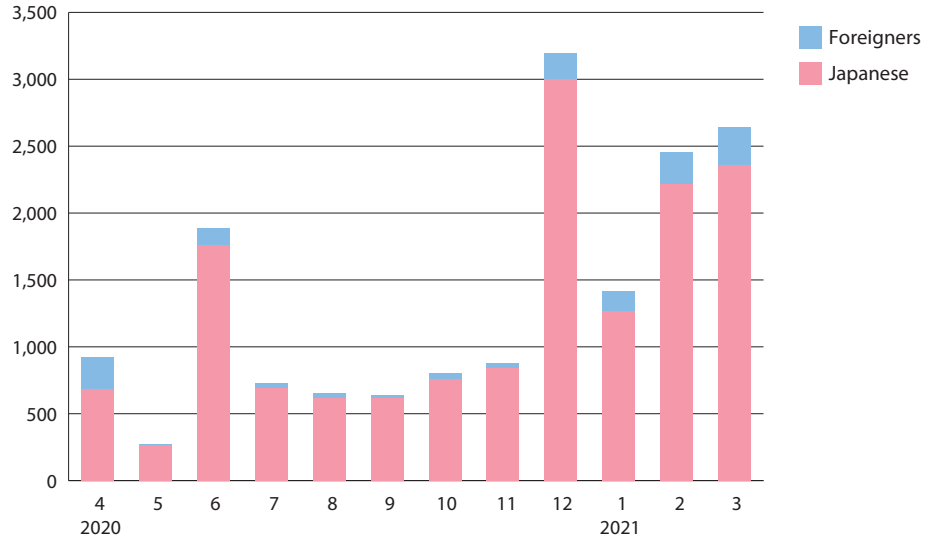

Users in 2020 (according to facilities, person-days)

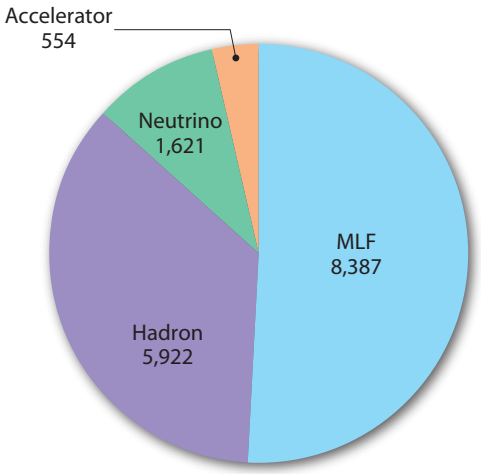

Users in 2020 (according to organizations, person-days)

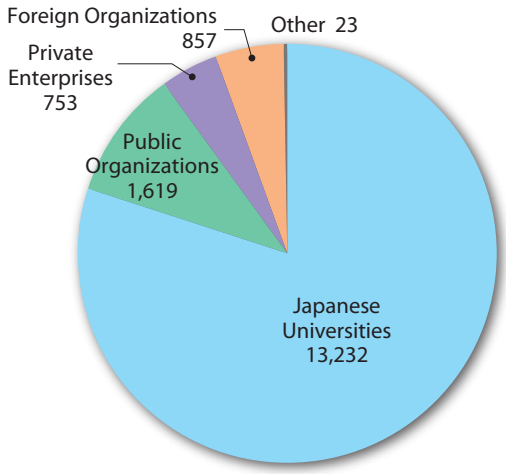

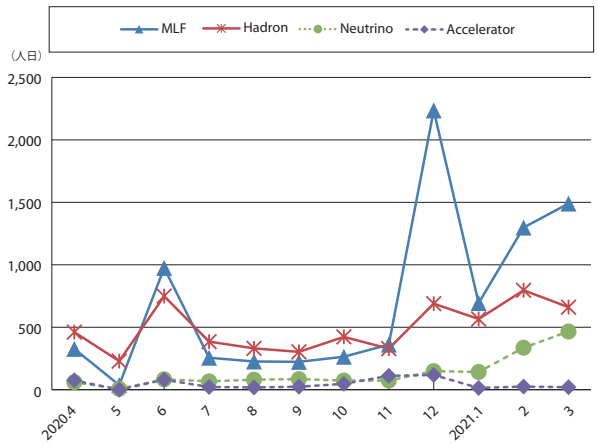

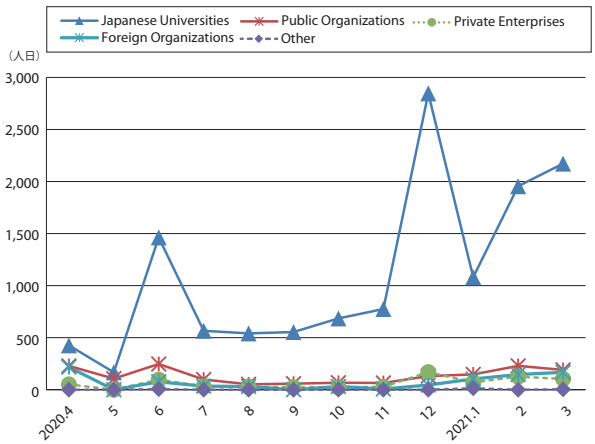

MLF Proposals Summary - FY2020

Due to the COVID-19 situation, 2020B and 2021A were combined into one proposal round. The experiment period for the proposals for "2020B+2021A" was from December 2020 to July 2021. Therefore, the proposals for 2021A are included in the FY2020 data as they cannot be counted separately.

Table 1. Breakdown of Proposals Numbers for the 2020 Rounds

Beam-line	Instrument		2020A		2020B+2021A		Full Year			
			Submitted	Approved	Submitted	Approved	Submitted		Approved	
			GU	GU	GU	GU	PU/S	IU	PU/S	IU
BL01	4D-Space Access Neutron Spectrometer - ***4SEASONS***		25(0)	10(0)	31(0)	11(0)	0	1	0	1
BL02	Biomolecular Dynamics Spectrometer - ***DNA***		24(0)	5(0)	36(2)	15(1)	2	2	2	2
BL03	IBARAKI Biological Crystal Diffractometer - ***iBIX***	(100-β)‡	0	0	3	3	0	0	0	0
		(β)†	0	0	0	0	48※	0	47※	0
BL04	Accurate Neutron-Nucleus Reaction Measurement Instrument - ***ANNRI***		5	4	11	5	1	1	1	1
BL05	Neutron Optics and Physics - ***NOP***		2	2	4	4	1	0	1	0
BL06	Village of Neutron Resonance Spin Echo Spectrometers - ***VIN ROSE***		1	1	7	4	1	0	1	0
BL08	Super High Resolution Powder Diffractometer - ***SuperHRPD***		13	8	19	11	1	0	1	0
BL09	Special Environment Powder Diffractometer - ***SPICA***		2	2	1	1	1	0	1	0
BL10	Neutron Beamline for Observation and Research Use - ***NOBORU***		10	7	15	10	3	1	3	1
BL11	High-Pressure Neutron Diffractometer - ***PLANET***		21(0)	15(0)	14(0)	12(0)	0	1	0	1
BL12	High Resolution Chopper Spectrometer - ***HRC***		5	4	11	8	1	0	1	0
BL14	Cold-Neutron Disk-Chopper Spectrometer - ***AMATERAS***		25	8	36	7	3	1	3	1
BL15	Small and Wide Angle Neutron Scattering Instrument - ***TAIKAN***		35(0)	15(0)	50(2)	20(2)	2	3	2	3
BL16	Soft Interface Analyzer - ***SOFIA***		14	14	29	25	0	1	0	1
BL17	Polarized Neutron Reflectometer - ***SHARAKU***		18(2)	11(1)	20(1)	14(1)	2	3	2	3
BL18	Extreme Environment Single Crystal Neutron Diffractometer - ***SENJU***		18(0)	9(0)	28(0)	10(0)	1	1	1	1
BL19	Engineering Materials Diffractometer - ***TAKUMI***		14	11	31	21	1	1	1	1
BL20	IBARAKI Materials Design Diffractometer - ***iMATERIA***	(100-β)‡	9	6	8	6	0	0	0	0
		(β)†	26	26	36	36	22	0	22	0
BL21	High Intensity Total Diffractometer - ***NOVA***		25	19	20	10	1	0	1	0
BL22	Energy Resolved Neutron Imaging System - ***RADEN***		10(0)	10(0)	24(0)	16(0)	2	3	2	3
BL23	Polarized Neutron Spectrometer - ***POLANO***		1	1	2	2	1	0	1	0
D1	Muon Spectrometer for Materials and Life Science Experiments - ***D1***		15(0)	6(0)	20(0)	12(0)	1	1	1	1
D2	Muon Spectrometer for Basic Science Experiments - ***D2***		3(1)	3(1)	8(0)	4(0)	1	1	1	1
S1	General purpose μSR spectrometer - ***ARTEMIS***		22(2)	16(2)	46(0)	24(0)	1	1	1	1
U1A	Ultra Slow Muon Microscope - ***U1A***		0	0	0	0	0	1	0	1
U1B	Transmission Muon Microscope - ***U1B***		0	0	0	0	0	1	0	1
Total			***343***	***213***	***509***	***290***	***87***	***24***	***86***	***24***

GU : General Use **PU** : Project Use or Ibaraki Pref. Project Use **S** : S-type Proposals
IU : Instrument Group Use
† : Ibaraki Pref. Exclusive Use Beamtime (β = 80% in FY2020)
‡ : J-PARC Center General Use Beamtime (100-β = 20% in FY2020)
( ) : Proposal Numbers under the New User Promotion (BL01, BL02, BL11, BL15, BL17, BL18, BL22) or P-type proposals (D1,D2, S1) in GU

※ Proposal rounds are held twice per year (for each of the A and B periods), with only the yearly total shown above.
The actual total number of proposals in each beamline named in the table does not match the number shown in the "Total" cell, because some proposals are submitted or approved across multiple beamlines.

Table 2. Proposals Numbers of Long Term Proposal for the 2020 Rounds

Application FY	Submitted	Approved
2018	9	5
2019	9	4
2020	13	3

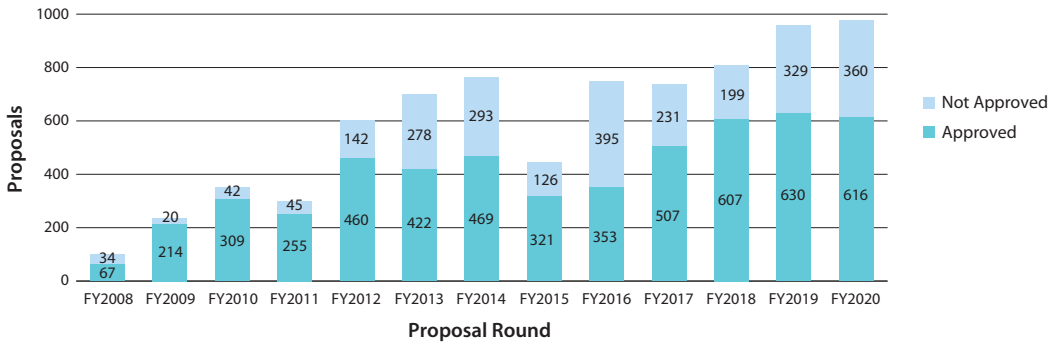

Fig. 1. MLF Proposal Numbers over Time

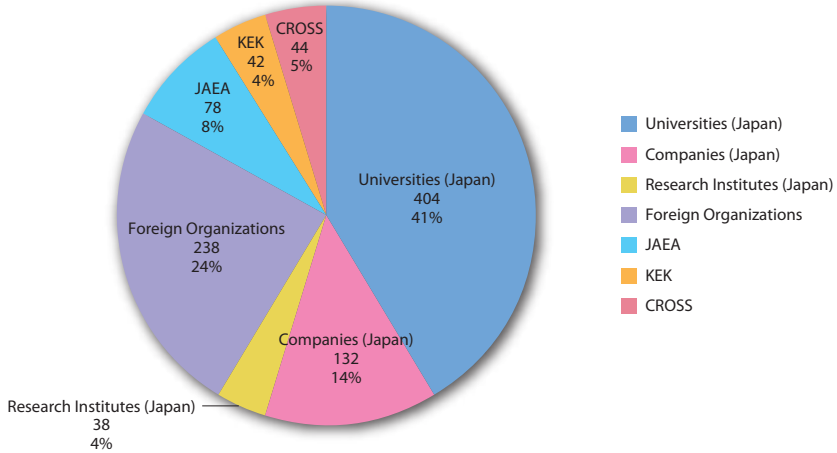

Fig. 2. Origin of Submitted Proposals by affiliation - FY2020 (2020A, 2020B+2021A)

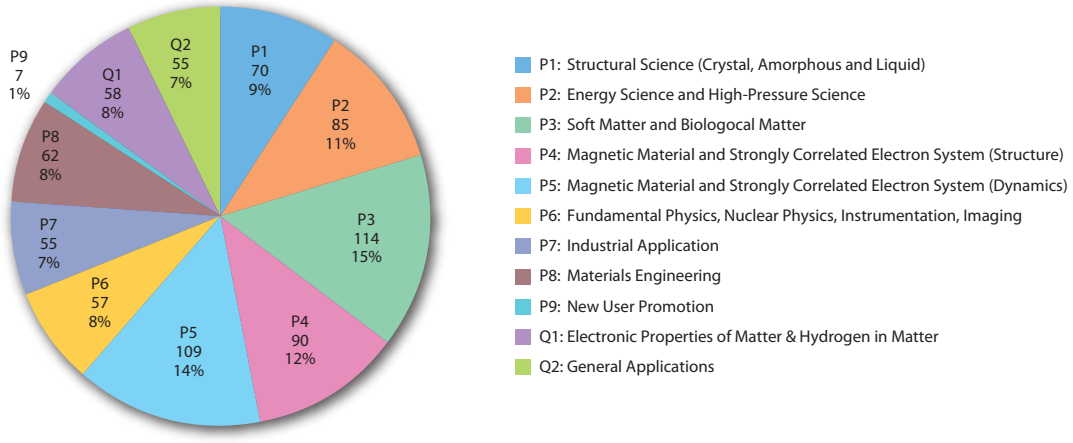

Fig. 3. Submitted Proposals by Sub-committee/Expert Panel –2020 (2020A, 2020B+2021A)

J-PARC PAC Approval Summary for the 2020 Rounds

	(Co-) Spokespersons	Affiliation	Title of the experiment	Approval status (PAC recommendation)	Beamline	Status
E03	K.Tanida	JAEA	Measurement of X rays from X^- Atom	Stage 2	K1.8	Data taking
P04	J.C.Peng, S.Sawada	U of Illinois at Urbana-Champaign; KEK	Measurement of High-Mass Dimuon Production at the 50-GeV Proton Synchrotron	Deferred	Primary	
E05	T.Nagae	Kyoto U	Spectroscopic Study of X-Hypernucleus, $^{12}_{X}$Be, via the ^{12}C(K^-, K^+) Reaction	Stage 2 New experiment E70 based on the S-2S spectrometer	K1.8	Finished
E06	J.Imazato	KEK	Measurement of T-violating Transverse Muon Polarization in $K^+ \to p^0 m^+ n$ Decays	E36 as the first step	K1.1BR	
E07	K.Imai, K.Nakazawa, H.Tamura	JAEA, Gifu U, Tohoku U	Systematic Study of Double Strangeness System with an Emulsion-counter Hybrid Method	Stage 2	K1.8	Finished Data analysis
E08	A.Krutenkova	ITEP	Pion double charge exchange on oxygen at J-PARC	Stage 1	K1.8	
E10	A.Sakaguchi, T.Fukuda	Osaka U, Osaka EC U	Production of Neutron-Rich Lambda-Hypernuclei with the Double Charge-Exchange Reaction (Revised from Initial P10)	Stage 2	K1.8	Li run finished, Be target run with S-2S
E11	A.K.Ichikawa, F.Sanchez	KEK	Tokai-to-Kamioka (T2K) Long Baseline Neutrino Oscillation Experimental Proposal	Stage 2	neutrino	Data taking
E13	H.Tamura	Tohoku U	Gamma-ray spectroscopy of light hypernuclei	Stage 2	K1.8	Finished
E14	T.Yamanaka	Osaka U	Proposal for $K_L \to p^0$ n n-bar Experiment at J-PARC	Stage 2	KL	Data taking
E15	M.Iwasaki, T.Nagae	RIKEN, Kyoto U	A Search for deeply-bound kaonic nuclear states by in-flight 3He(K-, n) reaction	Stage 2	K1.8BR	Finished
E16	S.Yokkaichi	RIKEN	Measurements of spectral change of vector mesons in nuclei (previously "Electron pair spectrometer at the J-PARC 50-GeV PS to explore the chiral symmetry in QCD")	Stage 2 for Run 0	High p	Data taking
E17	R.Hayano, H.Outa	U Tokyo, RIKEN	Precision spectroscopy of Kaonic ^{3}He 3d->2p X-rays	Registered as E62 with an updated proposal	K1.8BR	
E18	H.Bhang, H.Outa, H.Park	SNU, RIKEN, KRISS	Coincidence Measurement of the Weak Decay of $^{12}_{\Lambda}$C and the three-body weak interaction process	Stage 2	K1.8	
E19	M.Naruki	KEK	High-resolution Search for Q^+ Pentaquark in $p^-p \to K^-X$ Reactions	Stage 2	K1.8	Finished
E21	Y.Kuno	Osaka U	An Experimental Search for μ – e Conversion at a Sensitivity of 10^{-16} with a Slow-Extracted Bunched Beam	Phase-I Stage 2 PAC recommends producing a more detailed schedule to ensure a timely start.	COMET	
E22	S.Ajimura, A.Sakaguchi	Osaka U	Exclusive Study on the Lambda-N Weak Interaction in A=4 Lambda-Hypernuclei	Stage 1	K1.8	
T25	S.Mihara	KEK	Extinction Measurement of J-PARC Proton Beam at K1.8BR	Test Experiment	K1.8BR	Finished
E26	K.Ozawa	KEK	Search for w-meson nuclear bound states in the $p-+^AZ \to n+^{(A-1)}_{w}(Z-1)$ reaction, and for w mass modification in the in-medium $w \to p^0 g$ decay	Stage 1	K1.8	
E27	T.Nagae	Kyoto U	Search for a nuclear Kbar bound state K^-pp in the d(p^+, K^+) reaction	Stage 2	K1.8	Fisnished
E29	H.Ohnishi	RIKEN	Search for f-meson nuclear bound states in the pbar + $^AZ \to f + ^{(A-1)}_{f}(Z-1)$ reaction	Stage 1	K1.1	
E31	H.Noumi	Osaka U	Spectroscopic study of hyperon resonances below KN threshold via the (K^-,n) reaction on Deuteron	Stage 2	K1.8BR	Finished Data analysis
T32	A.Rubbia	ETH, Zurich	Towards a Long Baseline Neutrino and Nucleon Decay Experiment with a next-generation 100 kton Liquid Argon TPC detector at Okinoshima and an intensity upgraded J-PARC Neutrino beam	Test Experiment	K1.1BR	Finished
P33	H.M.Shimizu	Nagoya U	Measurement of Neutron Electric Dipole Moment	Deferred	Linac	
E34	T. Mibe	KEK, RIKEN	An Experimental Proposal on a New Measurement of the Muon Anomalous Magnetic Moment g-2 and Electric Dipole Moment at J-PARC	Stage 2	MLF	
E36	M.Kohl, S.Shimizu	Hampton U, Osaka U	Measurement of $G(K^+ \to e^+ n)/G(K^+ \to m^+ n)$ and Search for heavy sterile neutrinos using the TREK detector system	Stage 2	K1.1BR	Finished Data analysis
E40	K.Miwa	Tohoku U	Measurement of the cross sections of Σp scatterings	Stage 2	K1.8	Finished Data analysis
P41	M.Aoki	Osaka U	An Experimental Search for μ – e Conversion in Nuclear Field at a Sensitivity of 10^{-14} with Pulsed Proton Beam from RCS	Deferred	MLF	Reviewed in MLF/IMSS
E42	J.K.Ahn	Pusan National U	Search for H-Dibaryon with a Large Acceptance Hyperon Spectrometer	Stage 2	K1.8	
E45	K.H.Hicks, H.Sako	Ohio U, JAEA	3-Body Hadronic Reactions for New Aspects of Baryon Spectroscopy	Stage 2 PAC requests that the group further examine ways to reduce the total beam time requested and to find an efficient running scheme, including quick but careful beam tuning.	K1.8	
T46	K.Ozawa	KEK	EDIT2013 beam test program	Test Experiment	K1.1BR	Abandonded
T49	T.Maruyama	KEK	Test for 250L Liquid Argon TPC	Test Experiment	K1.1BR	Withdrawn

	(Co-) Spokespersons	Affiliation	Title of the experiment	Approval status (PAC recommendation)	Beamline	Status
E50	H.Noumi	Osaka U	Charmed Baryon Spectroscopy via the (π, D^{*-}) reaction	Stage 1 The FIFC, IPNS, and E50 should investigate the beam-line feasibility	High p	
T51	S.Mihara	KEK	Research Proposal for COMET(E21) Calorimeter Prototype Beam Test	Test Experiment	K1.1BR	had to be stopped
T52	Y.Sugimoto	KEK	Test of fine pixel CCDs for ILC vertex detector	Test Experiment	K1.1BR	not performed yet
T53	D.Kawama	RIKEN	Test of GEM Tracker, Hadron Blind Detector and Lead-glass EMC for the J-PARC E16 experiment	Test Experiment	K1.1BR	not performed yet
T54	K.Miwa	Tohoku U	Test experiment for a performance evaluation of a scattered proton detector system for the Σp scattering experiment E40	Test Experiment	K1.1BR	not performed yet
T55	A.Toyoda	KEK	Second Test of Aerogel Cherenkov counter for the J-PARC E36 experiment	Test Experiment	K1.1BR	had to be stopped
E56	T.Maruyama	KEK	A Search for Sterile Neutrino at J-PARC Materials and Life Science Experimental Facility	Stage 2	MLF	Data taking
E57	J. Zmeskal	Stefan Meyer Institute for Subatomic Physics	Measurement of the strong interaction induced shift and width of the 1s state of kaonic deuterium at J-PARC	Stage 1	K1.8BR	in preparation
P58	M. Yokoyama	U. Tokyo	A Long Baseline Neutrino Oscillation Experiment Using J-PARC Neutrino Beam and Hyper-Kamiokande	Deferred	neutrino	
T59	A. Minamino	Kyoto U	A test experiment to measure neutrino cross sections using a 3D grid-like neutrino detector with a water target at the near detector hall of J-PARC neutrino beam-line	To be arranged by IPNS and KEK-T2K	neutrino monitor bld	Finished
T60	T. Fukuda	Toho U	Proposal of an emulsion-based test experiment at J-PARC	Arranged by IPNS and KEK-T2K	neutrino monitor bld	Finished
E61	M. Wilking	Stony Brook U	NuPRISM/TITUS	Superseded. E61 has been adopted in Hyper-K as IWCD. IWCD is reviewed by HK-PAC.	neutrino	
E62	R. Hayano, S. Okada, H. Outa	U. Tokyo, RIKEN	Precision Spectroscopy of kaonic atom X-rays with TES	Stage 2	K1.8BR	Finished
E63	H. Tamura	Tohoku U	Gamma-ray spectroscopy of light hypernuclei II	Stage 2	K1.1	BL not ready yet. Exp. in preparation
T64	Y. Koshio	Okayama U	Measurement of the gamma-ray and neutron background from the T2k neutrino/anti-neutrino at J-PARC B2 Hall	Arranged by IPNS and KEK-T2K	neutrino	
E65	A.K.Ichikawa, F.Sanchez	Kyoto U	Proposal for T2K Extended Run	Stage-2	neutrino	
T66	T. Fukuda	Nagoya U	Proposal of an emulsion-based test experiment at J-PARC	Test Experiment	neutrino	
P67	I. Meigo	JAEA	Measurement of displacement cross section of proton in energy region between 3 and 30 GeV for high-intensity proton accelerator facility	Carry out the experiment within the framework of facility development	MR	
T68	T. Fukuda	Nagoya U	Extension of T60/T66 Experiment: Proposal for the Run from 2017 Autumn	Test Experiment	neutrino	
E69	A. Minamino	Yokohama National U	Study of neutrino-nucleus ineraction at around 1GeV using cuboid lattice neutrino detector, WAGASHI, muon range detectors and magnetized spectrometer, Baby MIND, at J-PARC neutrino monitor hall	Superseded. Merged with T2K.	neutrino	
E70	T. Nagae	Kyoto U	Proposal for the next E05 run with the S-2S spectrometer	Stage-2	K1.8	
E71	T. Fukuda	Nagoya U	Proposal for precise measurement of neutrinop-water cross-section in NINJA physics run	Stage-2	neutrino	Data taking
E72	K. Tanida	JAEA	Search for a Narrow Λ* Resonance using the p(K-, Λ)η Reaction with the hypTPC Detector	Stage-2	K1.8BR	
E73	Yue Ma	RIKEN	$^{3}_{\Lambda}$H and $^{4}_{\Lambda}$H mesonic weak decay lifetime measurement with ^{3,4}He(K^-,π^0)$^{3,4}_{\Lambda}$H reaction	Stage-1	K1.8BR	
P74	A.Feliciello	INFN, Torino	Direct measurement of the 3ΛH and 4ΛH lifetimes using the 3,4He(π-,K0)3,4ΛH reactions	Rejected	K1.1	
E75	H.Fujioka	Tokyo Inst. Tech,	Decay Pion Spectroscopy of 5$\Lambda\Lambda$H Produced by Ξ-hypernuclear Decay	Stage-1	K1.8	
P76	H.M.Shimizu	Nagoya U	Searches for the Breaking of the Time Reversal Invariance in Polarized Epithermal Neutron Optics	Deferred	MLF	
T77	Yue Ma	RIKEN	Feasibility study for 3ΛH mesonic weak decay lifetime measurement with 3,4He(K-,π0)3,4ΛH reaction	PAC supoorts the ontinuation of T77 by an explorative run with the 3He target.	K1.8BR	
T78	H.Nishiguchi	KEK	8GeV Operation Test and Extinction Measurement	Test Experiment	K1.8BR	
P79	T.Ishikawa	Tohoku U	Search for an I=3 dibaryon resonance	PAC suggests stage-1 status	High p	
P80	F.Sakuma	RIKEN	Systematic investgatin of the light kaonic nuclei	PAC suggests stage-1 status	K1.8BR	
T81	T.Fukuda	Nagoya U	Proposal of test experiment for technical improvements of neutrino measurements with nuclear emulsion detector	Test Experiment	neutrino	
P82	T.Maruyama	KEK	JSNS2-II	PAC suggests stage-1 status	MLF	

Organization and Committees

Organization Structure

J-PARC Center Management System Chart

as of April 1, 2020

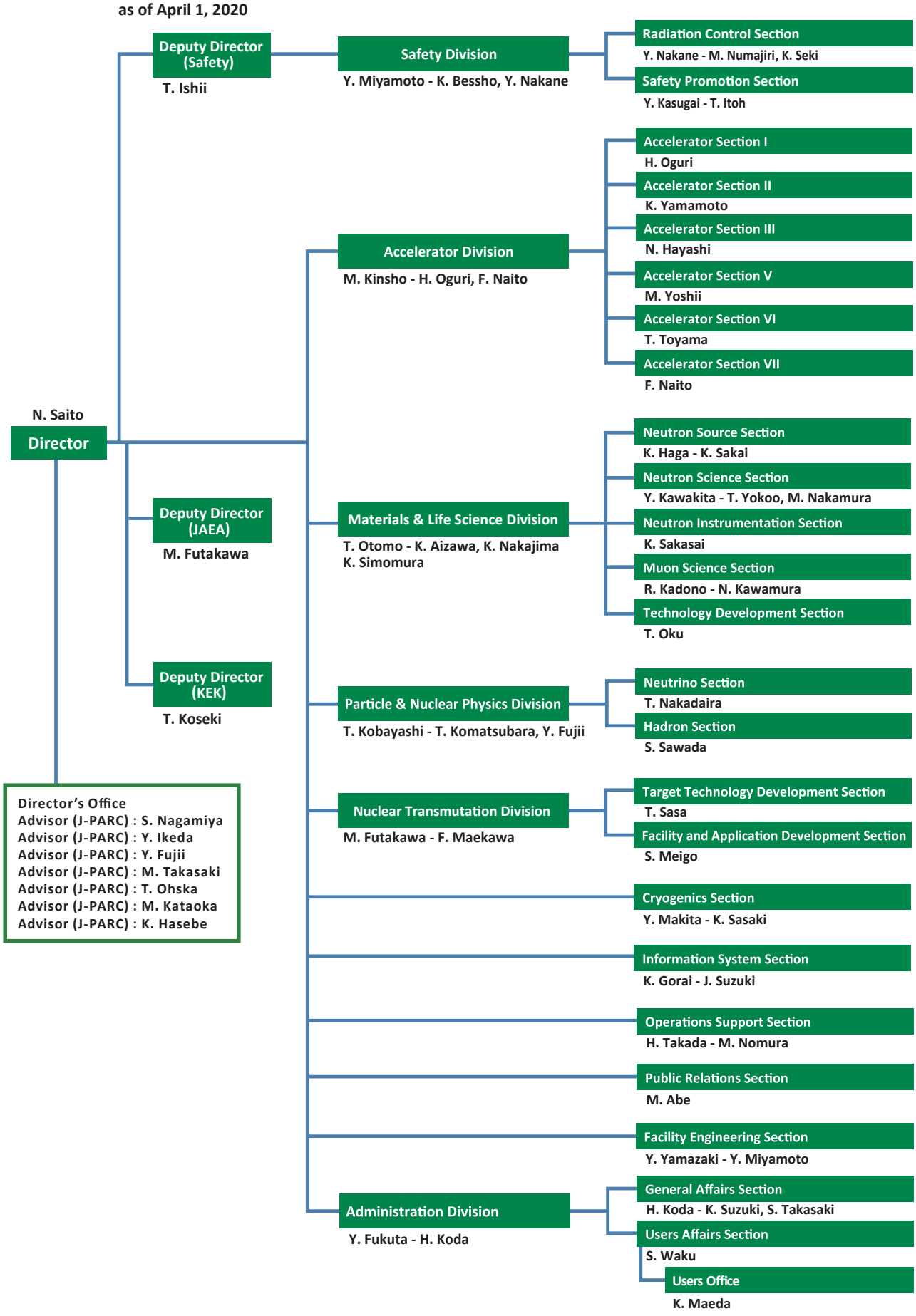

Members of the Committees Organized for J-PARC

(as of March, 2020)

1) Steering Committee (*) Chair

Junji Haba (*)	High Energy Accelerator Research Organization (KEK), Japan
Koki Uchimaru	High Energy Accelerator Research Organization (KEK), Japan
Katsuo Tokushuku	High Energy Accelerator Research Organization (KEK), Japan
Nobuhiro Kosugi	High Energy Accelerator Research Organization (KEK), Japan
Seiya Yamaguchi	High Energy Accelerator Research Organization (KEK), Japan
Yukitoshi Miura (*)	Japan Atomic Energy Agency (JAEA), Japan
Kenji Sudo	Japan Atomic Energy Agency (JAEA), Japan
Masayasu Takeda	Japan Atomic Energy Agency (JAEA), Japan
Toshiyuki Momma	Japan Atomic Energy Agency (JAEA), Japan
Hiroyuki Oigawa	Japan Atomic Energy Agency (JAEA), Japan
Naohito Saito	J-PARC Center, Japan

2) International Advisory Committee (*) Chair

Jean-Michel Poutissou (*)	TRIUMF, Canada
Thomas Prokscha	Paul Scherrer Institute (PSI), Switzerland
Jun Sugiyama	Comprehensive Research Organization for Science and Society (CROSS), Japan
Jie Wei	Michigan State University, USA
Roland Garoby	European Spallation Source (ERIC), Sweden *Retired
Eckhard Elsen	European Organization for Nuclear Research (CERN), Switzerland
Patricia McBride	Fermi National Accelerator Laboratory (FNAL), USA
Robert Tribble	Brookhaven National Laboratory (BNL), USA
Donald F. Geesaman	Argonne National Laboratory, USA
Paolo Giubellino	GSI Helmholtzzentrum für Schwerionenforschung, Germany
Hamid Aït Abderrahim	SCK • CEN, Belgium
Akira Hasegawa	Tohoku University, Japan
Paul Langan	Oak Ridge National Laboratory (ORNL), USA
Hidetoshi Fukuyama	Tokyo University of Science, Japan
Dan Alan Neumann	National Institute of Standards and Technology (NIST), USA
Andrew Dawson Taylor	Science and Technology Facilities Council (STFC), UK
Helmut Schober	Institut Laue–Langevin, France

3) User Consultative Committee for J-PARC (*) Chair

Tsuyoshi Nakaya	Kyoto University, Japan
Taku Yamanaka	Osaka University, Japan
Toshinori Mori	University of Tokyo, Japan
Takashi Kobayashi	High Energy Accelerator Research Organization (KEK), Japan
Hirokazu Tamura	Tohoku University, Japan
Tomofumi Nagae (*)	Kyoto University, Japan
Hiroyuki Noumi	Osaka University, Japan
Shinya Sawada	High Energy Accelerator Research Organization (KEK), Japan
Fuminori Sakuma	RIKEN, Japan
Masaki Fujita	Tohoku University, Japan
Naoya Torikai	Mie University, Japan
Osamu Yamamuro	University of Tokyo, Japan
Yasushi Idemoto	Tokyo University of Science, Japan
Kazuhisa Kakurai	Comprehensive Research Organization for Science and Society (CROSS), Japan
Toshiya Otomo	High Energy Accelerator Research Organization (KEK), Japan
Jun Akimitsu	Okayama University/Hiroshima University, Japan
Tadashi Adachi	Sophia University, Japan
Koichiro Shimomura	High Energy Accelerator Research Organization (KEK), Japan
Jun Sugiyama	Comprehensive Research Organization for Science and Society (CROSS), Japan
Hiroyuki Kishimoto	Sumitomo Rubber Industries, Ltd. Japan
Hideto Imai	Nissan Analysis and Research Center, Japan
Masahiro Hino	Kyoto University, Japan
Hironori Kodama	Ibaraki Prefecture, Japan
Satoru Yamashita	University of Tokyo, Japan
Cheol-Ho Pyeon	Kyoto University, Japan
Kazufumi Tsujimoto	Japan Atomic Energy Agency (JAEA), Japan

4) Accelerator Technical Advisory Committee (*) Chair

Wolfram Fischer	Brookhaven National Laboratory (BNL), USA
Mats Lindroos	European Spallation Source, Sweden
John Thomason	Science and Technology Facilities Council (STFC), UK
Sheng Wang	Institute of High Energy Physics (IHEP), China
Toshiyuki Shirai	National Institutes for Quantum and Radiological Science and Technology (QST),Japan
Alexander V Aleksandrov	Oak Ridge National Laboratory (ORNL), USA
Jie Wei (*)	Michigan State Univ., USA
Robert Zwaska	Fermi National Accelerator Laboratory (FNAL), USA
Simone Gilardoni	European Organization for Nuclear Research (CERN), Switzerland

5) Neutron Advisory Committee (*) Chair

Robert McGreevy (*)	Science and Technology Facilities Council (STFC), UK
Bertrand Blau	Paul Scherrer Institut (PSI), Switzerland
Michael Dayton	Oak Ridge National Laboratory (ORNL), USA
Yoshiaki Kiyanagi	Nagoya University, Japan
Christiane Alba-Simionesco	Laboratoire Leon Brilloin (LLB), France
Jamie Schulz	Australian Nuclear Science and Technology Organization(ANSTO), Australia
Andreas Schreyer	European Spallation Source, Sweden
Sung-Min Choi	Korea Advanced Institute of Science and Technology, Korea
Yoshie Otake	RIKEN, Japan
Masaaki Sugiyama	Kyoto University, Japan
Christian Rüegg	Paul Scherrer Institute (PSI), Switzerland

6) Muon Advisory Committee (*) Chair

Martin Månsson	KTH Royal Institute of Technology, Sweden
Thomas Prokscha (*)	Paul Scherrer Institut (PSI), Switzerland
Andrew MacFarlane	University of British Columbia, Canada
Klaus Kirch	Paul Scherrer Institut (PSI), Switzerland
Kenya Kubo	International Chiristian University, Japan
Tadayuki Takahashi	University of Tokyo, Japan
Takashi Nakano	Osaka University, Japan
Hiroshi Amitsuka	Hokkaido University, Japan

7) Radiation Safety Committee (*) Chair

Yoshitomo Uwamino (*)	Japan Radioisotope Association, Japan
Yoshihiro Asano	High Energy Accelerator Research Organization (KEK), Japan
Hiroshi Watabe	Tohoku University, Japan
Takeshi Iimoto	University of Tokyo, Japan
Takeshi Murakami	National Institutes for Quantum and Radiological Science and Technology (QST), Japan
Hitoshi Kobayashi	High Energy Accelerator Research Organization (KEK), Japan
Yoshihito Namito	High Energy Accelerator Research Organization (KEK), Japan
Shinichi Sasaki	High Energy Accelerator Research Organization (KEK), Japan
Hiroyuki Oigawa	Japan Atomic Energy Agency (JAEA), Japan
Takumi Nemoto	Japan Atomic Energy Agency (JAEA), Japan
Nobuyuki Kinouchi	Japan Atomic Energy Agency (JAEA), Japan

8) Radiation Safety Review Committee (*) Chair

Tetsuro Ishii (*)	Japan Atomic Energy Agency (JAEA), Japan
Yukihiro Miyamoto	Japan Atomic Energy Agency (JAEA), Japan
Masaharu Numajiri	High Energy Accelerator Researchi Organization (KEK), Japan
Hidetoshi Kikunaga	Tohoku University, Japan
Hiroshi Yashima	Kyoto Univaersity, Japan
Kanenobu Tanaka	Institute of Physical and Chemical Research (RIKEN), Japan
Nobuyuki Chiga	National Institute for Quantum and Radiological Science and Technoloty (QST), Japan
Toshiro Itoga	Japan Synchrotron Radiation Research Institute (JASRI), Japan
Koji Kiriyama	Comprehensive Reserch Organization for Science and Society (CROSS), Japan
Akira Hirose	Japan Atomic Energy Agency (JAEA), Japan
Makoto Kobayashi	Japan Atomic Energy Agency (JAEA), Japan
Nobukazu Toge	High Energy Accelerator Researchi Organization (KEK), Japan
Kazuyoshi Masumoto	High Energy Accelerator Researchi Organization (KEK), Japan
Michikazu Kinsho	Japan Atomic Energy Agency (JAEA), Japan
Yoshiaki Fujii	High Energy Accelerator Researchi Organization (KEK), Japan
Takeshi Komatsubara	High Energy Accelerator Researchi Organization (KEK), Japan
Kazuya Aizawa	Japan Atomic Energy Agency (JAEA), Japan

9) MLF Advisory Board (*) Chair

Takamitsu Kohzuma	Ibaraki University, Japan
Takahisa Arima	University of Tokyo, Japan
Taku Sato	Tohoku University, Japan
Yoji Koike	Tohoku University, Japan
Masaaki Sugiyama (*)	Kyoto University, Japan
Yoshiharu Sakurai	Japan Synchrotron Radiation Research Institute(JASRI), Japan
Jun Takahara	Kyusyu University, Japan
Takashi Kamiyama	Hokkaido University, Japan
Toshio Yamaguchi	Fukuoka University, Japan
Hiroshi Amitsuka	Hokkaido University, Japan
Kenya Kubo	International Christian University, Japan
Toshiya Otomo	High Energy Accelerator Research Organization (KEK), Japan
Hideki Seto	High Energy Accelerator Research Organization (KEK), Japan
Takashi Kamiyama	High Energy Accelerator Research Organization (KEK), Japan
Shinichi Itoh	High Energy Accelerator Research Organization (KEK), Japan
Koichiro Shimomura	High Energy Accelerator Research Organization (KEK), Japan
Ryosuke Kadono	High Energy Accelerator Research Organization (KEK), Japan
Kazuhisa Kakurai	Comprehensive Research Organization for Science and Society (CROSS), Japan
Kazuya Aizawa	Japan Atomic Energy Agency (JAEA), Japan
Masayasu Takeda	Japan Atomic Energy Agency (JAEA), Japan
Kazuhiko Soyama	Japan Atomic Energy Agency (JAEA), Japan
Kenji Nakajima	Japan Atomic Energy Agency (JAEA), Japan
Yukinobu Kawakita	Japan Atomic Energy Agency (JAEA), Japan
Jun-ichi Suzuki	Comprehensive Research Organization for Science and Society (CROSS), Japan

10) Program Advisory Committee (PAC) for Nuclear and Particle Physics Experiments at the J-PARC 50Gev Proton Synchrotron

(*) Chair

Ichiro Adachi	High Energy Accelerator Research Organization (KEK), Japan
Motoi Endo	High Energy Accelerator Research Organization (KEK), Japan
Yoshitaka Itow	Nagoya University, Japan
Takahiro Kawabata	Osaka University, Japan
Hiroaki Ohnishi	Tohoku University, Japan
Akira Ohnishi	Kyoto University, Japan
Kohei Yorita	Waseda University, Japan
Patrick Achenbach	Mainz University, Germany
Monika Blanke	Karlsruhe Institute of Technology, Germany
Laura Fields	Fermi National Accelerator Laboratory (FNAL), USA
David Jaffe	Brookhaven National Laboratory (BNL), USA
Francois Le Diberder	The French National Institute of Nuclear and Particle Physics (IN2P3), France
Kam-Biu Luk	University of California at Berkley, USA
Anthony William Thomas	University of Adelaide, Australia
Nu Xu	Lawrence Berkeley National Laboratory, USA
Rikutaro Yoshida (*)	Argonne National Laboratory, USA

11) TEF Technical Advisory Committee

(*) Chair

Marc Schyns (*)	SCK • CEN, Belgium
Michael Butzek	Forschungszentrum Jülich, Germany
Michael Wohlmuther	Paul Scherrer Institut (PSI), Switzerland
Yoshiaki Kiyanagi	Nagoya University, Japan
Keishi Sakamoto	National Institutes for Quantum and Radiological Science and Technology (QST), Japan
Georg Müller	Karlsruhe Institute of Technology, Germany
Masatoshi Kondo	Tokyo Institute of Technology, Japan

Main Parameters

Present main parameters of Accelerator

Linac	
Accelerated Particles	Negative hydrogen
Energy	400 MeV
Peak Current	50 mA
Pulse Width	0.385 ms for MLF 0.50 ms for MR-FX 0.20 ms for MR-SX
Repetition Rate	25 Hz
Freq. of RFQ, DTL, and SDTL	324 MHz
Freq. of ACS	972 MHz
RCS	
Circumference	348.333 m
Injection Energy	400 MeV
Extraction Energy	3 GeV
Repetition Rate	25 Hz
RF Frequency	0.938 MHz → 1.67 MHz
Harmonic Number	2
Number of RF cavities	12
Number of Bending Magnet	24
Main Ring	
Circumference	1567.5 m
Injection Energy	3 GeV
Extraction Energy	30 GeV
Repetition Rate	~0.4 Hz
RF Frequency	1.67 MHz → 1.72 MHz
Harmonic Number	9
Number of RF cavities	9
Number of Bending Magnet	96

Key parameters of Materials and Life Science Experimental Facility

Injection energy	3 GeV
Repetition rate	25 Hz
Neutron Source	
Target material	Mercury
Number of moderators	3
Moderator material	Liquid hydrogen
Moderator temperature/pressure	20 K/1.5 MPa
Number of neutron beam extraction ports	23
Muon production target	
Target material	Graphite
Number of muon beam extraction ports	4
Neutron instruments *	
Open for user program (general use)	21
Under commissioning/construction	0
Muon Instruments *	
Open for user program (general use)	3
Under commissioning/construction	1/0

(* As of August, 2021)

Events

Events

The University of Toyama and the J-PARC Center Signed a "Cooperative Agreement for Using the Experimental Facilities of the J-PARC Center in Promotion of Materials and Life Sciences Research and Hydrogen Isotopes Research"

On May 1, the University of Toyama and the J-PARC Center signed a cooperative agreement. Both organizations will build and promote close relationship to conduct research in fields, such as materials and life science and hydrogen isotope studies.

The University of Tokyo and KEK Sign MoU to promote the Hyper-Kamiokande Project

On May 25, the University of Tokyo and the High Energy Accelerator Research Organization (KEK) signed a memorandum of understanding (MoU) regarding the promotion of the Hyper-Kamiokande project. J-PARC accelerators will dramatically expedite the experiment.

Held 2020 General Assembly Meeting of the MLF

On June 9, the General Assembly of the J-PARC Materials and Life Science and Life Science Experimental Facility (MLF) was held remotely on Zoom. About 140 people participated in it, including the J-PARC Center, Comprehensive Research Organization for Science and Society (CROSS) Neutron Science and Technology Center, Ibaraki Prefecture and the universities in charge of the experimental equipment.

The Zoom meeting (PC screen view)

Arrangement on Research Cooperation between JAEA and the Karlsruhe Institute of Technology in the Field of ADS Development

JAEA and the Karlsruhe Institute of Technology (KIT) in Germany concluded the arrangement on the research cooperation in the field of Accelerator Driven nuclear transmutation System (ADS) development on June 18. Both organizations will exchange information in the area of the lead-Bismuth technology.

Toyota Group and J-PARC Collaborative Special Lecture Held Online

J-PARC and Toyota Group have advanced comprehensive collaborative research, which uses neutrons at J-PARC as a part of the development of hydrogen energy related to taking measures against global warming. On June 30, the J-PARC Center held an online lecture event for collaboration. Participants exchanged information on the FC technology.

Group photo with participants

30th J-PARC PAC Held Online

The J-PARC Program Advisory Committee for Nuclear and Particle Physics Experiments (J-PARC PAC) was held as an online three-day meeting starting on July 20. The advice by the committee regarding new research proposals and group reports will be compiled.

Tokai Village, KEK Sign "Agreement on Facility Use in Event of Disaster"

On August 4, the Inter-University Research Institute Corporation High Energy Accelerator Research Organization (KEK) and Tokai Village have signed "Agreement on Facility Use in the Event of a Disaster".

It aims to make J-PARC users' accommodations available as evacuation shelters upon request of the Tokai Village for cooperation in a disaster. The J-PARC Center Director Naohito Saito, Deputy Director Tadashi Koseki, Tokai Village Mayor Osamu Yamada and KEK Director General Masanori Yamauchi attended the signing ceremony.

From the left, Deputy Director T. Koseki, Director N. Saito, Village Mayor O. Yamada, Associate Village Mayor H. Hagitani

"Safety Day"

The J-PARC Center established May 23 as a "Safety Day" after a radioactive material leak accident in 2013. Due to the spread of the novel coronavirus, the annual event was held on September 9.

The J-PARC Director Naohito Saito gave awards for six good practices on safety. The category is divided into four fields of "The most Frequent Good Practices Award", "Safety Consideration Award", "Creativity Award", and "Sanitation Consideration Award".

After the ceremony, there was a lecture on safe behavior, and the event was closed with the remarks of the Deputy Director of Safety of the J-PARC Center, Tetsuro Ishii.

Mr. D. Yamazaki of the Neutron Instrumentation Section receiving a commendation (right)

6th J-PARC Media Meeting Held Online

The 6th J-PARC Media Meeting was held on September 30 by videoconference. Nine people from seven companies participated. Neutron Science Section's Takenao Shinohara, who is in charge of the neutron imaging system RADEN, gave examples of non-destructive observation. Other discussed topics were the plan of the Muon g-2/EDM experiment, the ongoing experiment at the US Fermilab, and the visualization of water in a fuel cell using neutrons.

J-PARC Science Class "Can World's Smallest Top Explain Nobel Prize-class Discovery?!- Accelerator Research to Elucidate Small World Using Large Device-"

The J-PARC Center organized a science experiment class at the Hitachi Civic Center Science Museum on October 4. The instructors were Dr. Tsutomu Mibe of Hadron Section, Deputy Director of the MLF Division Dr. Koichiro Shimomura, and Dr. Masashi Otani of Accelerator Section VII. All of them are specialists on muon research. Eight elementary school pupils attended the class and experimented with the movement of the spinning axis of a top.

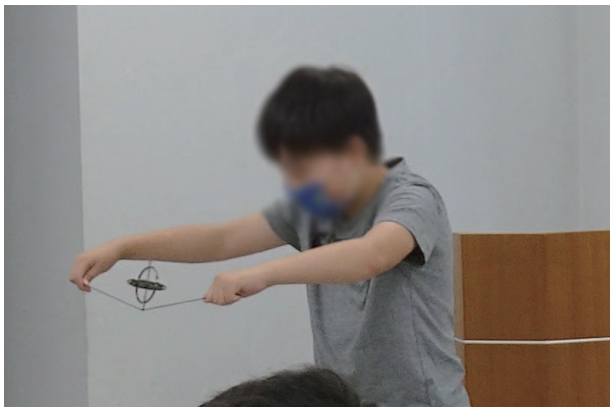

Why doesn't a gyroscope fall off the string?

J-PARC Virtual Open House 2020/Live Streamed J-PARC Facilities

The J-PARC Center held the annual open house online this year. The special website was activated on October 7. On the 10, there was a live-streamed event on YouTube.

In the opening session, the Tokai Village Mayor Osamu Yamada and the J-PARC Center Director Naohito Saito discussed the relationship between the village

Quiz show hosted by Imozo and staffs from Tokai Village office

Live streaming at MLF

and the center. It was followed by talks and facility introductions by researchers. They answered the viewers' questions.

This time, viewers were able to observe the inside of some facilities which are not shown in normal situations.

2020 J-PARC Emergency Drill on October 21 at the Hadron Experimental Facility

On October 21, the J-PARC Center conducted the emergency drill of JFY2020 at the Hadron Experimental Facility. The assumed situation was a large-dose exposure during a beam operation with workers in an experimental area.

A variety of trainings were done regarding initial response, evaluation of exposure level, communications between the incident site and the command office and the NSRI (Nuclear Science Research Institute, in which J-PARC locates).

Activities at the On-site Command Office

J-PARC Hello Science "There is an Accelerator in the Development of Science"

Accelerators have made significant contributions to the development of science. Dr. Tatsunobu Shibata of the Accelerator Division talked about the role of accelerators at science talk event Hello Science on October 30. He explained that the ones at J-PARC succeeded in finding new particles and J-PARC can produce proton beams with the world's highest power level, which are essential for use in secondary particles research.

Participation at JASIS 2020 Exhibition

JASIS (Japan Analytical & Scientific Instruments Show) is one of the largest scientific instrument exhibitions in Asia. J-PARC exhibited in collaboration with JRR-3 in order to introduce the analytical technique using neutron beam. Mitsutaka Nakamura, Sub Leader of the Neutron Science Section of MLF explained the recent results.

J-PARC Hello Science at Tokai Village Children's Science Club

A three-day event of the Tokai Village Children's Science Club was held in November. The instructors were Dr. Satoshi Mihara of the Particle and Nuclear Physics Division, Dr. Yasuyuki Sugiyama and Dr. Tomohiro Takayanagi of the Accelerator Division.

The themes were on light, electricity and magnetism. Seven 5th and 6th grade elementary pupils participated in the experiments. Some children commented that they wanted to learn more about J-PARC because they knew these experiments were connected with its research work.

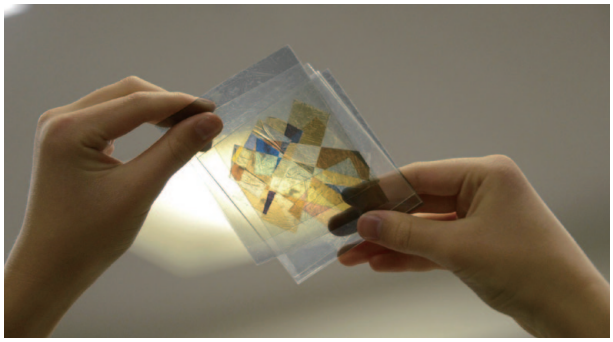

What will happen by layering polarizing plate, sheet with clear adhesive tape, and more?

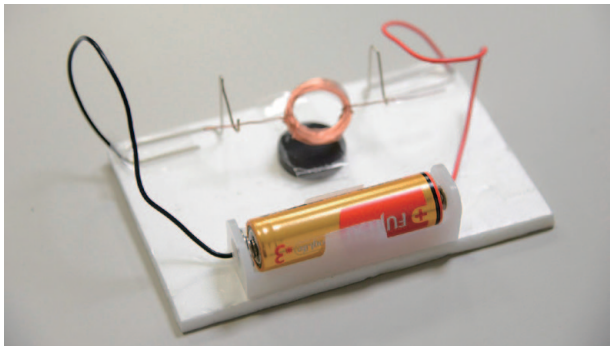

Paper clip motor made by a pupil

J-PARC Hello Science at Tama Rokuto Science Center "Let's Make a Top That Leans While Spinning! -The World of Accelerator Research Seem from Top's Rotation-"

The J-PARC Center introduced the world of its advanced research through craft-making and experiments at Tama Rokuto Science Center on November 29.

Two researchers and two public relations staffs attended the event. Dr. Masashi Otani of the Accelerator Division and Dr. Koichiro Shimomura, Deputy Head of the Material and Life Science Division and Public Relations Section Leader Minako Abe and science staff Naoko Inoue gave instructions to the participants.

They learned about the spin theory of elementary particles by electric current and magnet and also by making tops.

Participant observing magnetic field created by electric current (magnetic lines of force)

J-PARC Hello Science "Looking into Lithium-Ion Battery Using J-PARC Negative Muon"

At J-PARC Hello Science on December 25, Dr. Izumi Umegaki of Toyota Central R & D Labs., Inc. gave a lecture on lithium-ion battery research using a high-intensity negative muon beam in MLF. She showed that the research would further improve the safety of lithium-ion batteries, which are used in our everyday life, such as smartphones and automobiles and contribute to the development of eco-friendly reusable batteries.

J-PARC Center's Videos on the Official YouTube Channel of the Youngster's Science Festival in Hitachi

The 20th Youngster's Science Festival in Hitachi was canceled due to the spread of coronavirus infections and the organizer changed its style and held the festival online by collecting links of YouTube videos. The J-PARC Center offered two videos in December. One was about precession made by graduate students engaged in experiments at J-PARC. The other was about pendulum bell made by the Public Relations Section.

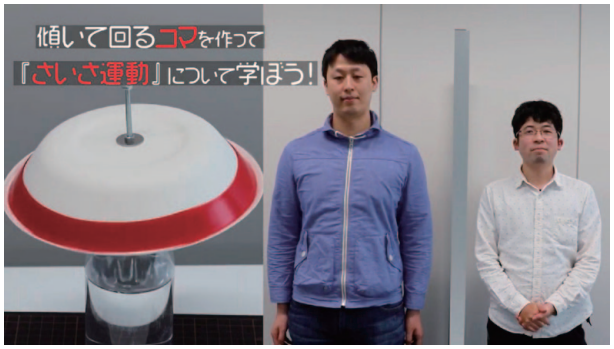

Let's learn about precession by making a top

Let's make a pendulum bell

J-PARC Advisory Committees Held Online

From January 22 to February 22, the J-PARC Center held four advisory committees online.

The committees were Transmutation Experimental Facility (T-TAC), Accelerator Facility (A-TAC), Muon Experimental Facility (MAC), and Neutron Experimental Facility (NAC). The purpose was to receive advice and suggestions from experts in and out of Japan. Their summaries will be reported, and the J-PARC International Advisory Committee (IAC) will discuss the contents in early March.

The 31st J-PARC PAC Held Remotely

The 31st Program Advisory Committee for Nuclear and Particle Physics Experiment at the J-PARC (PAC) was held on January 20-22. J-PARC holds PAC twice a year and this was the second time in JFY2020. There were presentations of one new proposal and two that have been deferred in the last PAC meeting in July. The presentations were followed by eight reports on the progress and future plans.

The 3rd "FC-Cubic Open Symposium" Streamed on YouTube

FC-Cubic, a technology research association consisting of 20 companies, has been conducting research for fuel cells with an aim to realize a hydrogen-based society. On February 2, under the co-sponsorship of NEDO (New Energy and Industrial Technology Development Organization), the FC-Cubic Open Symposium was held

online from the Tokyo International Exchange Center. J-PARC participated in it, because the main topic of this symposium was J-PARC and neutron. We also offered a facility tour by video. The total number of the symposium participants was over 1,800.

J-PARC Hello Science "Emergence of a New Type of Neutrino?!": Data Acquisition for the JSNS2 Experiment Begins at J-PARC

An experiment called JSNS2, which is searching for a new type of neutrino, "sterile neutrino", was started at J-PARC. Dr. Takasumi Maruyama, who is responsible for it gave a talk at Hello Science on February 26. He explained that its existence challenges the validity of the "Standard Model", which is accepted broadly in particle physics. For that reason, there were many questions among the participants.

At the event site

J-PARC International Advisory Committee

The meeting of the International Advisory Committee (IAC) was held on March 4 and 5. It was the summary of the four meetings of T-TAC, A-TAC, MAC, and NAC in January and February. On the second day, IAC announced its advice presented by the Chair of the committee, Jean-Michel Poutissou of the TRIUMF Research Center in Canada.

Quantum Beam Science Festa FY2020

The Quantum Beam Science Festa was held online on March 9-11. 614 people attended, mostly MLF and KEK Photon Factory (PF) users. On the first day, the MLF Symposium kicked off with an opening message by Kazuhiko Soyama, Senior Principal Research at the J-PARC Center. He announced that the operation of JRR-3 was resumed in February. Then Toshiya Otomo, Head of the Materials and Life Science Division presented a report on the current status of the MLF. After that, facility staffs delivered talks on the medium/long-term plans. Many requests were made by the participants under the COVID-19 crisis.

Visitors

Naokazu Takemoto, Minister of State for Special Missions, Cabinet Office (September 2)

Hiroyuki Ohta, President of Ibaraki University (September 16)

Hidehiro Mitsuya, Parliamentary Secretary of MEXT (October 20)

Takashi Shimazu, Representative of Toyota Central R&D Labs., Inc. (November 4)

Susumu Kajiwara, Deputy Minister's Secretariat (November 27)

Hinako Takahashi, Deputy Minister of MEXT (December 16)

There were 362 visitors to J-PARC for the period from April 2020, to the end of March 2021.

There were 2,767 visitors to J-PARC for the period from April 2019 to the end of March 2020.

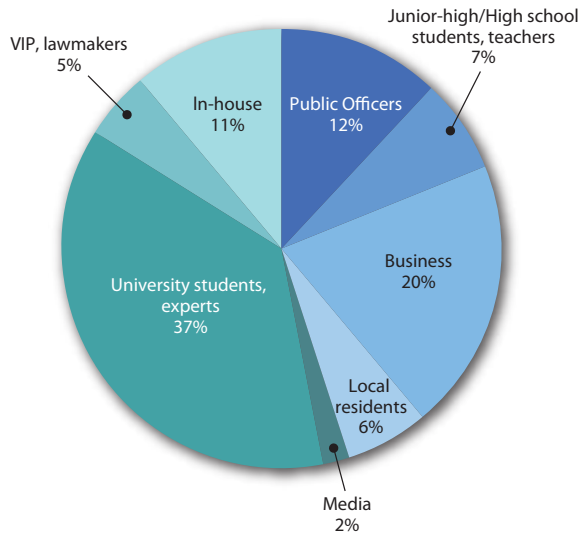

Publications

Publications in Periodical Journals

A-001
A. S. Tremsin, *et al*.
In-situ observation and analysis of solid-state diffusion and liquid migration in a crystal growth system: A segregation-driven diffusion couple
Acta Mater., 186 434-442 (2020)

A-002
M. Morgano, *et al*.
Investigation of the effect of Laser Shock Peening in Additively Manufactured samples through Bragg Edge Neutron Imaging
Addit. Manuf., 34 101201 (2020)

A-003
H. Iwamoto
Generation of nuclear data using Gaussian process regression
J. Nucl. Sci. Technol., 57, pp. 932-938

A-004
T. Hirata, *et al*.
A Facile Surface Functionalization Method for Polymers Using a Non-solvent
ACS Appl. Bio Mater., 3 2170-2176 (2020)

A-005
J. H. Hong, *et al*.
Design of a Bio-inert Interface Using an Amphiphilic Block Copolymer Containing a Bottlebrush Unit of Oligo(oxazoline)
ACS Appl. Bio Mater., 3 7363–7368 (2020)

A-006
K. Mori, *et al*.
Experimental Visualization of Interstitialcy Diffusion Pathways in Fast-Fluoride-Ion-Conducting Solid Electrolyte Ba0.6La0.4F2.4
ACS Appl. Energy Mater., 3 2873 (2020)

A-007
K. Shiino, *et al*.
Structural investigation of sulfonated polyphenylene ionomers for the design of better performing proton-conductive membranes
ACS Appl. Polym. Mater., 2 5558-5565 (2020)

A-008
S. Utsumi, *et al*.
Flux Growth and Magnetic Properties of Helimagnetic Hexagonal Ferrite Ba(Fe1–xScx)12O19 Single Crystals
ACS Omega, 5 24890-24897 (2020)

A-009
T. Sato, *et al*.
Crystal Structural Investigations for Understanding Hydrogen Storage Properties of YMgNi4-Based Alloys
ACS Omega, 5 31192 (2020)

A-010
M. Tanaka, *et al*.
Structure determination of the human TRPV1 ankyrin-repeat domain under nonreducing conditions
Acta Crystallogr. Sect. F Struct. Biol. Cryst. Commun., F76 130-137 (2020)

A-011
Y. Wang, *et al*.
Real time observation of martensite transformation for a 0.4 C low alloyed steel by neutron diffraction
Acta Mater., 184 30-40 (2020)

A-012
Y. Wang, *et al*.
Continuous and discontinuous yielding behaviors in ferrite-cementite steels
Acta Mater., 196 565-575 (2020)

A-013
S. Harjo, *et al*.
Neutron diffraction monitoring of ductile cast iron under cyclic tension–compression
Acta Mater., 196 584-594 (2020)

A-014
D. Fukui, *et al*.
Internal residual stress originated from Bain strain and its effect on hardness in Fe–Ni martensite
Acta Mater., 196 660-668 (2020)

A-015
T. N. Lam, *et al*.
Enhancement of fatigue resistance by overload-induced deformation twinning in a CoCrFeMnNi high-entropy alloy
Addit. Manuf., 34 101201 (2020)

A-016
L. Kong, *et al*.
Suppressed Lattice Disorder for Large Emission Enhancement and Structural Robustness in Hybrid Lead Iodide Perovskite Discovered by High-pressure Isotope Effect
Adv. Funct. Mater., 31 2009131 (2020)

A-017
K. Hayashi, *et al*.
Preparation, thermoelectric properties, and crystal structure of boron-doped Mg2Si single crystals
AIP Adv., 10 35115 (2020)

A-018
Y. Umegaki, *et al*.
Nondestructive High-Sensitivity Detections of Metallic Lithium Deposited on a Battery Anode Using Muonic X-rays
Anal. Chem., 92 8194 (2020)

A-019
T. Takami, *et al*.
A new Bi0.7Fe1.3O1.5F1.7 phase: Crystal structure, magnetic properties, and cathode performance in fluoride-ion batteries
APL Mater., 8 051103 (2020)

A-020
H. Seto, T. Yamada
Quasi-elastic neutron scattering study of the effects of metal cations on the hydration water between phospholipid bilayers
Appl. Phys. Lett., 116 133701 (2020)

A-021
H. K. Cho, S. Park
Magnetic structure of undistorted hexagonal ferrites, Lu0.2In0.8FeO3
Appl. Phys. Lett., 116 202902 (2020)

A-022
H. Yamamoto, *et al*.
Reversible thermally controlled spontaneous magnetization switching in perovskite-type manganite
Appl. Phys. Lett., 117 112404 (2020)

A-023
J. Kitanishi, *et al*.
Identification and Characterization of a Redox Sensor Phosphodiesterase from Ferrovum sp. PN-J185 Containing Bacterial Hemerythrin and HD-GYP Domains
Biochemistry, 59 983-991 (2020)

A-024
H. Kawaura, *et al*.
Operando Time-slicing Neutron Reflectometry Measurements of Solid Electrolyte Interphase Formation on Amorphous Carbon Surfaces of a Li-ion Battery
Bull. Chem. Soc. Jpn., 93 854-861 (2020)

A-025
H. Uchiyama, *et al*.
Single-stranded β-1,3–1,6-glucan as a carrier for improved dissolution and membrane permeation of poorly water-soluble compounds
Carbohydr. Polym., 247 116698 (2020)

A-026
Y. Fujii, *et al*.
Cation- and anion-ordered rutile-type derivative LiTeO3(OH)
Chem. Commun., 56 10042-10045 (2020)

A-027
J. Yamaura, *et al*.
Polar nano-region structure in oxynitride perovskite LaTiO2N
Chem. Commun., 56 1385-1388 (2020)

A-028
H. Yamauchi, *et al*.
High-temperature short-range order in Mn3RhSi
Commun. Mater., 1 43 (2020)

A-029
R. Sei, *et al*.
Tetragonality induced superconductivity in anti-ThCr2Si2-type RE2O2Bi (RE = rare earth) with Bi square nets
Dalton Trans., 49 3321-3325 (2020)

A-030
R. Kasai, *et al*.
Effect of Separator and Anode on Electrochemical Characteristics and Crystal Structure of Lithium-ion Battery Cathode Material 0.4Li2MnO3-0.6LiMn1/3Ni1/3Co1/3O2
Electrochemistry, 89 148-156 (2020)

A-031
T. Nakaya, K. Nishikawa
Long baseline neutrino oscillation experiments with accelerators in Japan
European Physical Journal C 80(2020) 334

A-032
T. Yamada, H. Seto,
Quasi-Elastic Neutron Scattering Studies on Hydration Water in Phospholipid Membranes
Front. Chem., 8 8 (2020)

A-033
J. Pallbo, *et al*.
NACore amyloid formation in the presence of phospholipids
Front. Physiol., 11 592117 (2020)

A-034
K. Komatsu, *et al*.
Developments of nano-polycrystalline diamond anvil cells for neutron diffraction experiments
High Press. Res., 40 184-193 (2020)

A-035
T. Hattori, *et al*.
Practical effects of pressure-transmitting media on neutron diffraction experiments using Paris-Edinburgh presses
High Press. Res., 40 325-338 (2020)

A-036
M. Nitta, *et al*.
High-Brightness Red-Emitting Phosphor La3(Si,Al)6(O,N)11:Ce3+ for Next-Generation Solid-State Light Sources
High-Brightness Red-Emitting Phosphor La3(Si,Al)6(O,N)11:Ce3+ for Next-Generation Solid-State Light Sources

A-037
M. Iio, *et al*.
Research and Development of Future Radiation-Resistant Superconducting Magnets With Mineral Insulated REBCO Coils
IEEE Trans. Appl. Supercond., 30 (2020), 4600505

A-038
W. Liao, *et al*.
Impact of the Angle of Incidence on Negative Muon-induced SEU Cross Sections of 65-nm Bulk and FDSOI SRAMs
IEEE Trans. Nucl. Sci., 67 1566-1572 (2020)

A-039
J. Kuroda, *et al*.
Measurement of Single-Event Upsets in 65-nm SRAMs Under Irradiation of Spallation Neutrons at J-PARC MLF
IEEE Trans. Nucl. Sci., 67 1599-1605 (2020)

A-040
N. Amemiya, *et al*.
AC Loss and Shielding-Current-Induced Field in a Coated-Conductor Test Magnet for Accelerator Applications under Repeated Excitations
IEEE Transactions on Applied Superconductivity 30 (2020) 4004105

A-041
T. Obana, T. Ogitsu
Design of Lightweight Superconducting Magnets for a Rotating Gantry With Active Shielding
IEEE Transactions on Applied Superconductivity 30 (2020) 4400305

A-042
K. TANAKA, *et al*.
New Types of Organic Resins for Insulation of Warm Magnets
IEEE Transactions on Applied Superconductivity 30 (2020) 7700105

A-043
T. Takayanagi, *et al*.
Comparative studies of three-dimensional analysis and measurement for establishing pulse electromagnet design
IEEE Transactions on Applied Superconductivity, 30(4)(2020), p.4901605_1 - 4901605_5

A-044
T. Kishishita, *et al*.
SliT: A Strip-Sensor Readout Chip With Subnanosecond Time Walk for the J-PARC Muon g - 2/EDM Experiment
IEEE Transactions on Nuclear Science 67 (2020) 2089

A-045
T. Matsubara, *et al*.
Cation distributions and magnetic properties of ferrispinel MgFeMnO4
Inorg. Chem., 59 17970-17980 (2020)

A-046
T. Yajima, *et al*.
Titanium Hydride Complex BaCa2Ti2H14 with a 9-Fold Coordination
Inorg. Chem., 59 4228-4233 (2020)

A-047
Y. Matsumoto, *et al*.
High-pressure Synthesis of Ba2CoO2Ag2Te2 with Extended CoO2 Planes
Inorg. Chem., 59 8121–8126 (2020)

A-048
H. Sato, *et al*.
Simultaneous Broadening Analysis of Multiple Bragg Edges Observed by Wavelength-resolved Neutron Transmission Imaging of Deformed Low-carbon Ferritic Steel
ISIJ International, 60 1254-1263 (2020)

A-049
N. Tsuchida, *et al*.
Analysis of Tensile Deformation Behavior by in situ Neutron Diffraction Experiments of 1 GPa-grade TRIP Steels with High Elongation
ISIJ International, 60 1349-1357 (2020)

A-050
Y. Hosoya, *et al*.
Mechanism of Improved Ductility of 1500 MPa-class Ultra-high Strength Cold-rolled Steel Sheet Produced by Rolling and Partitioning Method
ISIJ International, 60 2097 (2020)

A-051
T. Wakisaka, *et al*.
Rational Synthesis for a Noble Metal Carbide
J. Am. Chem. Soc., 142 1247 (2020)

A-052
X. Zhang, *et al*.
Distance-Selected Topochemical Dehydro-Diels-Alder Reaction of 1,4-Diphenylbutadiyne toward Crystalline Graphitic Nanoribbons
J. Am. Chem. Soc., 142 17662-17669 (2020)

A-053
N. L. Yamada, *et al*.
Application of Precise Neutron Focusing Mirror for Neutron Reflectometry - Latest Results and Future Prospects
J. Appl. Crystallogr., 53 1462-1470 (2020)

A-054
Y. Akahama, *et al*.
Structure refinement of black phosphorus under high pressure
J. Chem. Phys., 153 014704 (2020)

A-055
J. Matsuno, *et al*.
Synthesis and characterization of nanoemulsion-mediated core crosslinked nanoparticles, and in vivo pharmacokinetics depending on the structural characteristics
J. Control. Release, 324 405 (2020)

A-056
M. Aggarwal, *et al*.
Energy Resolved Neutron Imaging for Strain Reconstruction Using the Finite Element Method
J. Imaging, 6 13 (2020)

A-057
T. Aoyagi, *et al*.
Performance evaluation of a silicon strip detector for positrons/electrons from a pulsed a muon beam
J. Instrum., 15 P04027 (2020)

A-058
S. Okada, *et al*.
X-ray Spectroscopy of Muonic Atoms Isolated in Vacuum with Transition Edge Sensors
J. Low. Temp. Phys., 200 445-451 (2020)

A-059
T. E. Ashton, *et al*.
Multiple diffusion pathways in LixNi0.77Co0.14Al0.09O2 (NCA) Li-ion battery cathodes
J. Mater. Chem. A, 8 11545-11552 (2020)

A-060
H. Abe, *et al*.
CO2 capture and surface structures of ionic liquid-propanol solutions
J. Mol. Liq., 301 112445 (2020)

A-061
K. Sakai, *et al*.
Conceptual design of an abnormality sign determination system for the general control system of the Materials and Life Science Experimental Facility at J-PARC
J. Neutron Res., 22 337-343 (2020)

A-062
M. Kajimoto, *et al*.
Energy resolution and neutron flux of the 4SEASONS spectrometer revisited
J. Neutron Res., 22 99-107 (2020)

A-063
Y. Iwamoto, *et al*.
Estimation of reliable displacements-per-atom based on athermal-recombination-corrected model in radiation environments at nuclear fission, fusion, and accelerator facilities
J. Nucl. Mat. 538, pp. 152261

A-064
T. Ishida, *et al*.
Tensile behavior of dual-phase titanium alloys under high-intensity proton beam exposure: Radiation-induced omega phase transformation in Ti-6Al-4V
J. Nucl. Mater., 541 152413 (2020)

A-065
H. Matsuda, *et al*.
Measurement of Displacement Cross-Sections of Copper and Iron for Proton with Kinetic Energies in the Range 0.4 - 3 GeV
J. Nucl. Sci. Technol., 57, pp. 1141-1151

A-066
H. Takei, *et al*.
Low-power proton beam extraction by the bright continuous laser using the 3-MeV negativehydrogen linac in Japan Proton Accelerator Research Complex
J. Nucl. Sci. Technol., 58, pp. 580-603

A-067
H. Iwamoto, *et al*.
Estimation of uncertainty in lead spallation particle multiplicity and its propagation to a neutron energy spectrum
J. Nucl.Sci. Technol., 57, pp. 276 - 290

A-068
Y. Kameda, *et al*.
Solvation Structure of Li+ in Concentrated Acetonitrile and N,N-Dimethylformamide Solutions Studied by Neutron Diffraction with 6Li/7Li Isotopic Substitution Methods
J. Phys. Chem. B, 124 10456 (2020)

A-069
K. Yoshimoto, *et al*.
Principal Vibration Modes of the La2O3–Ga2O3 Binary Glass Originated from Diverse Coordination Environments of Oxygen Atoms
J. Phys. Chem. B, 124 5056-5066 (2020)

A-070
Z. Liu, *et al*.
Heterogeneity of Water Molecules on the Free Surface of Thin Reduced Graphene Oxide Sheets
J. Phys. Chem. C Nanomater. Interfaces, 124 11064-11074 (2020)

A-071
Y. Zhou, *et al*.
Dihydrogen Bonds in Aqueous NaBD4 Solution by Neutron and X-Ray Diffraction
J. Phys. Chem. Lett., 11 1622 (2020)

A-072
M. A. González, *et al*.
Nanoscale Relaxation in "Water-in-Salt" and "Water-in-Bisalt" Electrolytes
J. Phys. Chem. Lett., 11 7279 (2020)

A-073
T. Hiroto, *et al*.
Noncoplanar ferrimagnetism and local crystalline-electric-field anisotropy in the quasicrystal approximant Au70Si17Tb13
J. Phys. Condens. Matter, 32 415802 (2020)

A-074
M. Abe, *et al*.
Development of a μ-PIC with glass substrate aiming at high gas gain
J. Phys. Conf. Ser., 1498 012002 (2020)

A-075
M. Komabuchi, *et al*.
Crystal Structure and Cation Distribution of the X-type Hexaferrite Sr2Co2Fe28O46
J. Physical Soc. Japan, 89 034601 (2020)

A-076
M. Kofu, O. Yamamuro
Dynamics of Atomic Hydrogen in Palladium Probed by Neutron Spectroscopy
J. Physical Soc. Japan, 89 051002 (2020)

A-077
K. Iida, *et al*.
Horizontal line nodes in Sr2RuO4 proved by spin resonance
J. Physical Soc. Japan, 89 053702 (2020)

A-078
K. Sato, *et al*.
Coexistence of Two Components in Magnetic Excitations of La2-xSrxCuO4 (x = 0.10 and 0.16)
J. Physical Soc. Japan, 89 114703 (2020)

A-079
S. Ikeda, *et al*.
Multi-Step Magnetic Transitions in EuNiIn4
J. Physical Soc. Japan, 89 14707 (2020).

A-080
K. Otomo, *et al*.
Structural Studies of Hydrogen Storage Materials with Neutron Diffraction: A Review
J. Physical Soc. Japan, 89 51001 (2020)

A-081
T. U. Ito, *et al*.
Negatively Charged Muonium and Related Centers in Solids
J. Physical Soc. Japan, 89 51007 (2020)

A-082
T. Noda, *et al*.
Preparation, characterization, and dilute solution properties of four-branched cage-shaped poly (ethylene oxide)
J. Polym. Sci., 58 2098-2107 (2020)

A-083
R. Iizuka-Oku, W. Gui, K. Komatsu, T. Yagi, H. Kagi,
High-pressure responses of alkali metal hydrogen carbonates, RbHCO3and CsHCO3: Findings of new phases and unique compressional behavior
J. Solid State Chem., 283 121139 (2020)

A-084
J. Hendriks, *et al*.
Bayesian non-parametric Bragg-edge fitting for neutron transmission strain imaging
J. Strain Anal. Eng. Des., (2020)

A-085
K. Abe, *et al*.
Measurement of the charged-current electron (anti-)neutrino inclusive cross-sections at the T2K off-axis near detector ND280
Journal of High Energy Physics 10 (2020) 114

A-086
R. Acciarri, *et al*.
The Liquid Argon In A Testbeam (LArIAT) experiment
Journal of Instrumentation 15 (2020) P04026

A-087
T. Aoyagi, *et al*.
Performance evaluation of a silicon strip detector for positrons/electrons from a pulsed a muon beam
Journal of Instrumentation 15 (2020) P04027

A-088
A.Blondel, *et al*.
The SuperFGD Prototype charged particle beam tests
Journal of Instrumentation 15 (2020) P12003

A-089
J. S. Park(*), *et al*.
Performance of PMTs for the JSNS2 experiment
Journal of Instrumentation 15 (2020) T07003

A-090
J. S. Park(*), *et al*.
The JSNS2 data acquisition system
Journal of Instrumentation 15 (2020) T09002

A-091
T. Kishishita, *et al*.
LTARS: analog readout front-end ASIC for versatile TPC-applications
Journal of Instrumentation 15 (2020) T09009

A-092
T. Hashimoto, *et al*.
Integration of a TES-based X-ray spectrometer in a kaonic atom experiment
Journal of Low Temperature Physics 199 (2020) 1018

A-093
D. Kitahara, *et al*.
The location of Mn and Fe in axinite–(Fe) from Nandan, China determined by anomalous X–ray scattering (AXS)
Journal of Mineralogical and Petrological Sciences, 115 227-235 (2020)

A-094
M. Nagashima, *et al*.
Crystal chemistry of Sr–rich piemontite from manganese ore deposit of the Tone mine, Nishisonogi Peninsula, Nagasaki, southwest Japan
Journal of Mineralogical and Petrological Sciences, 115 391-406 (2020)

A-095
H. Matsuda, *et al*
Measurement of displacement cross-sections of copper and iron for proton with kinetic energies in the range 0.4 -- 3 GeV
Journal of Nuclear Science and Technology 57 (2020) 1141

A-096
F. Funama, *et al*.
Observation of TOF-MIEZE Signals with Focusing Mirrors at BL06, MLF, J-PARC
Journal of Surface Investigation: X-ray, Synchrotron and Neutron Techniques, 14 S50-S55 (2020)

A-097
K. Kataoka
Oxide single crystals with high lithium-ion conductivity as solid electrolytes for all-solid-state lithium secondary battery applications
Journal of the Ceramic Society of Japan, 128 7-18 (2020)

A-098
Z. Xu, *et al*.
Hydrogen states in hydrogen-passivated semiconducting barium disilicide measured via muon spin rotation
Jpn. J. Appl. Phys., 59 071004 (2020)

A-099
K. Ito, *et al*.
Water Distribution in Nafion Thin Films on Hydrophilic and Hydrophobic Carbon Substrates
Langmuir, 36 12830–12837 (2020)

A-100
T. Miyazaki, *et al*.
Neutron Reflectivity on the Mobile Surface and Immobile Interfacial Layers in the Poly(vinyl acetate) Adsorption Layer on a Si Substrate with Deuterated Toluene Vapor-Induced Swelling
Langmuir, 36 15181-15188 (2020)

A-101
T. Miyazaki, *et al*.
Detailed Structural Study on the Poly(vinyl alcohol) Adsorption Layers on a Si Substrate with Solvent Vapor-Induced Swelling
Langmuir, 36 3415-3424 (2020)

A-102
T. Sugahara, *et al*.
Structural change of α-gel (α-form hydrated crystal) induced by temperature and shear flow in an oleic acid-based gemini surfactant system
Langmuir, 36 4695-4701 (2020)

A-103
T. Kimura, *et al*.
Sublayered Thin Films of Hydrated Anion Exchange Ionomer for Fuel Cells Formed on SiO2 and Pt Substrates Analyzed by Neutron Reflectometry under Controlled Temperature and Humidity Conditions
Langmuir, 36 4955-4963 (2020)

A-104
T. Yoshimura, *et al*.
Adsorption and aggregation properties of Gemini-type amphiphilic dendrimers
Langmuir, 36 563 (2020)

A-105
K. Igata, *et al*.
Cationic Polymer Brush/Giant Polysaccharide Sacran Assembly: Structure and Lubricity
Langmuir, 36 6494-6501 (2020)

A-106
S. Yada, *et al*.
Microstructural Characterization of Foam Formed by a Hydroxy Group-Containing Amino Acid Surfactant Using Small-Angle Neutron Scattering
Langmuir, 36 7808–7813 (2020)

A-107
Y. Higaki, *et al*.
Hydration State Variation of Polyzwitterion Brushes through Interplay with Ions
Langmuir, 36 9015 (2020)

A-108
C.I. Gupit, *et al*.
Nanostructures and viscosities of nafion dispersions in water/ethanol from dilute to concentrated regimes
Macromolecules, 53 1464 (2020)

A-109
Y. Oda, *et al*.
Dynamic Interface based on Segregation of an Amphiphilic Hyperbranched Polymer Containing Fluoroalkyl and Oligo(ethylene oxide) Moieties
Macromolecules, 53 2380-2387 (2020)

A-110
M. Ohira, *et al*.
Quantitative structure analysis of a near-ideal polymer network with deuterium label by small-angle neutron scattering
Macromolecules, 53 4047 (2020)

A-111
A. Izumi, *et al*.
Interfacial Cross-Link Inhomogeneity of a Phenolic Resin on a Silica Surface As Revealed by X-ray and Neutron Reflection Measurements
Macromolecules, 53 4082-4089 (2020)

A-112
K. Tashiro, *et al*.
Introduction of Disorder in the Crystal Structures of Atactic Poly(vinyl Alcohol) and Its Iodine Complex To Solve a Dilemma between X-ray and Neutron Diffraction Data Analyses

Macromolecules, 53 6656-6671 (2020)

A-113
T. Nishimura, *et al*.
Determining the hydration in the hydrophobic layer of permeable polymer vesicles by neutron scattering
Macromolecules, 53 7546 (2020)

A-114
Y. Cui, *et al*.
A study on the micromechanical behavior of Ti-55531 titanium alloy with lamellar microstructure byin-situ neutron diffraction
MATEC Web of Conferences, 321 11013 (2020)

A-115
Y. Tomota, *et al*.
Influence of carbon concentration and magnetic transition on the austenite T lattice parameter of 30Mn-C steel
Mater. Charact., 163 110243 (2020)

A-116
D. Ma, *et al*.
In-situ neutron diffraction investigation on the martensite transformation, texture evolution and martensite reversion in high manganese TRIP steel
Mater. Charact., 163 110244 (2020)

A-117
Z. Wei, *et al*.
Transformation textures in pure titanium: Texture memory vs surface effect
Mater. Charact., 164 110359 (2020)

A-118
K. Itoh, *et al*.
Structural study of Ni67Zr33 amorphous alloy: Interatomic space analysis approach
Mater. Chem. Phys., 240 122214 (2020)

A-119
W. Woo, *et al*.
Comparison of dislocation density, twin fault probability, and stacking fault energy between CrCoNi and CrCoNiFe medium entropy alloys deformed at 293 and 140K
Mater. Sci. Eng. A Struct. Mater., 781 139224 (2020)

A-120
S. Harjo, *et al*.
Neutron Diffraction Monitoring of As-Cast Mg97Zn1Y2 during Compression and Tension
Mater. Trans., 61 828-832 (2020)

A-121
J. W. Bae, *et al*.
On the phase transformation and dynamic stress–strain partitioning of ferrous medium-entropy alloy using experimentation and finite element method
Materialia, 9 100619 (2020)

A-122
T. Kai, *et al*.
Feasibility Study of Two-Dimensional Neutron-Resonance Thermometry using Molybdenum in 316 Stainless-Steel
Materials Research Forum LLC, 15 149-153 (2020)

A-123
K. Oikawa, *et al*.
Pulsed Neutron Imaging Based Crystallographic Structure Study of a Japanese Sword made by Sukemasa in the Muromachi Period
Materials Research Forum LLC, 15 207-213 (2020)

A-124
J. D. Parker, *et al*.
Development of Event-Type Neutron Imaging Detectors at the Energy-Resolved Neutron Imaging System RADEN at J-PARC
Materials Research Proceedings, 15 102-107 (2020)

A-125
Y. Oba, *et al*.
Neutron Transmission Spectrum of Liquid Lead Bismuth Eutectic
Materials Research Proceedings, 15 160-164 (2020)

A-126
H. Sato, *et al*.
Crystallographic Microstructure Study of a Japanese Sword made by Noritsuna in the Muromachi Period by Pulsed Neutron Bragg-Edge Transmission Imaging
Materials Research Proceedings, 15 214-220 (2020)

A-127
Y. Matsumoto, *et al*.
Comparative Study of Ancient and Modern Japanese Swords using Neutron Tomography
Materials Research Proceedings, 15 221-226 (2020)

A-128
K. Ohmae, *et al*.
Crystallographic Structure Study of a Japanese Sword Masamitsu made in the 1969 using Pulsed Neutron Imaging
Materials Research Proceedings, 15 227-232 (2020)

A-129
O. Holderer, *et al*.
Fuel Cell Electrode Characterization Using Neutron Scattering
Materials, 13 1474 (2020)

A-130
T. N. Lam, *et al*.
Element Effects of Mn and Ge on the Tuning of Mechanical Properties of High-Entropy Alloys
Metall. Mater. Trans. A Phys. Metall. Mater. Sci., 51 5023-5028 (2020)

A-131
I. Tanaka, *et al*.
Current status and near future plan of neutron protein crystallography at J-PARC
Methods Enzymol., 634 101-123 (2020)

A-132
M. B. Spano, *et al*.
Large crystal growth for neutron protein crystallography
Methods Enzymol., 634 21-46 (2020)

A-133
S. Urakawa, *et al*.
X-ray and neutron study on the structure of hydrous SiO2 glass up to 10 GPa
Minerals, 10 84 (2020)

A-134
S. Kajiyama, *et al*.
Shear-induced liquid-crystalline phase transition behaviour of colloidal solutions of hydroxyapatite nanorod composites
Nanoscale, 12 11468-11479 (2020)

A-135
K. Watanabe, *et al*.
Highly asymmetric lamellar nanostructures from nanoparticle–linear hybrid block copolymers
Nanoscale, 12 16526-16534 (2020)

A-136
W. Zhang, *et al*.
Oxide-ion conduction in the Dion–Jacobson phase CsBi2Ti2NbO10−δ
Nat. Commun., 11 1224 (2020)

A-137
Q. Ren, *et al*.
Establishing the carrier scattering phase diagram for ZrNiSn-based half-Heusler thermoelectric materials
Nat. Commun., 11 3142 (2020)

A-138
M. Fujihala, *et al*.
Gapless spin liquid in a square-kagome lattice antiferromagnet
Nat. Commun., 11 3429 (2020)

A-139
F. B. Li, *et al*.
Understanding colossal barocaloric effects in plastic crystals
Nat. Commun., 11 4190 (2020)

A-140
K. Komatsu, *et al*.
Ice Ic without stacking disorder by evacuating hydrogen from hydrogen hydrate
Nat. Commun., 11 464 (2020)

A-141
T. Yamamoto, *et al*.
Strain-induced creation and switching of anion vacancy layers in perovskite oxynitrides
Nat. Commun., 11 5923 (2020)

A-142
X. Li, *et al*.
Ultralow Thermal Conductivity from Transverse Acoustic Phonon Suppression in Distorted Crystalline α-MgAgSb
Nat. Commun., 11 942 (2020)

A-143
K. Abe, *et al*.
Constraint on the matter-antimatter symmetry-violating phase in neutrino oscillations
Nature 580(2020) n339

A-144
M. L. Friend
A decade of science at J-PARC
Nature Reviews Physics 2 (2020) 2

A-145
R. Bauer, *et al*.
Slow compression of crystalline ice at low temperature
Nature, 585 E10 (2020)

A-146
P. Wu, *et al*.
Strong lattice anharmonicity exhibited by the high-energy optical phonons in thermoelectric material
New J. Phys., 22 083083 (2020)

A-147
P. Gwak, *et al*.
Slow Control and Monitoring programming for JSNS2
New Physics: Sae Mulli 70 (2020) 928

A-148
Z. Xu, *et al*.
Strong local moment antiferromagnetic spin fluctuations in V-doped LiFeAs
NPJ Quantum Mater., 5 11 (2020)

A-149
T. Okudaira, *et al*.
Development and application of a 3He neutron spin filter at J-PARC
Nucl. Instrum. Methods Phys. Res. A, 977 164301 (2020)

A-150
T. Naoe, *et al*.
Pressure wave induced sound measurement for diagnosing the operation status of the J-PARC pulsed spallation neutron source
Nucl. Instrum. Methods Phys. Res. A, 982 164566 (2020)

A-151
H. Matsuda, *et al*.
Measurement of thick target neutron yield at 180°for a mercury target induced by 3-GeV protons
Nucl. Instrum. Methods Phys. Res. B 483, pp. 33–40

A-152
R. Murayama, *et al*.
A new cylindrical photon-veto detector for the KL → π0νν experiment
Nucl. Instrum. Methods Phys. Res. Section A 953 (2020) 163255

A-153
Y. Nakazawa, *et al*.
Radiation hardness study for the COMET Phase-I electronics
Nucl. Instrum. Methods Phys. Res. Section A 955 (2020)n163247

A-154
T. Yamanaka, *et al*.
Positron tracking detector for J-PARC muon g--2/EDM experiment
Nucl. Instrum. Methods Phys. Res. Section A 958 (2020) 162786

A-155
H. Nishiguchi, *et al*.
Construction on vacuum-compatible straw tracker for COMET Phase-I
Nucl. Instrum. Methods Phys. Res. Section A 958 (2020) 162800

A-156
Y. Sato, *et al*.
Development of a front-end ASIC for silicon-strip detectors of the J-PARC muon g-2/EDM experiment
Nucl. Instrum. Methods Phys. Res. Section A 969 (2020) 164035

A-157
K. Sato, *et al*.
CsI calorimeter for the J-PARC KOTO experiment
Nucl. Instrum. Methods Phys. Res. Section A 982 (2020) 164527

A-158
A. W. Thomas, *et al*.
Ten Years of the Asian Nuclear Physics Association (ANPhA) and Major Accelerator Facilities for Nuclear Physics in the Asia Pacific Region
Nuclear Physics News 30 (2020· 3

A-159
Y. Zhou, *et al*.
The Structural Elucidation of Aqueous H3BO3 Solutions by DFT and Neutron Scattering
Phys. Chem. Chem. Phys., 22 17160-17170 (2020)

A-160
M. Kawano, *et al*.
Mixing states of imidazolium-based ionic liquid, [C4mim][TFSI], with cycloethers studied by SANS, IR, and NMR experiments and MD simulations
Phys. Chem. Chem. Phys., 22 5332-5346 (2020)

A-161
Y. Higuchi, *et al*.
Pulsed neutron imaging for differentiation of ice and liquid water towards fuel cell vehicle applications
Phys. Chem. Chem. Phys., 23 1062-1071 (2020)

A-162
M. Nagashima, *et al*.
Multi-methodical study of the Ti, Fe2+ and Fe3+ distribution in chevkinite-subgroup minerals: X-ray diffraction, neutron diffraction, 57Fe Mössbauer spectroscopy and electron-microprobe analyses
Phys. Chem. Miner., 47 29 (2020)

A-163
H. Hotchi
Effects of the Montague resonance on the formation of the beam distribution during multiturn injection painting in a high-intensity proton ring
Phys. Rev. Accel. Beams (Internet), 23(5), p.050401_1 - 050401_13, 2020/05

A-164
P. Saha, *et al*.
First measurement and online monitoring of the stripper foil thinning and pinhole formation to achieve a longer foil lifetime in high-intensity accelerators
Phys. Rev. Accel. Beams (Internet), 23(8), p.082801_1 - 082801_13, 2020/08

A-165
Y. Shobuda, *et al*.
Titanium nitride-coated ceramic break for wall current monitors with an improved broadband frequency response
Phys. Rev. Accel. Beams (Internet), 23(9), p.092801_1 - 092801_18, 2020/09

A-166
S. Meigo, *et al*.
Two-parameter model for optimizing target beam distribution with an octupole magnet
Phys. Rev. Accel. Beams 23, 062802

A-167
T. Morishita, *et al*.
Electromagnetic design and tuning of the four-vane radio frequency quadrupole with nonuniform intervane voltage profile
Phys. Rev. Accel. Beams 23, 111003-1 – 111003-9 (2020)

A-168
T.Yasui, *et al*.
Transverse emittance growth caused by

space-charge-induced resonance
Phys. Rev. Accel. Beams 23, 61001- (2020)

A-169
T. Oda, *et al*.
Tuning Neutron Resonance Spin-Echo Spectrometers with Pulsed Beams
Phys. Rev. Appl., 14 054032 (2020)

A-170
E. Fogh, *et al*.
Magnetic structures and quadratic magnetoelectric effect in LiNiPO4 beyond 30 T
Phys. Rev. B, 101 024403 (2020).

A-171
T. Uchino, *et al*.
Proximity coupling of superconducting nanograins with fractal distributions
Phys. Rev. B, 101 035146 (2020)

A-172
T. Sato, *et al*.
Magnetic phase diagram enriched by chemical substitution in a noncentrosymmetric helimagnet
Phys. Rev. B, 101 054414 (2020)

A-173
S. Klotz, *et al*.
Crystal structure and magnetism of MnO under pressure
Phys. Rev. B, 101 064105 (2020)

A-174
K. H. Lee, *et al*.
Stabilization of orthorhombic distortions in Cu- and Co-doped ferrimagnetic Mn3O4
Phys. Rev. B, 101 085126 (2020)

A-175
Z. Cai, *et al*.
Spin dynamics of a magnetic Weyl semimetal Sr1-xMn1-ySb2
Phys. Rev. B, 101 134408 (2020)

A-176
M. M. R. Bhuiyan, *et al*.
Spin order in the classical spin kagome antiferromagnet MgxMn4−x(OH)6Cl2
Phys. Rev. B, 101 134424 (2020)

A-177
H. Ueda, *et al*.
Emergent spin-1 Haldane gap and ferroelectricity in a frustrated spin-1/2 ladder
Phys. Rev. B, 101 140408(R) (2020)

A-178
S. Asai, *et al*.
Helical and collinear spin density wave order in the S=1/2 one-dimensional frustrated chain compound NaCuMoO4(OH) investigated by neutron scattering
Phys. Rev. B, 101 144437 (2020)

A-179
H. Masuda, *et al*.
Field-induced spin reorientation in the antiferromagnetic Dirac material EuMnBi2 revealed by neutron and resonant x-ray diffraction
Phys. Rev. B, 101 174411 (2020)

A-180
N. Abe, *et al*.
Magnetically induced electric polarization in Ba3Fe2O5Cl2 with tunable direction in three dimensions
Phys. Rev. B, 101 180407(R) (2020)

A-181
C. Tan, *et al*.
Slow magnetic fluctuations and critical slowing down in Sr2Ir1−xRhxO4
Phys. Rev. B, 101 195108 (2020)

A-182
S. Bao, *et al*.
Evidence for magnon-phonon coupling in the topological magnet Cu3TeO6
Phys. Rev. B, 101 214419 (2020)

A-183
M. Soda, *et al*.
Magnetic correlations in YBaCo4O7 on kagome and triangular lattices
Phys. Rev. B, 101 214444 (2020)

A-184
M. Hirschberger, *et al*.
High-field depinned phase and planar Hall effect in the skyrmion host Gd2PdSi3
Phys. Rev. B, 101 220401(R) (2020)

A-185
K. Iida, *et al*.
q=0 long-range magnetic order in centennialite CaCu3(OD)6Cl2 · 0.6D2O: A spin-1/2 perfect kagome antiferromagnet with J1−J2−Jd
Phys. Rev. B, 101 220408(R) (2020)

A-186
S. Gao, *et al*.
Crystal electric field excitations in the quantum spin liquid candidate NaErS2
Phys. Rev. B, 102 024424 (2020)

A-187
M. Fujita, *et al*.
Magnetic behavior of T′-type Eu2CuO4 revealed by muon spin rotation and relaxation measurements
Phys. Rev. B, 102 045116 (2020)

A-188
N. Katayama, *et al*.
Robust atomic orbital in the cluster magnet LiMoO2
Phys. Rev. B, 102 081106(R) (2020)

A-189
J. Sugiyama, *et al*.
Nuclear magnetic field in Na0.7CoO2 detected with μ−SR
Phys. Rev. B, 102 144431 (2020)

A-190
H. Takahashi, *et al*.
Competing spin modulations in the magnetically frustrated semimetal EuCuSb
Phys. Rev. B, 102 174425 (2020)

A-191
C. Kim, *et al*.
Spin waves in the two-dimensional honeycomb lattice XXZ-type van der Waals antiferromagnet CoPS3
Phys. Rev. B, 102 184429 (2020)

A-192
D. Zhang, *et al*.
Temporally decoherent and spatially coherent vibrations in metal halide perovskites
Phys. Rev. B, 102 224310 (2020)

A-193
H. Tamatsukuri, *et al*.
Magnetism induced by interlayer electrons in the quasi-two-dimensional electride Y2C: Inelastic neutron scattering study
Phys. Rev. B, 102 224406 (2020)

A-194
S. Uechi, *et al*.
Behavior of Sm in the boron cage of Sm-doped RB6 (R =Yb, La) observed by multiple-wavelength neutron holography
Phys. Rev. B, 102 54104 (2020)

A-195
Y. Araki, *et al*.
Metamagnetic transitions and magnetoelectric responses in the chiral polar helimagnet Ni2InSbO6
Phys. Rev. B, 102 54409 (2020)

A-196
T. Yamamoto, *et al*.
Transverse asymmetry of γ rays from neutron-induced compound states of 140La
Phys. Rev. C, 101 064624 (2020)

A-197
H. Singh, *et al*.
Probing the adsorption of nonionic micelles on different-sized nanoparticles by scattering techniques
Phys. Rev. E, 102 62601 (2020)

A-198
S. Allenspach, *et al*.
Multiple Magnetic Bilayers and Unconventional Criticality without Frustration in BaCuSi2O6
Phys. Rev. Lett., 124 177205 (2020)

A-199
K. Kuramochi, *et al*.
Synthesis and physical properties of the new iridium oxyfluoride Sr2Ir(O,F)6-d using a topochemical reaction method
Phys. Rev. Mater., 4 013403 (2020)

A-200
R. Takahama, *et al*.
Structural, magnetic, transport and thermoelectric properties of the pseudobrookite AlTi2O5-Ti3O5 system
Phys. Rev. Mater., 4 074401 (2020)

A-201
J. Guo, *et al*.
Magnetic-field and composition tuned antiferromagnetic instability in the quantum spin-liquid candidate NaYbO2
Phys. Rev. Mater., 4 64410 (2020)

A-202
K. Nawa, *et al*.
Bound spinon excitations in the spin- 1/2 anisotropic triangular antiferromagnet Ca3ReO5Cl2
Phys. Rev. Res., 2 043121(11pages) (2020)

A-203
S. Shamoto, *et al*.
Ultralow-energy magnon anomaly in yttrium iron garnet
Phys. Rev. Res., 2 33235 (2020)

A-204
T. Nakajima, *et al*.
Crystallization of magnetic skyrmions in MnSi investigated by neutron spin echo spectroscopy
Phys. Rev. Res., 2 43393 (2020)

A-205
N. Kitamura, *et al*.
Local Structures in Disordered Rocksalt-Type Li3NbO4- Based Positive Electrode Materials for a Lithium-Ion Battery
Phys. Status Solidi. B Basic Solid State Phys., 257 2000112-1-7 (2020)

A-206
Y. Sakaguchi, *et al*.
Excitation Light Energy Dependence of Silver Photodiffusion into Amorphous Germanium Sulfide: Neutron and X-Ray Reflectivity and X-Ray Diffraction
Phys. Status Solidi. B Basic Solid State Phys., 257 2000178 (2020)

A-207
H. Saitoh, *et al*.
Neutron diffraction study on the deuterium composition of nickel deuteride at high temperatures and high pressures
Physica B Condens. Matter., 587 412153 (2020)

A-208
Y. Sue, *et al*.
Development of a bunch-width monitor for low-intensity muon beam below a few MeV
Physical Review Accelerators and Beams, 23 022804 (2020).

A-209
T. Yamaga, *et al*.
Observation of a KNN bound state in the 3 He(K-, Λp)n reaction
Physical Review C 102 (2020) 44002

A-210
K. Abe, *et al*.
First combined measurement of the muon neutrino and antineutrino charged-current cross section without pions in the final state at T2K
Physical Review D 101 (2020) 112001

A-211
K. Abe, *et al*.
Simultaneous measurement of the muon neutrino charged-current cross section on oxygen and carbon without pions in the final state at T2K
Physical Review D 101 (2020) 112004

A-212
K. Abe, *et al*.
Measurement of the muon neutrino charged-current single π+ production on hydrocarbon using the T2K off-axis near detector ND280
Physical Review D 101 (2020) 12007

A-213
W. Foreman, *et al*.
Calorimetry for low-energy electrons using charge and light in liquid argon
Physical Review D 1010(2020) 12010

A-214
K. Abe, *et al*.
First measurement of the charged current νμ double differential cross section on a water target without pions in the final state
Physical Review D 102 (2020) 12007

A-215
N. Shimizu, *et al*.
First search for KL → π0γ
Physical Review D 102 (2020) 51103

A-216
K. Abe, *et al*.
Search for Electron Antineutrino Appearance in a Long-Baseline Muon Antineutrino Beam
Physical Review Letters 124 (2020) 161802

A-217
T. Kitahara, *et al*.
New Physics Implications of Recent Search for KL → π0νν at KOTO
Physical Review Letters 124 (2020) 71801

A-218
Tatsumi AOYAMA, *et al*.
The anomalous magnetic moment of the muon in the Standard Model
Physics Reports-Review Section of Physics Letters 887 (2020) 1

A-219
Y. Kimura, *et al*.
Folded amphiphilic homopolymer micelles in water: uniform self-assembly beyond amphiphilic random copolymers
Polym. Chem., 11 5156 (2020)

A-220
D. Ito, *et al*.
efficient synthesis to crystallinity control
Polym. Chem., 11 5181 (2020)

A-221
K. A. Suyama, *et al*.
Fine-structure analysis of perhydropolysilazane-derived nano layers in deep-buried condition using polarized neutron reflectometry
Polymers, 12 2180 (2020)

A-222
H. Natori
Development of very slow negative muon beam
PoS (NuFACT2019), 369 090 (2020)

A-223
S. Makimura, *et al*.
Status and Future Prospect of Muon Target at J-PARC MLF
PoS (NuFACT2019), 369 124 (2020)

A-224
R.Abramishvili, *et al*.
COMET Phase-I technical design report
Prog. Theor. Exp. Phys., 033C01- (2020)

A-225
J. Beare, *et al*.
Study of muonium emission from laser-ablated silica aerogel
Prog. Theor. Exp. Phys., 2020 123C01 (2020)

A-226
K. Hirota, *et al*.
Neutron lifetime measurement with pulsed cold neutrons
Prog. Theor. Exp. Phys., 2020 123C02 (2020)

A-227
H. Ohnishi, *et al*.
Hadron Physics at J-PARC
Progress in Particle and Nuclear Physics 113 (2020) 103773

A-228
Y. Ichikawa, *et al*.
An event excess observed in the deeply bound region of the 12C(K^-,p) missing mass spectrum
Prog. Theor. Exp. Phys., 123D001 (2020)

A-229
T. Tanaka, *et al*.
Gamma-ray spectra from thermal neutron capture on gadolinium-155 and natural gadolinium
Prog. Theor. Exp. Phys., 2020 043D02 (2020)

A-230
O. Takahashi, *et al*.
Microstructural Features and Ductile-Brittle Transition Behavior in Hot-Rolled Lean Duplex Stainless Steels
Quantum Beam Science, 4 16 (2020)

A-231
Y. Wang
Phase Stress Measurement of Centrifugally Cast Duplex Stainless Steel by Neutron Diffraction
Quantum Beam Science, 4 28 (2020)

A-232
Y. Noda, *et al*.
The Large-Area Detector for Small-Angle Neutron Scattering on iMATERIA at J-PARC
Quantum Beam Science, 4 32 (2020)

A-233
Y. Noda, *et al*.
First Experiment of Spin Contrast Variation Small-Angle Neutron Scattering on the iMATERIA Instrument at J-PARC
Quantum Beam Science, 4 33 (2020)

A-234
K. Nakagawa, *et al*.
Characterization of Dislocation Rearrangement in FCC Metals during Work Hardening Using X-ray Diffraction Line-Profile Analysis
Quantum Beam Science, 4 36 (2020)

A-235
S. Koizumi, *et al*.
Advanced Small-Angle Scattering Instrument Available in the Tokyo Area. Time-of-Flight, Small-Angle Neutron Scattering Developed on the iMATERIA Di ractometer at the High Intensity Pulsed Neutron Source J-PARC
Quantum Beam Science, 4 42 (2020)

A-236
Y. Onuki, S. Sato
In Situ Observation for Deformation-Induced Martensite Transformation (DIMT) during Tensile Deformation of 304 Stainless Steel Using Neutron Diffraction. PART I: Mechanical Response
Quantum Beam Science, 4 44227 (2020)

A-237
A. Momose, *et al*.
Recent Progress in X-ray and Neutron Phase Imaging with Gratings
Quantum Beam Science, 4 9 (2020)

A-238
T. MIBE
Anomalous Magnetic Moment and Electric Dipole Moment of Muon
Radioisotopes 69 (2020)n 145

A-239
T. Shinohara, *et al*.
The energy-resolved neutron imaging system, RADEN
Rev. Sci. Instrum., 91 043302 (2020)

A-240
V. Sonnenschein, *et al*.
An experimental setup for creating and imaging 4He2* excimer cluster tracers in superfluid Helium-4 via neutron-3He absorption reaction
Rev. Sci. Instrum., 91 33318 (2020)

A-241
M. Wada, et a.
Measurement of a time dependent spatial beam profile of an RF-driven H- ion source
Rev. Sci. Instrum., Vol 91, 013330-1 - 013330-5 (2020)

A-242
K. Arai, *et al*.
Reconsideration of the conformation of methyl cellulose and hydroxypropyl methyl cellulose ethers in aqueous solution
RSC Adv., 10 19059 (2020)

A-243
M. Naeem, *et al*.
Cooperative deformation in high-entropy alloys at ultralow temperatures
Sci. Adv., 6 eaax4002 (2020)

A-244
S. Sato, *et al*.
Antiferromagnetism in perfectly ordered L10-MnAl with stoichiometric composition and its mechanism
Sci. Rep., 10 12489 (2020)

A-245
S. Yamamoto, *et al*.
Optical imaging of muons
Sci. Rep., 10 20790 (2020)

A-246
R. Inoue, *et al*.
Dynamics of proteins with different molecular structures under solution condition
Sci. Rep., 10 21678 (2020)

A-247
W. Woo, *et al*.
Stacking Fault Energy Analyses of Additively Manufactured Stainless Steel 316L and CrCoNi Medium Entropy Alloy Using In Situ Neutron Diffraction
Sci. Rep., 10 43845 (2020)

A-248
Y. K. Kshetri, *et al*.
Electronic structure, thermodynamic stability and high temperature sensing properties of Er-α-SiAlON ceramics
Sci. Rep., 10 4952 (2020)

A-249
H. Saitoh, *et al*.
Crystal and Magnetic Structures of Double Hexagonal Close-Packed Iron Deuteride
Sci. Rep., 10 9934 (2020)

A-250
E. Shoji, *et al*.
Neutron computed tomography of phase separation structures in solidified CuCo alloys and investigation of relationship between the structures and melt convection during solidification
Scr. Mater., 175 29 (2020)

A-251
K. Cho, *et al*.
Study on formation mechanism of {332} < 113 > deformation twinning in metastable β-type Ti alloy focusing on stress-induced α"martensite phase
Scr. Mater., 177 106-111 (2020)

A-252
T. Yamashita, *et al*.
Role of retained austenite in low alloy steel at low temperature monitored by neutron diffraction
Scr. Mater., 177 43992 (2020).

A-253
Z. Deng, *et al*.
Elinvar property of cold-rolled NiTi alloy
Scr. Mater., 187 197-201 (2020)

A-254
M. Naeem, *et al*.
Extremely high dislocation density and deformation pathway of CrMnFeCoNi high entropy alloy at ultralow temperature
Scr. Mater., 188 21-25 (2020)

A-255
N. Ishida, *et al*.
Synthesis, cathode property and crystal, electronic and local structures of Mg2Mo3O8 as Mg rechargeable battery cathode material
Solid State Ion., 354 115413 (2020)

A-256
R. Li, *et al*.
Anomalous sub-diffusion of water in biosystems: From hydrated protein powders to concentrated protein solution to living cells
Struct. Dyn., 7 054703 (2020)

A-257
J. Kim, *et al*.
Pyroelectric power generation from the

waste heat of automotive exhaust gas
Sustain. Energy Fuels, 4 1143 (2020)

A-258
Y. Hosoya, *et al*.
Mechanism of improved ductility of 1,500 MPa-class ultra-high strength cold-rolled steel sheet produced by rolling and partitioning method
Tetsu to Hagane, 106 154-164 (2020)

A-259
Y. Tomota, *et al*.
In situ Neutron Diffraction on Ferrite and Pearlite Transformations for a 1.5Mn-1.5Si-0.2C Steel
Tetsu to Hagane, 106 262-271 (2020)

A-260
Y. Onuki, *et al*.
Mutual Verification of Phase Fraction Analysis Techniques for Steels Comprising Deformation Induced Martensite Phases: Neutron-Diffraction-Based Rietveld Texture Analysis and Saturation Magnetization Measurement
Tetsu to Hagane, 106 457 (2020)

A-261
Y. Sakaguchi, *et al*.
Silver photodiffusion into amorphous Ge chalcogenides - Excitation photon energy dependence of the kinetics probed by neutron reflectivity
The European Physical Journal Applied Physics, 90 30101 (2020)

A-262
Y. Sakaguchi, K. Tamura
Photo-induced effects on amorphous and liquid selenium by pulsed laser illumination -Photo-induced structural changes in a network of selenium chains
Z. Phys. Chem., 235 189-212 (2020)

Conference Reports and Books

B-001
S. Meigo, *et al*.
Measurement of displacement cross section with the kinematic energy above 400 MeV for structural materials in the proton accelerator facilities
JPS Conf. Proc. 28, 061004

B-002
F. Sakuma, *et al*.
K- pp bound system at J-PARC
AIP Conference Proceedings 2249 (2020) 20005

B-003
A. Kimura, *et al*.
Neutron capture and total cross-section measurements of 155Gd and 157Gd at ANNRI in J-PARC
EPJ Web Conf., 239 1012 (2020)

B-004
G. Rovira, *et al*.
Measurement of the neutron capture cross-section of 237Np using ANNRI at MLF/J-PARC
EPJ Web Conf., 239 1017 (2020)

B-005
T. Katabuchi, *et al*.
Fast Neutron Capture Reaction Data Measurement of Minor Actinides for Development of Nuclear Transmutation Systems
EPJ Web Conf., 239 1044 (2020)

B-006
S. Iwamoto, *et al*.
Evaluation of gamma-ray strength function based on measured gamma-ray pulse-height spectra in time-of-flight neutron capture experiments
EPJ Web Conf., 239 17016 (2020)

B-007
H. Iwamoto, *et al*.
A comprehensive study of spallation models for proton-induced spallation products yields utilized in transport calculation
EPJ Web of Conferences 239, 06001

B-008
H. Matsuda, *et al*.
Measurement of nuclide production cross section for lead and bismuth with proton in energy range from 0.4 GeV to 3.0 GeV
EPJ Web of Conferences 239, 06004

B-009
S. Meigo, *et al*.
Measurement of displacement cross section in J-PARC for proton in the energy range from 0.4 GeV to 3 GeV
EPJ Web of Conferences 239, 06006

B-010
Y. Iwamoto, *et al*.
Calculation of athermal recombination corrected dpa cross sections for proton, deuteron and heavy-ion irradiations using the PHITS code
EPJ Web of Conferences 239, 20011

B-011
M. Yoshimoto, *et al*.
Progress status in fabrication of HBC stripper foil for 3-GeV RCS at J-PARC in Tokai site
EPJ Web of Conferences, 229(2020), p.01001_1 - 01001_7

B-012
S. Abe, *et al*.
Impact of Hydrided and Non-Hydrided Materials Near Transistors on Neutron-Induced Single Event Upsets
IEEE International Reliability Physics Symposium Proceedings, (2020)

B-013
T. Okamura, *et al*.
Helium Transfer Line with Conduction-Cooled Nb-Ti Superconducting Wires for COMET Muon Transport Solenoid
IOP Conf. Ser. Mater. Sci. Eng., 755 (2020), 12058

B-014
T. Okamura, *et al*.
Helium Transfer Line with Conduction-Cooled Nb-Ti Superconducting Wires for COMET Muon Transport Solenoid
IOP Conference Series Materials Science and Engineering 755 (2020) 12058

B-015
T. Mibe
Precise Measurement of Anomalous Magnetic Moment of Muon
Journal of Computer Chemistry, Japan 19 (2020) 64

B-016
H. Hotchi, *et al*.
J-PARC 3-GeV RCS; 1-MW beam operation and beyond
Journal of Instrumentation (Internet), 15(7), p.P07022_1 - P07022_16, 2020/07

B-017
A. Nakamura, *et al*.
R&D on the gas injection system of Beam Induced Fluorescence Monitor toward MW beam power at the J-PARC Neutrino Beam-line
Journal of Physics: Conference Series 1468 (2020) 12213

B-018
T. Nomura
A future K0L → π0νν experiment at J-PARC
Journal of Physics: Conference Series 1526 (2020) 12027

B-019
T Onji, *et al*.
Superconducting Properties of a Prototype Pancake Coil using a MgB2 Rutherford-type Stranded Conductor
Journal of Physics: Conference Series 1559 (2020) 12057

B-020
M Hira, *et al*.
Theoretical and experimental investigation of R&W and W&R SMES coils wound with large-scale MgB2 Rutherford cables operated around liquid hydrogen temperature
Journal of Physics: Conference Series 1590 (2020) 12058

B-021
K. Tanaka
Major Accelerator Facilities for Nuclear Physics in Asia Pacific
Journal of Physics: Conference Series 1643 (2020) 12041

B-022
T. Gogami, *et al*.
Study on the baryon interaction by Ξ hypernuclear spectroscopy with the (K-, K+) reaction
Journal of Physics: Conference Series 1643 (2020) 12133

B-023
K. Miwa, *et al*.
Study of ΣN interaction from the Σp scattering experiment at J-PARC
Journal of Physics: Conference Series 1643 (2020) 12174

B-024
S. Kumano
Tensor-polarized structure functions: Tensor structure of deuteron in 2020's
Journal of Physics: Conference Series 543 (2020) 12001

B-025
Y. Iwamoto, *et al*.
Measurement of defect induced electrical resistivity change of tungsten wire at cryogenic temperature using high energy proton irradiation
JPS Conf. Proc. 28, 061003

B-026
S. Saito, *et al*.
Current Status of R&D and PIE Program for ADS Material Development in JAEA
JPS Conf. Proc. 28, p.071003_1 - 071003_6, 2020/02

B-027
S. Makimura, *et al*.
Feasibility Study for NITE SiC/SiC as the Target Material for Pions/Muons Production at High-Power Proton Accelerator Facilities
JPS Conf. Proc., 28 031005 (2020)

B-028
T. Naoe, *et al*.
Change in Mechanical Properties by High-Cycle Loading Up to Gigacycle for 316L Stainless Steel
JPS Conf. Proc., 28 061009 (2020)

B-029
N. Nakamura, *et al*.
μSR and Neutron Scattering Studied on Possible Partially-Disordered Magnetic State Coexisting with Heavy Quasiparticles in SmPt2Si2
JPS Conf. Proc., 29 012009 (2020)

B-030
N. Metoki, *et al*.
The f-electron State of the Heavy Fermion Superconductor NpPd5Al2 and the Isostructural Family
JPS Conf. Proc., 30 011123 (2020)

B-031
S. Nakazato, *et al*.
Successive Phase Transitions in R3Ir4Sn13 (R: La and Ce) Investigated Using Neutron and X-ray Diffraction
JPS Conf. Proc., 30 011128 (2020)

B-032
K. Iba, *et al*.
Magnetic Structure of a Chiral Magnet DyNi3Al9
JPS Conf. Proc., 30 011164 (2020)

B-033
D. Hirai, *et al*.
Muon Spin Rotation, High-Field Magnetization, and Structural Study on a Spin–Orbit-Entangled Mott Insulator Ba2MgReO6
JPS Conf. Proc., 30 11143 (2020)

B-034
S. Tsunoda, *et al*.
μSR study of the magnetic state in hole and electron doped Sr2IrO4
JPS Conf. Proc., 30 11145 (2020)

B-035
K. A. Suyama, *et al*.
Metal catalyzed H-D exchange methods using D2O as a deuterium source: A comparative study in different sealed devices
JPS Conf. Proc., 33 011150 (2020)

B-036
C. Ohmori
Improvements of Beam Acceleration Systems and μSR
Meson

B-037
Makoto Yoshida
COMET Experiment
Meson, 52 (2020), 20

B-038
Ken-ichi SASAKI
Precise Magnetic Field Shimming and Absolute Magnetic Field Measurement
Meson, 52 (2020), 24

B-039
T. Asami, *et al*.
DEVELOPMENT OF REAL-TIME COD CORRECTION SYSTEM FOR THE HIGH INTENSITY PROTON SYNCHROTRONS
Proc. 17th Ann. Mtg. Part. Accel. Soc. Jpn. (Internet), 20- (2020)

B-040
K. Kadowaki, *et al*.
THE DESIGN OF THE NEW BEAM DUMP FOR J-PARC MR UPGRADE
Proc. 17th Ann. Mtg. Part. Accel. Soc. Jpn. (Internet), 205- (2020)

B-041
T. Shibata, *et al*.
THE NEW HIGH-FIELD SEPTUM MAGNET FOR UPGRADING OF FAST EXTRACTION IN MR J-PARC(2)
Proc. 17th Ann. Mtg. Part. Accel. Soc. Jpn. (Internet), 388- (2020)

B-042
Y. Komatsu, *et al*.
BEAM COMMISSIONING OF A NEW PRIMARY PROTON BEAM LINE AT J-PARC HADRON EXPERIMENTAL FACILITY
Proc. 17th Ann. Mtg. Part. Accel. Soc. Jpn. (Internet), 485- (2020)

B-043
M. Furusawa, *et al*.
REPLACEMENT AND UPGRADE OF RF POWER SUPPLY CONTROL DEVICES IN J-PARC SYNCHROTRONS
Proc. 17th Ann. Mtg. Part. Accel. Soc. Jpn. (Internet), 521- (2020)

B-044
M. Yang, *et al*.
UPGRADED RADIATION DOSE MONITOR SYSTEM WITH XBEE DISPATCHER PROGRAM
Proc. 17th Ann. Mtg. Part. Accel. Soc. Jpn. (Internet), 524- (2020)

B-045
T. Shibata, *et al*.
THE NEW LOW-FIELD SEPTUM MAGNET FOR UPGRADING OF FAST EXTRACTION IN MR J-PARC(6)
Proc. 17th Ann. Mtg. Part. Accel. Soc. Jpn. (Internet), 594- (2020)

B-046
K. SATO, *et al*.
LONG-TERM ELECTRICITY POWER CONSUMPTION TRENDS AT J-PARC

ACCELERATOR FACILITIES
Proc. 17th Ann. Mtg. Part. Accel. Soc. Jpn. (Internet), 620- (2020)

B-047
M. Nomura, *et al*.
APPLYING IMAGE RECOGNITION TECHNOLOGY BY CONVOLUTIONAL NEURAL NETWORKS TO MOUNTAIN PLOT IMAGES
Proc. 17th Ann. Mtg. Part. Accel. Soc. Jpn. (Internet), 64- (2020)

B-048
M. Tomizawa, *et al*.
DESIGN AND STATUS OF CURRENT BEAM DUMP SYSTEM IN J-PARC MAIN RING
Proc. 17th Ann. Mtg. Part. Accel. Soc. Jpn. (Internet), 665- (2020)

B-049
H. Okita, *et al*.
BENCHMARKING OF LONGITUDINAL CALCULATION CODE BLOND FOR APPLICATION TO J-PARC RCS
Proc. 17th Ann. Mtg. Part. Accel. Soc. Jpn. (Internet), 674- (2020)

B-050
F. Tamura, *et al*.
TOWARDS WIDESPREAD USE OF MTCA IN ACCELERATORS
Proc. 17th Ann. Mtg. Part. Accel. Soc. Jpn. (Internet), 68- (2020)

B-051
A. Kobayashi, *et al*.
STUDY OF THE TRANSVERSE BEAM INSTABILITY CAUSED BY THE RESISTIVE-WALL IMPEDANCE AT THE J-PARC MAIN RING
Proc. 17th Ann. Mtg. Part. Accel. Soc. Jpn. (Internet), 684- (2020)

B-052
T. Toyama, *et al*.
ANALYSIS OF COLLECTIVE INSTABILITIES OF UNEVEN FILLED BEAMS INCLUDING LONG RANGE WAKE FIELDS USING AN IIR FILTER
Proc. 17th Ann. Mtg. Part. Accel. Soc. Jpn. (Internet), 689- (2020)

B-053
T. Shibata, *et al*.
THE REDUCTION OF THE LEAKAGE FIELD OF THE NEW INJECTION SEPTUM MAGNET 1 BY USING A NEW MAGNETIC SHIELD IN MR J-PARC
Proc. 17th Ann. Mtg. Part. Accel. Soc. Jpn. (Internet), 793- (2020)

B-054
T. Sugimoto, *et al*.
PERFORMANCE OF NEW TERMINATION RESISTORS OF J-PARC MAIN RING INJECTION KICKER MAGNET
Proc. 17th Ann. Mtg. Part. Accel. Soc. Jpn. (Internet), 798- (2020)

B-055
M. Shirakata
PROTOTYPE OF SIX-AXIS MOUNT FOR QSC MAGNET IN BEAM COLLIMATOR AREA
Proc. 17th Ann. Mtg. Part. Accel. Soc. Jpn. (Internet), 802- (2020)

B-056
Y. Kawabata, *et al*.
CONSTRUCTION OF DISASTER PREVENTION SYSTEM BY DEDICATED NETWORK DEVICES AND MOBILE APPLICATION IN J-PARC MR
Proc. 17th Ann. Mtg. Part. Accel. Soc. Jpn. (Internet), 845- (2020)

B-057
T. SHIMOGAWA, *et al*.
STATUS OF NONDESTRUCTIVE DEVICE DEVELOPMENT FOR SLOW EXTRACTION
Proc. 17th Ann. Mtg. Part. Accel. Soc. Jpn. (Internet), 875- (2020)

B-058
H. Yamaguchi, *et al*.
FEASIBILITY STUDY ON DOSIMETRY USING ALANINE DOSIMETER AROUND HIGH-INTENSITY PROTON ACCELERATOR
Proc. 17th Ann. Mtg. Part. Accel. Soc. Jpn. (Internet), 93- (2020)

B-059
Y. SATO, *et al*.
Operation of a new multi-ribbon beam profile monitor in the beam abort line of J-PARC main ring
Proc. 17th Ann. Mtg. Part. Accel. Soc. Jpn. (Internet), FRPP17- (2020)

B-060
Y. HASHIMOTO, *et al*.
Development of a wide dynamic-range beam-profile monitor using OTR and fluorescence for Injected beams in J-PARC Main Ring
Proc. 17th Ann. Mtg. Part. Accel. Soc. Jpn. (Internet), FRPP19- (2020)

B-061
N. KAMIKUBOTA, *et al*.
Twelve-year operation and upgrade experiances of J-PARC MR control
Proc. 17th Ann. Mtg. Part. Accel. Soc. Jpn. (Internet), WEOOP04- (2020)

B-062
K. Noguchi, *et al*.
Improvement of proton beam extinction and optimization of the compensation kicker magnet of J-PARC main ring for the COMET experiment
Proc. 17th Ann. Mtg. Part. Accel. Soc. Jpn. (Internet), WEOT02- (2020)

B-063
B. Yee-Rendon, *et al*.
Error studies for the JAEA-ADS linac
Proc. 17th Ann. Mtg. Part. Accel. Soc. Jpn. (2020), 33

B-064
M. Sugita, *et al*.
PRECISE OPERATION OF SUPERCONDUCTING MAGNET FOR BEAM CAPTURE APPLYING WHOLE-BODY MRI MAGNET TECHNOLOGY
Proc. Ann. Mtg Part. Accel. Soc. Jpn. 13 (2020)

B-065
F. Muto, *et al*.
BEAM PROFILE MEASUREMENT SYSTEM IN THE NEIGHBORHOOD OF THE J-PARC HIGH-MOMENTUM BEAMLINE TARGET
Proc. Ann. Mtg Part. Accel. Soc. Jpn. 130 (2020)

B-066
S. Makimura, *et al*.
PRESENT STATUS OF COMET TARGET AT J-PARC
Proc. Ann. Mtg Part. Accel. Soc. Jpn. 150 (2020)

B-067
Y. Nakazawa, *et al*.
CURRENT STATUS FOR HIGH-POWER TESTS OF AN APF IH-DTL PROTOTYPE IN THE MUON LINAC
Proc. Ann. Mtg Part. Accel. Soc. Jpn. 154 (2020)

B-068
H. Yasuda, *et al*.
SPIN DYNAMICS SIMULATION IN MUON ACCELERATOR
Proc. Ann. Mtg Part. Accel. Soc. Jpn. 173 (2020)

B-069
Y. Nakazawa, *et al*.
DEVELOPMENT OF A DIAGNOSTIC BEAMLINE FOR THE DEMONSTRATION OF THE MUON ACCELERATION WITH AN APF IH-DTL
Proc. Ann. Mtg Part. Accel. Soc. Jpn. 254 (2020)

B-070
H. Hirayama, *et al*.
THE STATUS REPORT OF DEMONSTRATIVE EXPERIMENT OF 3D SPIRAL BEAM INJECTION FOR J-PARC MUON G-2/EDM EXPERIMENT
Proc. Ann. Mtg Part. Accel. Soc. Jpn. 29 (2020)

B-071
R. Kurasaki, *et al*.
DEVELOPMENT OF A ROTATING-DISC TYPE TARGET FOR J-PARC HADRON BEAMLINE (2)
Proc. Ann. Mtg Part. Accel. Soc. Jpn. 402 (2020)

B-072
Y. Komatsu, *et al*.
BEAM COMMISSIONING OF A NEW PRIMARY PROTON BEAM LINE AT J-PARC HADRON EXPERIMENTAL FACILITY
Proc. Ann. Mtg Part. Accel. Soc. Jpn. 485 (2020)

B-073
H. Takahashi, *et al*.
DEVELOPMENT OF NEW RADIATION-RESISTANT MAGNETS USING CYANATE ESTER RESIN

Proc. Ann. Mtg Part. Accel. Soc. Jpn. 599 (2020)

B-074
H. Watanabe, *et al*.
DEVELOPMENT OF A BELLOWS DUCT WITH A SEMI-REMOTE HANDLING SYSTEM AT J-PARC HADRON FACILITY
Proc. Ann. Mtg Part. Accel. Soc. Jpn. 786 (20209)

B-075
M. Abe, *et al*.
TRIAL DESIGN OF A STEERING MAGNET TO BE PLACED IN MUON STORAGE MAGNET FOR G-2/EDM PRECISION MEASUREMENT
Proc. Ann. Mtg Part. Accel. Soc. Jpn. 807 (2020)

B-076
M. Saito, *et al*.
OPERATION STATUS AND ANALYSIS OF THE NEW PRODUCTION TARGET AT J-PARC HADRON EXPERIMENTAL FACILITY
Proc. Ann. Mtg Part. Accel. Soc. Jpn. 822 (2020)

B-077
S. Makimura, *et al*.
Development of Toughened Fine-Grained Recrystallized Tungsten for high-heat-load device in accelerators
Proc. Ann. Mtg Part. Accel. Soc. Jpn. HGKP04 (2020)

B-078
K. Noguchi, *et al*.
Improvement of proton beam extinction and optimization of the compensation kicker magnet of J-PARC main ring for the COMET experiment
Proc. Ann. Mtg Part. Accel. Soc. Jpn. WEOT02 (2020)

B-079
S. V. Cao, M. L. Friend
INVESTIGATION OF AN OPTICAL-FIBER BASED BEAM LOSS MONITOR AT THE J-PARC EXTRACTION NEUTRINO BEAMLINE
Proc. IBIC 119 (2020)

B-080
S. V. Cao, *et al*.
FIRST BEAM PROFILE MEASUREMENTS BY BEAM INDUCED FLUORESCENCE AT THE J-PARC NEUTRINO EXTRACTION BEAMLINE
Proc. IBIC 184 (2020)

B-081
T. Murakawa, *et al*.
Neutron crystallography of copper amine oxidase reveals keto/enolate interconversion of the quinone cofactor and unusual proton sharing
Proc. Natl. Acad. Sci. U. S. A., 117 10818-10824 (2020)

B-082
Y. Fukuda, *et al*.
High-resolution neutron crystallography visualizes an OH-bound resting state of a copper-containing nitrite reductase
Proc. Natl. Acad. Sci. U. S. A., 117 4071-4077 (2020)

B-083
K. Komatsu, *et al*.
Anomalous hydrogen dynamics of the ice VII-VIII transition revealed by high-pressure neutron scattering
Proc. Natl. Acad. Sci. U. S. A., 117 6356-6361 (2020)

B-084
K. Yanai, *et al*.
Beam measurement of medium energy beam transport line (MEBT1) to improve injection beam matching in J-PARC linac DTL
Proc. of 17th Annual Meeting of Particle Accelerator Society of Japan (Internet), 127-129 (2020)

B-085
Y. Nakazawa, *et al*.
Current status for high-power tests of an APF IH-DTL prototype in the muon LINAC
Proc. of 17th Annual Meeting of Particle Accelerator Society of Japan (Internet), 154-157 (2020)

B-086
Y. Takeuchi, *et al*.
Development of Disk-and-Washer cavity for muon linear accelerator
Proc. of 17th Annual Meeting of Particle Accelerator Society of Japan (Internet), 158-162 (2020)

B-087
H. Yasuda, *et al*.
Spin Dynamics Simulation in the Muon Accelerator
Proc. of 17th Annual Meeting of Particle Accelerator Society of Japan (Internet), 173-176 (2020)

B-088
M. Otani, *et al*.
Study of Muon Acceleration by Auto-resonance Cyclotron
Proc. of 17th Annual Meeting of Particle Accelerator Society of Japan (Internet), 202-204 (2020)

B-089
Y. Kondo, *et al*.
Conceptual design of a L-band linac for muon acceleration
Proc. of 17th Annual Meeting of Particle Accelerator Society of Japan (Internet), 218-221 (2020)

B-090
R. Kitamura, *et al*.
Evaluation of the bunch-shape monitor for the high-intensity proton beam
Proc. of 17th Annual Meeting of Particle Accelerator Society of Japan (Internet), 251-253 (2020)

B-091
Y. Nakazawa, *et al*.
Development of a diagnostic beamline for the demonstration of the muon acceleration with an APF IH-DTL
Proc. of 17th Annual Meeting of Particle Accelerator Society of Japan (Internet), 254-257 (2020)

B-092
Y. Fuwa, *et al*.
Analysis on Voltage Droop on J-PARC Klystron High Voltage Power Supply
Proc. of 17th annual Meeting of Particle Accelerator Society of Japan (internet), 780-782 (2020)

B-093
H. Takahashi, *et al*.
MACHINE STATUS MONITORING SYSTEM FOR J-PARC RCS
Proc. of the 17th Annual Meeting of Particle Accelerator Society of Japan, 275-279 (2020).

B-094
P. K. Saha, *et al*.
Status of the proof-of-principle demonstration of 400 MeV H- laser stripping at J-PARC
Proc. of the 17th Annual Meeting of Particle Accelerator Society of Japan, 436-440 (2020).

B-095
H. Harada, *et al*.
Status of laser development for laser stripping experiment at J-PARC
Proc. of the 17th Annual Meeting of Particle Accelerator Society of Japan, 441-445 (2020).

B-096
K. Okabe
CHARGE EXCHANGE METHOD OF H- BEAM BY ELECTRON BEAM
Proc. of the 17th Annual Meeting of Particle Accelerator Society of Japan, 446-448 (2020).

B-097
N. Hayashi
Intensity dependence of the beam current monitors at J-PARC RCS
Proc. of the 17th Annual Meeting of Particle Accelerator Society of Japan, 478-481 (2020).

B-098
A. Kobayashi, *et al*.
Study of the transverse beam instability caused by the resistive-wall impedance at the J-PARC main ring
Proc. of the 17th Annual Meeting of Particle Accelerator Society of Japan, 684-688 (2020).

B-099
T. Toyama, *et al*.
Analysis of collective instabilities of uneven

filled beams including long range wake fields using an IIR filter
Proc. of the 17th Annual Meeting of Particle Accelerator Society of Japan, 689-692 (2020).

B-100
K. Yamamoto, *et al*.
Results of 1-MW Operation in J-PARC 3 GeV Rapid Cycling Synchrotron
Proc. of 17th Annual Meeting of Particle Accelerator Society of Japan, (2020), 209 - 213

B-101
T. Takayanagi, *et al*.
Semiconductor switch power supply for RCS kicker
Proc. of 17th Annual Meeting of Particle Accelerator Society of Japan, (2020), 25 - 28

B-102
H. Harada, *et al*.
Status of laser development for laser stripping experiment at J-PAR
Proc. of 17th Annual Meeting of Particle Accelerator Society of Japan, (2020), 441 - 445

B-103
S. Hatakeyama, *et al*.
High voltage dependence measurement of beam loss monitor in J-PARC RCS
Proc. of 17th Annual Meeting of Particle Accelerator Society of Japan, (2020), 475 - 477

B-104
A. Ono, *et al*.
Development of ignitron alternative semiconductor switch and new kicker power supply for J-PARC accelerator
Proc. of 17th Annual Meeting of Particle Accelerator Society of Japan, (2020), 590 - 593

B-105
M. Nomura, *et al*.
Applying image recognition technology by convolutional neural networks to mountain plot images
Proc. of 17th Annual Meeting of Particle Accelerator Society of Japan, (2020), 64 - 67

B-106
H. Okita, *et al*.
Benchmarking of Longitudinal Calculation Code BLOND for Application to J-PARC RCS
Proc. of 17th Annual Meeting of Particle Accelerator Society of Japan, (2020), 674 - 678

B-107
F. Tamura, *et al*.
Towards widespread use of MTCA in accelerators
Proc. of 17th Annual Meeting of Particle Accelerator Society of Japan, (2020), 68 - 72

B-108
K. Moriyama, T. Nakatani
Public cloud-based remote access infrastructure for neutron scattering experiments at MLF, J-PARC
Proc. of the 17th International Conference on Accelerator and Large Experimental Physics Control Systems, 707-713 (2020)

B-109
A. Ueno
J-PARC $\mathbf{H}-$ ion source and space-charge neutralized LEBT for 100-mA high energy and high duty factor LINACs
Review of Scientific Instruments 91, 033312 (2020)

KEK Reports

C-001
Safety Division, J-PARC Center
Annual Report on the Activities of Safety in J-PARC, FY2019
KEK Internal 2020-6

JAEA Reports

D-001
Safety Division, J-PARC Center
Annual Report on the Activities of Safety in J-PARC, FY2019
JAEA-Review 2020-067(2020)

Others

E-001
T. Nakadaira
Recent Progress of Neutrino Oscillation Experiments at J-PARC
Kasokuki, 17 (2020) 174

J-PARC Annual Report 2020
Vol.1: Highlight

December 2021

J-PARC

JAPAN PROTON ACCELERATOR RESEARCH COMPLEX

High Energy Accelerator Research Organization (KEK)
Japan Atomic Energy Agency (JAEA)

2-4 Shirakata, Tokai-mura, Naka-gun, Ibaraki 319-1195, Japan

http://j-parc.jp/